THE BEHAVIOUR OF FERROCEMENT SLABS UNDER DIFFERENT LOADS

A Thesis Submitted
In Partial Fulfilment of the Requirements
for the Degree of
DOCTOR OF PHILOSOPHY

by

MURLIDHAR RAISINGHANI

to the

DEPARTMENT OF CIVIL ENGINEERING
INDIAN INSTITUTE OF TECHNOLOGY KANPUR

AUGUST, 1976

IN MEMORY OF

MY BELOVED FATHER

CERTIFICATE

This is to certify that the thesis entitled 'THE BEHAVIOUR OF FERROCEMENT SLABS UNDER DIFFERENT LOADS' by Mr. Murlidhar Raisinghani for the award of the degree of Doctor of Philosophy is a record of bonafide research work carried out by him under my supervision, and has not been submitted elsewhere for a degree.

August, 1976

(SRI RANGA SAI ADIDAM)
Assistant Professor
Department of Civil Engineering
Indian Institute of Technology
Kanpur (INDIA)

ACKNOWLEDGEMENTS

The author wishes to express his profound gratitude to his thesis supervisor Dr. Sri Ranga Sai Adidam for valuable advices, encouragement and helpful criticisms throughout the course of this work.

The author is thankful to the authorities of Malaviya Regional Engineering College, Jaipur for sponsoring him under Quality Improvement Programme. He is, in particular, obliged to Prof. M.M. Dandekar, Head of Civil Engineering Department, M.R. Engineering College, Jaipur and to the late Principal R.M. Advani for all the help he has received from them.

He is indebted to Dr. Y.C. Das, Dr. P. Dayaratnam and Dr. M.P. Kapoor of Indian Institute of Technology, Kanpur, for their encouragement.

The author highly appreciates the assistance rendered by M/S S.C. Goel, S.V. Kapoor, K.V. Lakshmidhar, R.P. Trivedi, Hark Singh, Siddiqui, Verma and the supporting staff of the Structural Engineering Laboratory.

The help of Major M.B. Rekhi of the E.M.E; Indian Army in connection with blast loading tests is gratefully acknowledged.

The author is grateful to his friend Rahul Thakkar for all the help he has given during the preparation of the thesis. Special thanks are due to Dr. Surendra Mathur for the help and encouragement rendered by him during the closing stages of the manuscript. He also sincerely acknowledges the help rendered by his friends Major M.D. Advani, B.S.N. Reddy, B.N. Roy and Kamal Kedia.

The neat typing work of Mrs. B. Rukmini Devi, the good tracings prepared by Mr. S.D. Panesar and the help of M/S Kalyan Das and Maikoo Lal Gupta is also appreciated.

Finally the author finds it difficult to find words of appreciation for his beloved wife Leena and daughters, Renu, Ritu and Reshu for their understanding and tolerance in the course of this study.

MURLIDHAR RAISINGHANI

CONTENTS

LIST OF TABLES

LIST OF FIGURES

LIST OF SYMBOLS

A - a constant

A_s - area of skeletal steel per unit width per layer

A'_s - area of steel in compression zone

a, a_1, a_2 - constants

$2a$ - length of existing crack or flaw

B - a constant

b, b_1, b_2 - constants

C - constant

c - creep

c_1, c_2 - constants

c/c - centre to centre

D - a constant

d_1, d_2 - constants

E - Young's modulus of elasticity for any material

E_c - modulus of elasticity of the composite

E_f - modulus of elasticity of the fibre

E_m - modulus of elasticity of the mortar

E_t - modulus of elasticity of composite in tension in the cracked range

F - fibre efficiency factor

$F(K)$ - a parameter for creep rate

f_1 - surface energy

f_2 - time dependent irrecoverable deformation

f_3 - kinetic energy of crack propagation

f_4 - energy of stress concentration

f_5 - energy of the applied stress field

$f^1_{ij}, f^2_{ij}, f^3_{ij}$ - scalar function of θ

h - thickness of the composite section

h_c - depth of the compression zone in cracked range

h'_c - depth of the compression zone at yield

h_s - depth of the skeletal steel from the extreme fibre of the slab

h_t - depth of the tension zone in cracked range

h'_t - depth of the tension zone at yield

IS - Indian Standard

K - age at loading

K_1, K_2, K_3 - stress intensity factor

LA - loading areas

M - bending moment per unit width of the section

M_i - the generalised stress, $i = 1,2$

M_r - the radial moment

M_o - ultimate moment in uniaxial bending, per unit width

M_1, M_2 - principal moment

M_θ - circumferential moment

mm - millimetre

N_r - number of cycles which cause fatigue failure at a given stress condition

n_r - number of cycles applied at a given stress condition

P_c - collapse load

P_l - total load carried by the slab

p - load intensity

Q_i - generalised stress, $i = 1,2,3, \ldots n$

q_i - generalised displacements $i = 1,2,3, \ldots n$

r - radius at a given point

S - specific energy of the material

TA - test area

T_f - tensile force due to fibres

T_s - tensile force due to skeletal steel

T' - total tensile force

t - time

U - strain energy due to crack

V - work done due to plastic deformation

v_f - volume fraction of the fibres

v_m - volume fraction of the matrix

W - surface energy absorbed by the surfaces of the crack

w - total deflection

α - angle between the directions of M_1 and M_x

α_1 - parameter defined in equation A.1.2.5

α_2 - parameter defined in equation A.1.2.6

β - $\sqrt{E_c/E_t}$

γ - angle

∂ - partial derivative

η - an arbitrary positive scalar

ϱ - polar coordinate

μ - Poisson's ratio

π - a constant

Γ - region boundary

σ_c - tensile or compressive stress in the composite

σ_c^* - compressive stress in bending

σ_{ca} - average compressive strength of the mortar cube

σ_{cr} - rupture modulus of mortar determined from the beam test

σ_f - tensile or compressive stress in the fibres

σ_{ij} - stress components

σ_m - tensile or compressive stress in the mortar/matrix

σ_t^* - tensile stress in bending

σ_y - yield stress of reinforcements

ϕ - diameter

Ψ - non-dimensional radius

SYNOPSIS

THE BEHAVIOUR OF FERROCEMENT SLABS UNDER DIFFERENT LOADS

(A thesis submitted in partial fulfilment of the requirement for the degree of Doctor of Philosophy by Murlidhar Raisinghani to the Department of Civil Engineering, Indian Institute of Technology, Kanpur in 1976)

In quest for a new building material, at present time, ferrocement is the subject of vigorous research and development activity. Since Nervi, the acknowledged pioneer of ferrocement material, several research workers around the world have carried out both experimental as well as theoretical studies to understand the behaviour and mechanical properties of ferrocement. But most of the works reported in the literature are on the behaviour of ferrocement slab elements under direct tension, direct compression, flexure and torsion, which are in no way sufficient to characterise the mechanical and engineering properties of the material.

The present study is primarily aimed at investigating experimentally and analytically,

i) the behaviour of ferrocement slabs under sustained static loads,

ii) the behaviour of ferrocement slabs under repeated loads,

iii) the fatigue characteristics of ferrocement slabs,

iv) the yield criterion and the plastic analysis of ferrocement slabs and

v) the response of ferrocement cylindrical tank and slabs to blast loading.

In a composite material the visco-elastic deformations depend not only on the properties of the individual constituents but also on the way in which

they combine and interact. Since time-dependent deflection of structures is an important factor in design, ferrocement slabs were tested under various sustained loads for a period upto ninety days. Based on the observations, the time-deflection curves are plotted and a model to estimate the time-dependent flexural deflection is suggested.

Structures, floating as well as non floating, may be subjected to repeated stresses from waves, machinery, wind etc. In order to understand the behaviour of ferrocement under repeated stresses, several slabs were tested under pulsating loads of constant magnitude. The observed fatigue creep deflections have been plotted against cycles of load. The effect of repeated loads on the flexural rigidity of slabs has been discussed and the load-deflection hysteresis loops have been plotted. Based on the limited experimental data on fatigue failure, the S-N curveshave been presented.

The ferrocement may easily be treated as a homogeneous material and its behaviour under flexural loads has been observed to be very ductile. Since its behaviour is quite different from ordinary reinforced concrete material, the yield criterion for the slabs of ferrocement is expected to be different. Based on the observations and experimental data of twenty slabs tested under biaxial end moments, sixteen slabs tested under centre point loads and a circular slab tested under central punch load through a boss, a yield criterion for the slabs has been suggested.

CHAPTER I

INTRODUCTION

1.1 General

Ferrocement is a highly versatile form of reinforced mortar made of wire mesh, mild steel rods, sand, cement and water which possesses unique qualities of strength and serviceability. Ferrocement was developed by Nervi (1)* who based his thinking on the observation that elasticity of a reinforced concrete member increased in proportion to the subdivision and distribution of reinforcement in the mass. After considerable practical and laboratory experimentation, it became clear that several layers of mesh reinforcement in combination with steel rods embedded in a rich mortar, produced a very strong resilient material. It is essentially a form of reinforced concrete although it exhibits a structural behaviour different from conventional reinforced concrete in performance and strength. It can be fabricated into almost any shape to meet the needs of the user. The skills for ferrocement construction are quickly acquired and include many skills traditional in India and other developing countries. Ferrocement construction is labour intensive and a side benefit of its development is the creation of much needed jobs for unskilled labour in those countries.

Proven suitable for boat building, it has many other potential applications in agriculture, industry and housing. Ferrocement suits well to those structures that owe their strength to form such as thin shells and corrugated surfaces. Other applications of ferrocement are for under water

---

* Indicates reference number.

structures and container vessels to store liquid natural gases and explosives. To a certain extent grain storage silos (2), water tanks (3) and roofs have been constructed using ferrocement. Other applications like irrigation canal lining and culverts are being investigated. Ferrocement has been used in the lining of shafts and tunnels in Eastern Europe. Precast elements of ferrocement have been used as water proofing and decorative covers. More potential applications of ferrocement for developing countries are summarised in the National Academy of Science Report (3). Ferrocement is especially suitable for hanging roofs because of its higher extensibility.

There is a saving in the basic materials, viz. steel and cement, since it is possible to cast very thin sections with ferrocement. This is especially advantageous in spatial structures, as they can be built very slender, thereby, making the best use of their efficient form. Because of its dead weight, the handling and the erection of ferrocement elements is easier, thus making it suitable for prefabrication. Considerable advance has been made in the Soviet Union (4, 5) on the application of prefabrication techniques to ferrocement structures. Techniques such as Vibrobending and Vibropressing have been developed. Vibrobending is the technique of bending ferrocement plate to the required shape when mortar is fresh. In Vibropressing method, casting, vibrating and pressing are performed simultaneously.

1.2 Concept of Ferrocement

In the light of fracture mechanics for brittle materials as proposed by Griffith (6) and with experimental evidence it is now concluded that the low tensile strength of concrete is due to the naturally occuring internal flaws and microcracks present in the concrete. The unstable crack propagation in the presence of tensile loads for materials with small internal flaws or microcracks is the main reason why tensile strength of such materials is much less than their compressive strength. To explain this phenamenon Griffiths hypothesis states that the crack will begin to propagate unstably if the rate of elastic energy release is equal to or greater than the energy required in extending the crack. It is obvious from the relation derived by Griffith that the resistance of material with a particular specific surface energy can be increased by keeping the applied stress level low, reducing the flaw length and/or increasing the modulus of elasticity. Reducing the applied stress defeats the purpose of using the material efficiently. In ferrocement, the closely spaced wire mesh, well dispersed in the matrix not only decreases the flaw length but also increases the value of modulus of elasticity.

The use of small diameter wire mesh helps in reducing the stress concentration at the flaw tip. Romualdi and Mandel (7) postulated that a crack traversing through a material is arrested by the pinching action of shear bond between the wire and the mortar. This action reduces the strain energy release in the propagation of crack. The crack arresting action of

the wire mesh continues even after the crack has crossed the wire. If ultimate shear bond is exceeded, irrecoverable work is done in stripping off the wire out of mortar. Otherwise the ductile failure of the wire occurs.

1.3 Law of Mixture

In a composite material like ferrocement consisting of a matrix reinforced with uniformly dispersed continuous fibres, it is assumed that the fibres are firmly bonded so that when stressed no slippage occurs at the interface of the fibres and the matrix. The modulus of elasticity and the other relevant properties of the composite can be determined from the relation commonly known in literature as 'law of mixture' (8).

1.4 Specific Surface and Volume Fraction

The crack arrest mechanism is considerably influenced by the specific surface and the mechanical properties of the wire mesh. The specific surface or the degree of dispersity of ferrocement can be expressed as the surface area of fibres in contact with the matrix per unit volume of the composite. The ultimate load carrying capacity increases with the increase of the volume fraction of the reinforcement which is defined as the volume of steel (fibre and skeletal steel) per unit volume of the composite. It should be noted that the contribution of the skeletal steel in the crack arrest mechanism is insignificant, as verified by the experimental results(9).

This is due to the fact that, unlike the wire mesh, it is not dispersed sufficiently in the matrix; however, its contribution in load carrying capacity is quite appreciable.

1.5 Objectives of Study

Several research workers have carried out extensive experimental investigations and analytical studies to understand the mechanical properties and behaviour of ferrocement under direct tension, direct compression, torsion, flexure, impact etc. The trilinear load-deformation behaviour as exhibited by ferrocement slabs under transverse loads has also been studied by several authors. A critical literature review of the same has been presented in Chapter II. A cursory glance on the available literature, however, reveals that the research has been concentrated mainly on the forementioned characteristics of ferrocement.

Floating as well as non-floating structures may be subjected to repeated stresses due to wind, earthquake, waves and machines. A ferrocement boat in water is subjected to repeated stresses due to hydrodynamic effect of waves and/or machines fitted inside it. But it appears that hardly any work has been done on the fatigue creep and fatigue life of the material. Due to viscoelastic nature of the material, the deflection of ferrocement members increases with time under sustained loading. Furthermore, the increase in deflection leads to the formation of additional cracks. Hence, a knowledge of creep is of considerable importance in structural

mechanics and design. Ferrocement containers are also being used to store explosives. To evaluate and characterise ferrocement as a structural material, it is essential that the behaviour of material under different type of stresses is well established through experimental and analytical studies. Perhaps no attempt has been made so far to establish a generally acceptable yield criterion to determine the load carrying capacity of ferrocement slabs subjected to biaxial stresses.

1.6 Scope of Study

The present study is primarily aimed at investigating experimentally and analytically

i) the behaviour of ferrocement slabs under sustained static loads,

ii) the behaviour of ferrocement slabs under repeated stresses,

iii) the yield criterion and the plastic analysis of ferrocement slabs and

iv) the response of ferrocement slabs and a cylindrical tank to blast loading.

The flexural creep characteristics of ferrocement have been studied with particular reference to twenty rectangular slabs subjected to sustained central line load for a period upto ninety days. The tests for fatigue life and fatigue creep of ferrocement slabs have been carried out on thirty six similar slabs as for creep and under the central line loading only. Sixteen rectangular slabs under central line loads, twenty square slabs

under uniaxial and biaxial end moments and a circular slab subjected to a central punch load applied through the boss have been tested to determine the yield criterion and the collapse loads. The experimental observations have been compared with the theoretical predictions. The tests for blast loading were carried out on a ferrocement cylindrical tank and the slabs for which only a qualitative discussion has been presented.

CHAPTER II

SELECTIVE LITERATURE REVIEW

2.1 General

Nervi (1) obtained the mechanical properties of ferrocement from a series of tests and utilized these results in the design of several shell roofs which even today remain models of aesthetics in structural design. Since Nervi's demonstration of sea-worthiness of his ferrocement motor sailor, several investigators have studied engineering properties of ferrocement. Although microcracks are inherent in ferrocement even at no load, it can be designed to be watertight under service loads. For all intents and purposes, ferrocement is completely fire resistant and its conductivity is one sixth of that of steel. The material offers resistance to impact, shock and explosive loading. Romualdi and Batson (10), Aveston and Kelly (11) and Shah and Rangan (12) studied the crack arrest mechanism of brittle material reinforced with closely spaced wires and presented various theories.

2.2 Tension

Naaman and Shah (13) investigated the properties of ferrocement in direct tension by varying the type, size and volume of the wire mesh. It was observed that the ultimate strength of ferrocement in axial tension is the same as that of wire mesh alone and its modulus of elasticity can be predicted from those of mortar and wire mesh by law of mixture (8). It was

also observed that the specific surface of reinforcement strongly influences the cracking behaviour of reinforcement. An analytical expression for the crack spacing and specific surface of reinforcement was presented. Lee, Raisinghani and Pama (9) and Walkus (14) also concluded from the tests that the tensile stress at first crack and number of cracks at ultimate failure increased upto an optimum value with increasing specific surface. All the authors are of the view that the composition and strength of mortar do not appreciably influence the tensile strength of composite.

2.3 Compression

Studies by Bezukladov, Amel Yanovich, Verbitakiy and Bogoyavlensky (15), Rao and Gowdar (16), Lee, Raisinghani and Pama (9) and Kelly and Mouat (17) show that compressive strength of ferrocement depends primarily on that of cement mortar and is independent of specific surface or volume fraction. In axial compression the local buckling of the wire mesh causes mortar to split longitudinally, hence the ultimate compressive strength is less than that of mortar. Close tying of wire mesh may partly prevent this action. In the uncracked range the law of mixture was shown to predict well the modulus of elasticity of composite. In the mathematical derivation for the ultimate strength of composite, contribution of wire mesh and skeletal steel is neglected.

2.4 Flexure

Experiments performed by Lee, Raisinghani and Pama (9), Claman (18) and Bezukladov, Amel Yanovich, Verbitakiy and Bogoyavlensky (15) indicated

that the load-deformation curve for ferrocement plates under transverse loads can be approximated to a trilinear behaviour without much loss of accuracy. The response is elastic till cracks develop on the tensile face. The elastic range is followed by strain hardening range. Increasing number of cracks are seen with increasing stress. The cracks are very fine in this stage (crack width of 0.005 to 0.5 mm) and increasing mortar strains are due to increasing number of cracks rather than increasing width of cracks. This range terminates at a point where the deflection starts to increase significantly without an appreciable increase in load. The increase in deflection is mainly due to increasing width of cracks. Russians and others have analysed the post cracking strength of ferrocement slabs in bending by considering ferrocement as layered plate. The method of analysis has been presented in Appendix A.

Walkus (14) suggested that it is desirable to differentiate each stage according to performance of a structure e.g., water tightness, corrosion resistance etc. Based on his experimental research, Walkus (19), presented a theory of bending of ferrocement. Three states of serviceability for ferrocement structures have been distinguished and defined by the permissible width of microcracks. Using the more precise definition of cracking moment and the hitherto known knowledge of ferrocement behaviour in axial tension, the numerical correlation of stresses and strains and crackwidth have been determined. For watertightness permissible crackwidth is 20 microns and for corrosion 50-100 microns depending upon the environment.

Based on experimental investigations, Oberti (20), reported that for steel upto 200 kg/M^3, the extensibility of ferrocement was of the same order as for unreinforced mortar. When steel content was increased to 100-500 kg/M^3, the extensibility increased by about 5 times.

Cracking behaviour and moment capacity of ferrocement in flexure have been studied by Bezukladov, Amel Yanovich, Verbitakiy and Bogoyavlensky (15), Desayi and Jacob (21), Muhlert (22), Lee, Raisinghani and Pama (9), Rajgopalan and Parmeswaran (23) and Logan and Shah (24). It was observed that the flexural tensile stress at first crack increases with increasing specific surface. Specific surface in this case is defined as the total longitudinal surface area of reinforcement per unit volume of the mortar in tension. The flexural strength was shown to be accurately predicted by ultimate strength theory developed for conventional reinforced concrete. Rajagopalan and Parmeswaran (23) suggested a method to compute the cracking moment of ferrocement based on the assumption of a linear strain-space relationship and a nonlinear stress-space relationship in tension zone taking into account the plastification of mortar in that region. A methodology to predict the ultimate strength based on the assumed mechanism of failure was also given. Austriaco (25) derived moment-curvature relations of a ferrocement section on the assumption that wire mesh yields as soon as it is impinged by a crack. These moment-curvature relations led to an idealized trilinear moment-curvature curve which was used in the analytical studies and verified experimentally. The comparison of the theoretical results and experimentally obtained values were shown to be satisfactory. The

experimental results indicated that the composite load-deflection curve constructed by joining the two segments obtained by the trilinear and bi-linear analysis gave a good approximation of load-deformation behaviour of the circular ferrocement slabs.

In tensile state of stress, Pama, Sutharatanachaiyaporn and Lee (26) found out that in the cracked range mortar contributes to the modulus of elasticity of the composite section depending upon the volume fraction of wire mesh. It is also reported that modulus of shear rigidity and Poisson's ratio increase with increasing volume fraction of wire mesh and these mechanical properties can be calculated from the law of mixtures. Bezukladov, Amel Yanovich, Verbitakiy, Bogoyavlensky (15) reported on the basis of experimental results that Poisson's ratio decreases with increasing volume fraction contradictory to the findings of Pama, Sutharatanachaiyaporn, and Lee (26).

2.5 Impact

The resistance of ferrocement to moderate impact is one of its assets in marine use. Its behaviour is unique, for, the fabric remains largely intact after a part of energy due to blow has been observed. Apart from Nervi's (1) initial tests, Kelly and Mouat (17), Sintzow, Libow and Antipow (27), Lessard (30), Shah and Key (28), Chang, Gibson and Gibbons (29) and Bezukladov, Amel Yanovich, Verbitakiy and Bogoyavlensky (15) have carried out impact tests on ferrocement panels. It is reported that the effect of impact loads on ferrocement is localised and failure is characterised by a

widely dispersed area of shattered mortar and even under such conditions the material remained fairly impervious. Instead of measuring the width of cracks due to variable total potential energy of blows, Shah and Key (28), measured the effect of constant potential energy interms of flow of water (leakage rate) at a constant water head. This method of evaluating the impact resistance of ferrocement appears to be more rational. It was concluded that the higher the specific surface of reinforcement or the higher the yield strength of ferrocement the lesser the damage (that is leakage rate) due to impact loading.

2.6 Permeability

Tests for permeability and punching strength of ferrocement were reported by Lachance and Fugere (31). These tests showed that ferrocement was perfectly waterproof but permeable to oil, necessitating special coating for oil tankers. Punching strength of ferrocement was found to be four times that of fir ply wood of the same thickness.

2.7 Creep

Experimental studies on the flexural creep of ferrocement slabs under sustained loads were carried out by Bezukladov, Amel Yanovich, Verbitakiy and Bogoyavlensky (15). It was reported that the increase in deflection during initial period of application of load and with increasing time, the rate decreased. The slabs were subjected to flexural stress of 50 kg/cm^2.

Later on, hardly any work has been published on the time-dependent deflection of ferrocement slabs under static loads.

2.8 Fatigue

Although very little information is available on fatigue strength of ferrocement, fatigue may be critical property of ferrocement ship hulls. It is known that for reinforced and prestressed concrete structures, the fatigue resistance of the reinforcement is often the controlling property for the fatigue characteristics of the composite structures. Greenius (32) reported from the experimental tests that for imposed repeated loads of constant magnitude ferrocement slabs under flexure could withstand 2×10^5 cycles of load at an apparent fibre stress of 123 kg/cm^2 and under constant deflection condition it could withstand many thousand load cycles at an upper fibre stress of about 70 kg/cm^2. The endurance limit at 10^6 or 10^7 cycles has not yet been established.

2.9 Shear

The behaviour of ferrocement in pure planar shear had been studied by Bezukladov, Amel Yanovich, Verbitakiy and Bogoyavlensky (15). The stress-strain relation was observed to be bilinear giving rise to two different shear moduli each corresponding to one stage of loading. Initial shear modulus linearly varied with specific surface of wire reinforcement oriented in the direction of the tensile diagonal of plate. The shear modulus in the second phase was the same for all values of specific surface.

Further information on ferrocement was presented by Suryakumar, Narayanaswamy and Sharma (33), Walkus and Kowalski (34) etc.

2.10 Plasticity and Yield Criteria

Since one of the objectives of the present work is to develop a yield criterion for ferrocement slabs under general state of stress, a brief review of the literature on plasticity is presented here.

A detailed discription of historical developments in the theory of plasticity can be found in various survey papers and books (35,36,37 and 38). Tresca (39,40) is considered to be one of the pioneers in the field of plasticity for introducing a piecewise linear yield criterion for ductile materials. Von Mises (41,42) introduced the nonlinear yield criterion bearing his name and advanced the hypothesis that the strain rate vector is normal to the yield surface. Subsequently Drucker (43,44) gave a mathematical proof to the previously hypothesized normality of the strain rate vector and further showed that yield surface is convex.

Prager (45) and Melan (46) carried out general studies in plasticity, some of which can be applied to reinforced concrete slabs, especially the derivation to determine whether an upper bound solution is an exact solution or not. Nielsen (47) followed to a certain extent the same line as Prager and found both the upper and lower bound solutions. Where the two solutions coincide, the result is exact.

Koiter (48) introduced that the plastic strain rate vector at corners is a linear combination of the strain rate vectors from all loading surfaces

forming corners and falling within the fan of normals to the contributing surfaces.

Prager (49) introduced the kinematic strain hardening model which treats the initial yield surface as a rigid body and is free to translate but maintain its size and orientation. Prior to this, theories of strain hardening solids assumed a mechanism for contributing plastic flow based on a linear isotropic hardening theory. Hodge (50) presented a general theory which includes isotropic and kinematic hardening as a special case. Hodge (51,52,53) has solved various plate problems using the theory of linear isotropic strain hardening.

In the present study, works of Nielsen (54), Baus and Tolaccia (55) and Kwiecinski (56) on the yield criterion of reinforced concrete are of particular interest in addition to work of Austriaco (25).

Nielsen (54) tested reinforced concrete plates subjected to pure torsion. For isotropic reinforcement the loading condition would correspond to corners of square yield criterion in quadrants 2 and 4. Two forces, one upward and one downward were applied through steel channels welded to reinforcement along plate edges to transmit torsional moment. A close correlation was obtained between measured and calculated values which supported Johansen's (57) findings.

The first systematic experimental research to determine yield criterion of reinforced concrete plates under uniaxial and biaxial moments was carried out by Baus and Tolaccia (55). The shape of the yield criterion found out

from experimental research was different from that of square yield criterion. The investigators observed increase of moment capacity in going from uniaxial to biaxial bending and advanced several reasons in support of their findings. For biaxial moment of the same sign, the concrete on the compression side was subjected to biaxial compression, which caused an effect analogous to that of precompression of the specimen. This effect is most important when the compressive stress and Poisson's ratio of concrete are quite high. Kwiecinski's (56) main objective of study was kinking of reinforcement. From the interpretation of the test results, it was concluded that the maximum enhancement of moment capacity attributed to kinking was 18.8 percent which was in reasonable agreement with corresponding magnitude of 16 percent as reported by Wood (58). Lenschow and Sozen (59) carried out an exhaustive experimental and analytical work to develop a yield criterion for reinforced concrete plates under general state of stress. They have shown that there is no increase in the yield moment as a result of biaxial stress and the kinking of a bar across a yield line is so small that the increase in moment capacity is negligible.

Based on recent work of McLaughlin (60), Austriaco (25) has presented trilinear analysis of ferrocement rectangular plates under cylindrical bending and circular slabs under a central punch load. McLaughlin reported that in case where the current, and subsequent yield surfaces become tangent to or coincide with the limit surface over a finite segment, the limit surface is convex and the strain rate vector is normal to it within this segment. It is also proved that the theorems of limit analysis (61) are equally valid

for strain hardening materials with unique limit surface. Austriaco (25) showed that in ferrocement circular plates, under central punch load, non-regular progression of stress points occurs at certain stage of loading. This was treated by Thorn, Kao and Lee (62), in the analysis of long circular cylindrical shells under uniform internal pressure in which integration of flow laws led to a point function which was obtained by successive iteration.

From the foregoing selective literature survey it appears that not enough work has been done in the area of creep, fatigue and yield criterion of ferrocement slabs. Hence, the present study encompasses these important aspects.

CHAPTER III

THE EXPERIMENTAL PROGRAMME

3.1 General

The experimental part of investigation consisted of testing 72 slabs of size 300 x 600* under static flexural loads, sustained static loads and pulsating loads and 20 slabs of size 600 x 600 under biaxial end moments. In addition to these, one circular slabs of size 1575 with a central rigid core of diameter 300 and one cylindrical tank of size 1525 x 1525 were also tested. The slabs for biaxial end moments had overhangs of 240 x 600 which were heavily reinforced for applying the moments. To provide holes in these overhangs at 40 from the edges and 300 centre to centre (hereafter c/c), 16 ø steel pipes cut to the size of the thickness of the slabs were kept in position. The Figures 3.1 and 3.2 show the details of size and shape of the test specimens. The variables in all the specimens cast were, the number of layers of wire mesh, the gauge size of the wire mesh and the thickness of the slabs. The skeletal reinforcement for all these specimens except the circular slab and the cylindrical tank consisted of 6.6 ø bars at 150 c/c in two orthogonal directions. The skeletal reinforcement for cylindrical tank was at 100 c/c and for circular slab it was at 75 c/c in two orthogonal directions. The central rigid core of circular slab consisted of 6 ø bars in double U shape at 75 c/c with circular rings of the same diameter at 50 c/c.

The pertinent details of the test specimens are shown in Table 3.1. The letters S,C,F,UM,BM,CT and CS in the tables denote respectively, the static, creep, fatigue, uniaxial moment, biaxial moment, cylindrical tank

---

*all dimensions are in mm unless otherwise mentioned.

and circular slab. The numbers preceeding and following these letters denote respectively the total number of layers of wire mesh and number of the specimen. The circular slab was cast and tested by the author at Asian Institute of Technology, Bangkok, the pertinent details of the same are given in Table 3.1.

3.2 Material Preparation and Test Specimens

Skeletal grids of 6.6 ø steel bars spaced at 150 c/c each way were formed to conform with the desired dimensions of the samples. Two to four layers of galvanised hexagonal wire mesh, gauge # 19 or # 22 (wire diameter 0.9 and 0.6 respectively), were tied on both sides of the grid. To obtain a homogeneous composite mat and to avoid the effect of weaving of the wire mesh, the layers were arranged in alternate directions. In specimens with gauge # 22 wire mesh, small strips of the wire mesh were used as spacers. In larger slabs and tanks, the different layers of wire mesh were provided with an overlap of 100 to get a stronger joint. Care was also taken to stagger all such joints throughout the specimen. A typical cross-section of ferrocement slab is shown in Figure 3.3.

The mortar used for all these specimens had a cement-sand ratio of 1:1.75 with a water-cement ratio of 0.37 by weight. Ordinary portland cement conforming to IS269 and natural fine river sand from Kalpi passing IS sieve 240 were used throughout this investigation. In circular slab Plastet II (7 ml/kg of cement) was used as an admixture to control the quality of mix. The water-cement ratio in mortar for circular slab was 0.35 by weight.

Normally, no form work is required in applying the mortar on the wire mesh but, to get the exact dimensions and true surfaces, plywood moulds with thin tin sheets nailed to them were used in casting the samples. The cylindrical tank was cast without any mould. Wet mixing of the mortar was done in 0.05 cubic meter capacity laboratory mixer. The moulds were oiled and reinforcement placed in position properly. The Figure 3.4 shows the reinforcement for a biaxial moment specimen placed in position in the mould. The mortar was manually pressed inside the mesh. The moulds were then vibrated on the table vibrator to obtain uniform compaction. Six to eight standard cubes of 50 cm^2 face area were also cast from each batch of mix. The smaller specimens (300 x 600) were removed from the mould after 24 hours and larger ones after 48 hours and were cured in a water tank for 28 days. The cylindrical tank and the circular slab were cured with wet gunny bags and the control cylinders and cubes cast along with these were also cured under similar conditions. All samples were properly white washed, to obtain a clear picture of cracks, before subjecting them to test.

The electrical resistance strain gauges SR-4, gauge length 20 were fixed to the circular slab at strategic points as shown in Figure 3.2. The cylindrical tank was fixed with Rohit (India) strain gauges (gauge length 20). For all the specimens under test, deflection measurements at various critical points of interest were taken by means of deflection gauges with 0.01 accuracy.

3.3 Control Specimens

The mechanical properties of the wire mesh and skeletal steel were determined from the standard tension tests performed on the Instron Testing

Machine with an automatic plotter. Typical load-deformation curves for the skeletal steel, #19 and #22 wire mesh are shown in Figure 3.5. The curves shown are the average of three specimens tested for each case. Fifty percent of the cubes, cast from each batch of mix, were tested for their compressive strength after 28 days and remaining fifty percent on the day the specimens were put to test. The rupture strength of mortar was determined from 7 days and 28 days beam tests (150 x 150 x 750) under two point loads. The relevant mechanical properties of the control specimens are given in Table 3.2. The Table 3.3 shows the mechanical properties of the control specimens for circular slab.

3.4 The Test Setups

3.4.1 Creep Setup (Figure 3.6)

Six steady and compact setups were fabricated in the laboratory to perform flexure creep tests on slabs. These setups consisted of two plane rectangular frames made from rolled channel sections welded together. These frames were interconnected by a heavier channel section to give a clear span of 400. To make the setup more stable, the four legs of the setup were firmly embedded inside the concrete pedestals. The heavier channel section supported the lever arrangement (1:11). A dead load system was used for loading the slabs. The slabs tested under flexure creep were clamped at two ends and free at the other two. The slabs were subjected to a central line load. To avoid eccentricity in loading, the load was applied through a steel ball. The setups were also provided with an arrangement to fix up

dial gauge for measuring the central deflection to an accuracy of 0.01. Prior to clamping the ends, the slabs were properly levelled and centred. Plaster of paris and coir mats were used for transferring uniform pressure at the ends which also helped in avoiding cracking of slabs due to tightening of bolts. All the tests were performed at room temperature. To account for shrinkage, temperature and humidity etc., one of the slabs under test was kept free from load and the changes in the dial gauge reading with time noted.

3.4.2 Fatigue and Static Test Setup (Figure 3.7)

Both, the fatigue and the static tests were performed on the same setup. The setup consisted of two rigid abutments fixed firmly to the structural reaction floor by means of 50 ϕ studs. The abutments had c/c span of 500 and a clear span of 385 to receive the slab vertically. The slab specimens were clamped to the abutment, as shown in Figure 3.7 by means of 10 ϕ bolts and rigid rolled steel channels. It was observed during the first two tests that two 10 ϕ bolts on each end were not sufficient to create perfect clamped ends under pulsating loads, hence a modification was carried out to clamp the slabs firmly. This was achieved by tightening the slab between two flanges of the channels by means of two 12 ϕ U hooks at each end of the slab in addition to two 10 ϕ bolts.

A laboratory fabricated (lab-fab) pulsating jack, capacity 4000 kg, was fixed to the reaction girder bolted to two rigid abutments which were firmly fixed to the structural floor. The Figure 3.8 shows that the test

setup. This setup had two advantages. Firstly, a clear view of the tension side to observe the crack propagation was available and secondly the effect of self weight of the slab was avoided. The slabs were tested under a central line load. To avoid eccentricity in loading, the load from jack to slab was transferred through a lab-fab ball and socket arrangement.

The jack was connected to SC-10 Reihle Fatigue Testing Machine, which is single acting and can be used for fluctuating loads only. It consists of a combined pulsator and console unit. The machine has ten output hydraulic channels which can be connected to universal test cylinders of various capacities. The action of the pulsator is to increase the volume of the system on its down stroke and to decrease in the upward cycle. The frequency of load oscillation is controlled by a potentiometer. The operating frequency is indicated by a tachometer on the console which is electrically connected to a generator on pulsator drive. The pulsator drive transmits a pulse for each ten cycles of operation to electric cycle counter mounted on the console. The pulsator is provided with a self lubricating system which supplies pressure to release a self setting band type brake applied on the flywheel. This brake brings pulsator to stop quickly after the failure of the test specimen and causes machine to shut it self down.

The test specimens fixed to the setup were subjected to monotonically increasing loads in small increments and central deflection recorded through a deflection gauge with 0.01 accuracy. Deflection measurements were also taken at the clamped ends of the slab to check the rigidity of supports.

3.4.3 Biaxial End Moment Setup (Figure 3.9)

A special loading and supporting system was constructed for testing slab specimens under uniaxial and biaxial end moments. The main object was to eliminate undue influence from the load and the support during the stage at which test specimens would have significant deformations. In other words, the object was to maintain full control over the boundary conditions at all stages of loading. In addition to the advantages mentioned above a clear view of the tension side of the test specimen was available and hence, the development and propagation of cracks under loads could be observed conveniently.

The setup consisted of a square welded frame of size 600 x 600 made from rolled I-sections. 600 long pipe segments were welded to the top flanges of frame to receive a number of 30 ø smooth roller bearings in 140 lengths. The roller bearings were greased to reduce the frictional effects. This frame was bolted to two rolled I-sections resting on four rigid concrete column supports of 250 x 250 x 750. The slab specimens were properly centred over the square welded frame so that the test area* rested on the roller bearings. Through the holes in the loading areas on each side of the specimen, two 12 ø rods with hinges to permit rotation were connected to the angle iron box girders which in turn were connected through 16 ø rods, studded at both ends, to rigid box girders underneath the structural floor. The girders supported Simplex remote control hydraulic jacks of 10-30 ton capacity. The jacks were connected to the Reihle (280 kg/cm^2 pressure capacity, eight dials and four channel output) load measuring equipment. The slabs were

*TA and LA shown in Figure 3.1 are referred to as test areas and loading areas respectively for clarity.

tested under monotonically increasing loads and deflection readings noted for each increment to an accuracy of 0.01. The deflection gauges were fixed at strategic points on the specimen and also underneath the rigid supporting system. Figure 3.10 shows a test specimen under test.

3.4.4 Circular Slab Setup

A simply supported edge condition was achieved by resting the circular slab on a circular ring of mild steel 20 ϕ rod welded to a narrow annular steel plate. The narrow annular steel plate rested on the rigid support made from rolled steel channels. The slab specimen properly centred over the support was subjected to a central punch load through boss by means of a hydraulic jack and load was measured by 5 ton proving ring. The loaded specimen is shown in Figure 3.11. The deflections at the fifth points along the diameter of the slab were measured by dial gauges and the strain gauges readings taken by strain meter for every increment of load.

The detailed testing procedures, analysis of test results and discussions are presented in the chapters that follow.

Series*	Average Thickness mm	Gauge of Wire #	Volume Fraction		Total Volume Fraction of Reinforcement	Specific Surface of Reinforcement, cm^2/cm^3		Total Specific Surface cm^2/cm^3
			Skeletal Steel	Wire Mesh		Skeletal Steel	Wire Mesh	
4C, 4F, 4S	25.0	19	0.0460	0.0364	0.0824	0.2774	1.61	1.8874
6C, 6F	25.0	19	0.0460	0.0546	0.1006	0.2774	2.42	2.6974
8C, 8F	25.0	19	0.0460	0.0728	0.1188	0.2774	3.23	3.5074
6C, 6F, 6S, 6UM, 6BM	28.0	19	0.0408	0.0485	0.0893	0.246	2.15	2.396
8C, 8F, 8S, 8UM, 8BM	30.0	19	0.0383	0.0606	0.0989	0.231	2.7	2.931
4C, 4F, 4S, 4UM, 4BM	25.0	22	0.0460	0.0161	0.0521	0.2774	1.07	1.3474
6C, 6F, 6S	28.0	22	0.0408	0.0215	0.0623	0.246	1.42	1.666
8C, 8F, 8S	30.0	22	0.0383	0.0248	0.0631	0.231	1.782	2.013
6CT	25.0	19	0.068	0.0546	0.01126	0.408	2.42	2.828
8CS	28.0	19	0.046	0.046	0.092	0.456	2.70	3.156

* number of samples tested in each series are given in respective chapters.

Table 3.2 - Properties of Control Specimens (Mean Values)

Cube crushing strength of mortar	350 kg/cm^2
Initial tangent modulus of mortar	240×10^4 kg/cm^2
Rupture strength of mortar (beam test)	35.6 kg/cm^2
Yield strength of 6.6 ø bar	2612 kg/cm^2
Yield strength of // 19 gauge wire	2830 kg/cm^2
Yield strength of // 22 gauge wire	3538 kg/cm^2
Ultimate strength of 6.6 ø bar	3600 kg/cm^2
Ultimate strength of // 19 gauge wire	5268 kg/cm^2
Ultimate strength of // 22 gauge wire	5484 kg/cm^2
Modulus of elasticity of 6.6 ø bar	2×10^6 kg/cm^2
Modulus of elasticity of // 19 gauge wire	0.8×10^6 kg/cm^2
Modulus of elasticity of // 22 gauge wire	0.8×10^6 kg/cm^2

Table 3.3 - Properties of Control Specimens for Circular Slab (Mean Values)

Cylinder crushing strength of mortar	575 kg/cm^2
Poisson's ratio of mortar	0.185
Initial tangential modulus of mortar	30.9×10^4 kg/cm^2
Tangent modulus of mortar at 50% strength	23.56×10^4 kg/cm^2
Tensile strength of mortar (Brazilian test)	34.17 kg/cm^2
Yield strength of wire	2180.18 kg/cm^2
Ultimate strength of wire	3755.53 kg/cm^2
Modulus of elasticity of wire	96.70×10^4 kg/cm^2
Yield strength of 6 Ø bar	2756.87 kg/cm^2
Ultimate strength of 6 Ø bar	4008.72 kg/cm^2
Modulus of elasticity of 6 Ø bar	210.98×10^4 kg/cm^2

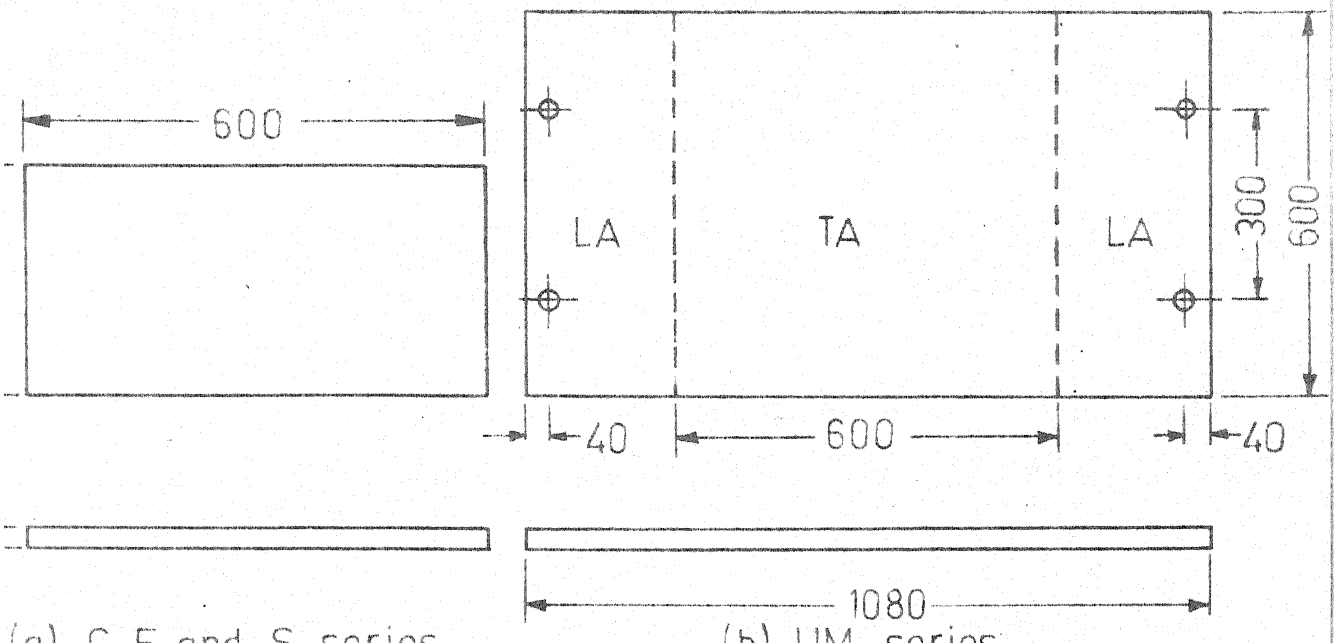

(a) C, F and S series. (b) UM series.

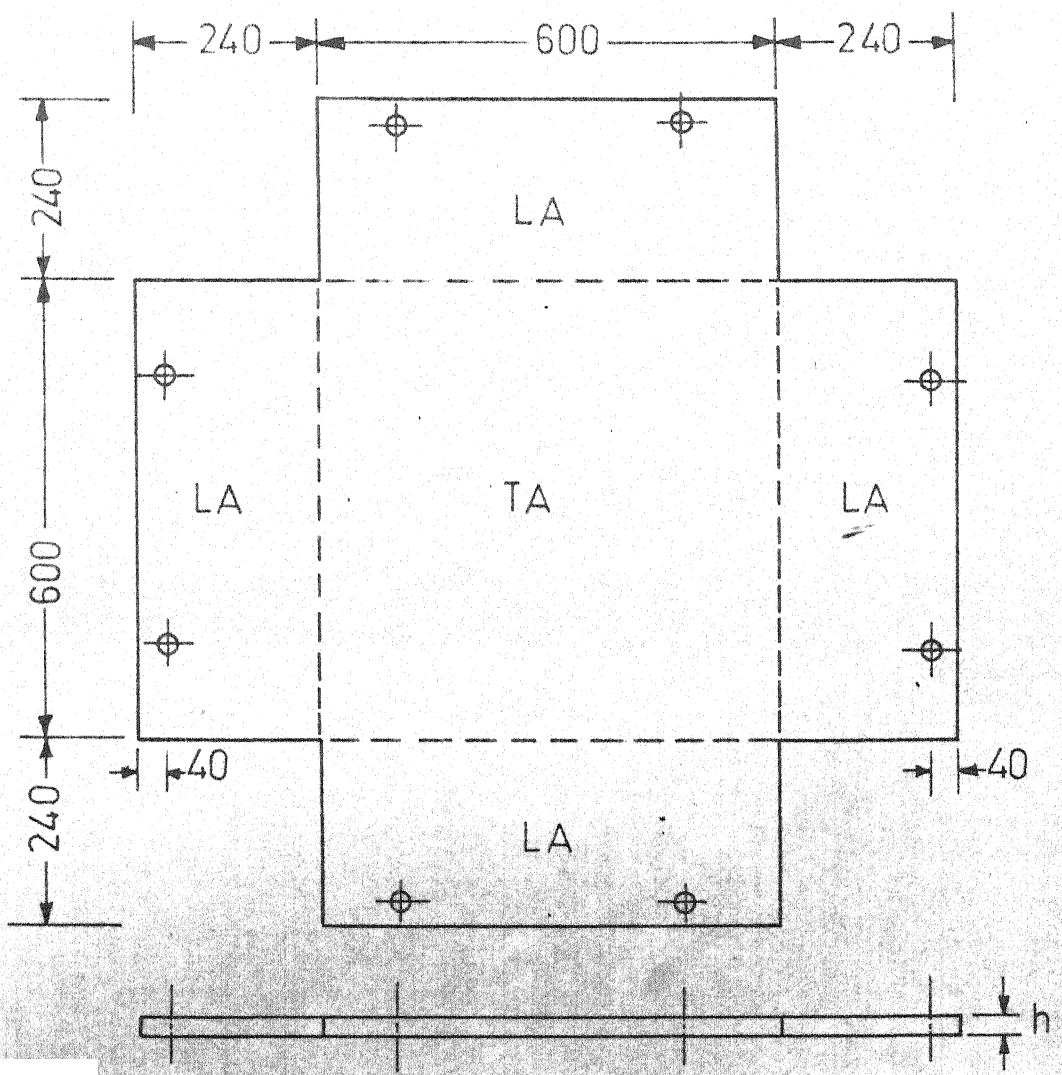

(c) BM series.

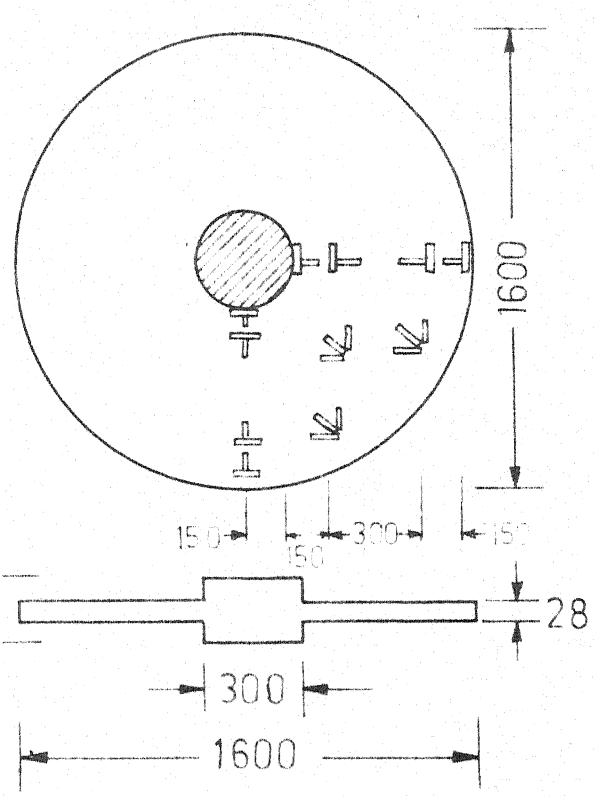

(a) Circular Slab with Rigid Core.

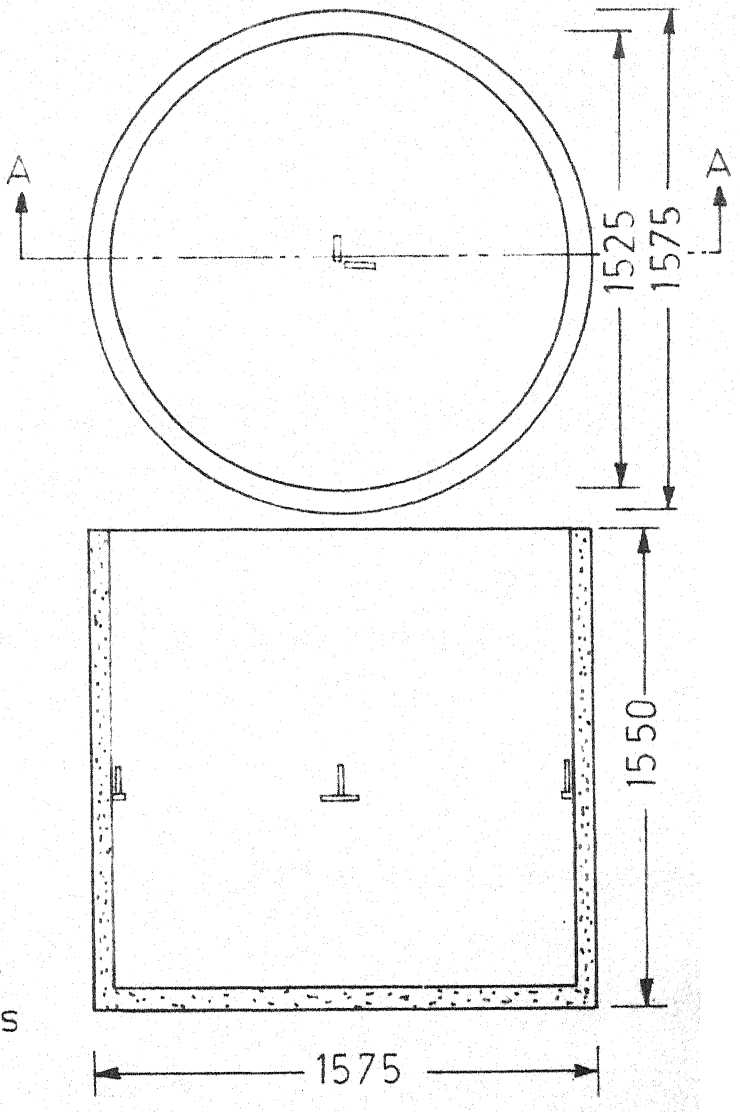

(b) Cylindrical Tank. (section at A-A)

ERS gauges

Figure 3.2 - Size and Shape of Specimens.

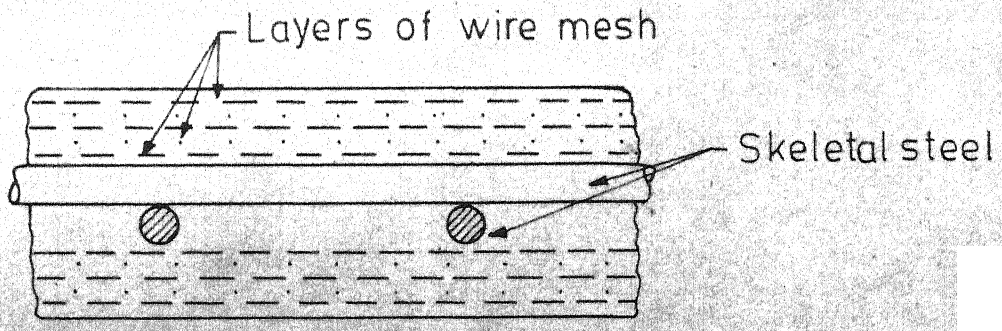

Figure 3.3 - A Typical Ferrocement Slab Element.

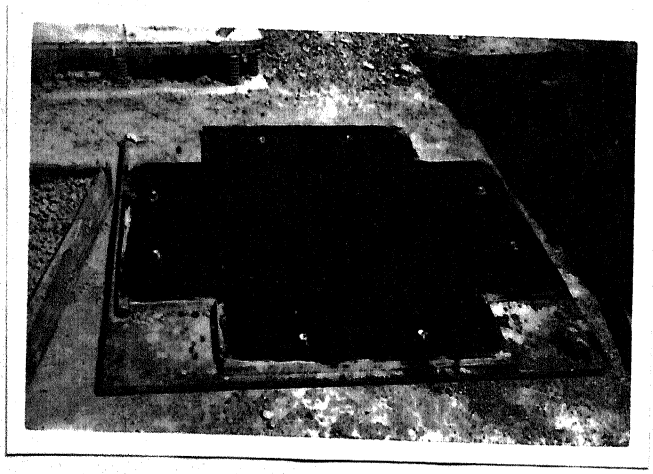

Figure 3.4 Reinforcement for Biaxial Moment Slabs

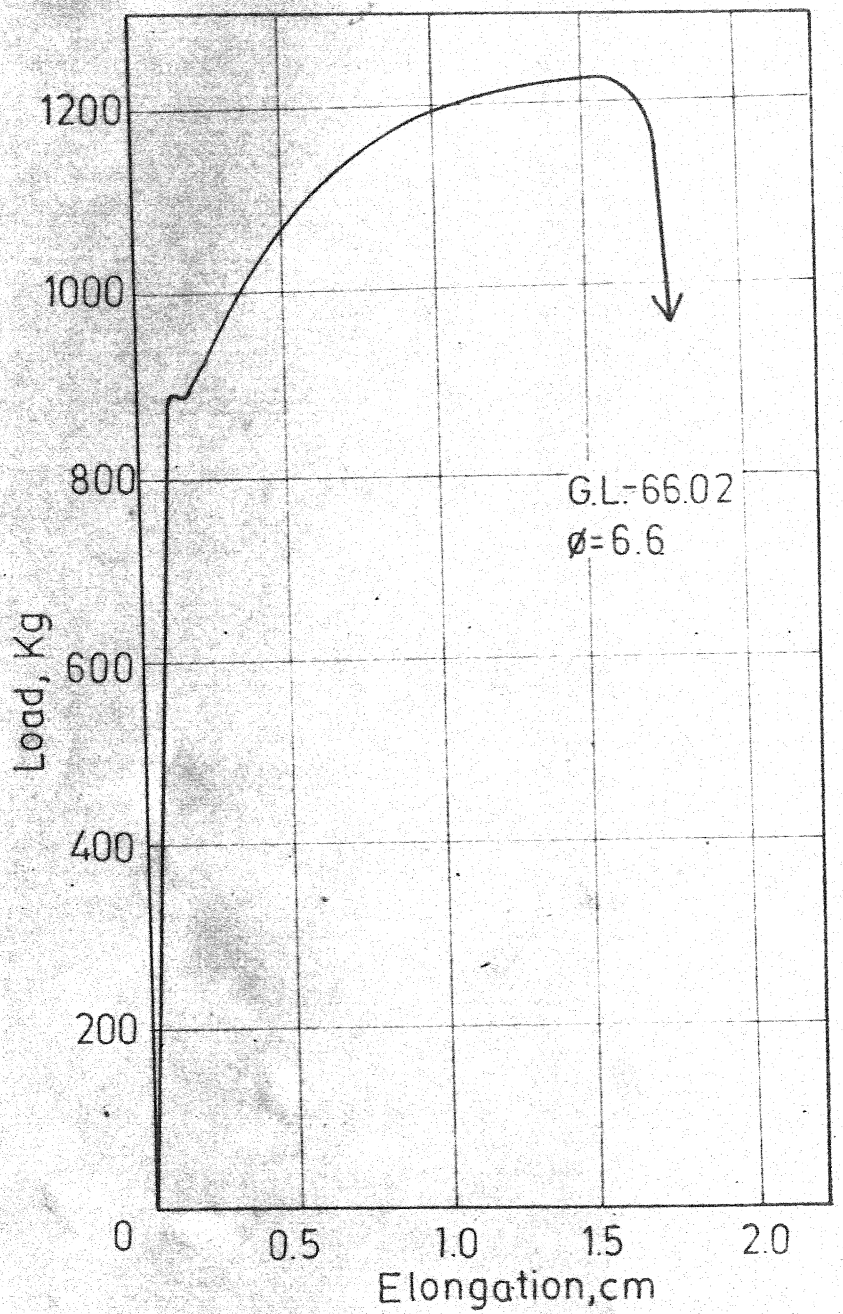

(a) Load-deformation curve for mild steel rod.

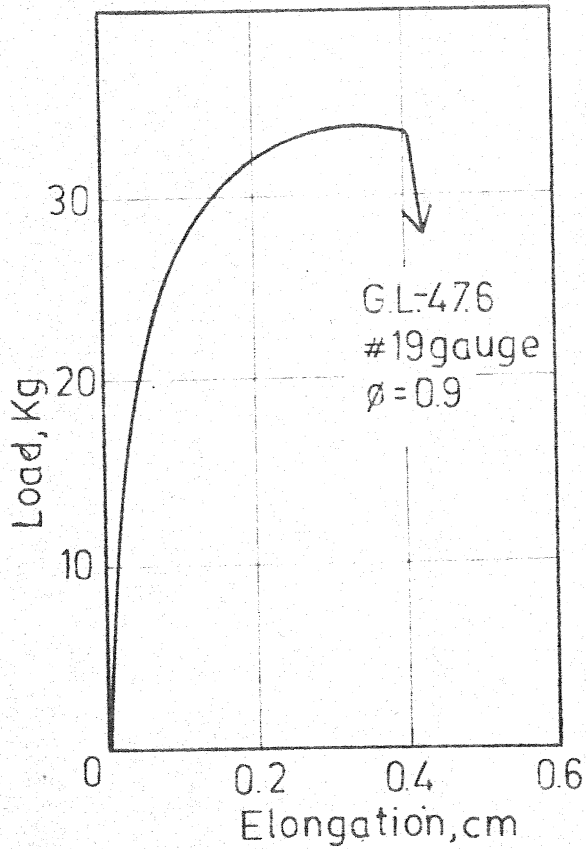

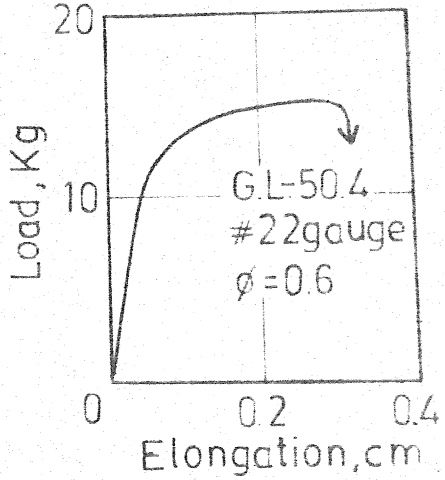

(b) Load-deformation curve for #19 and #22 gauge wire.

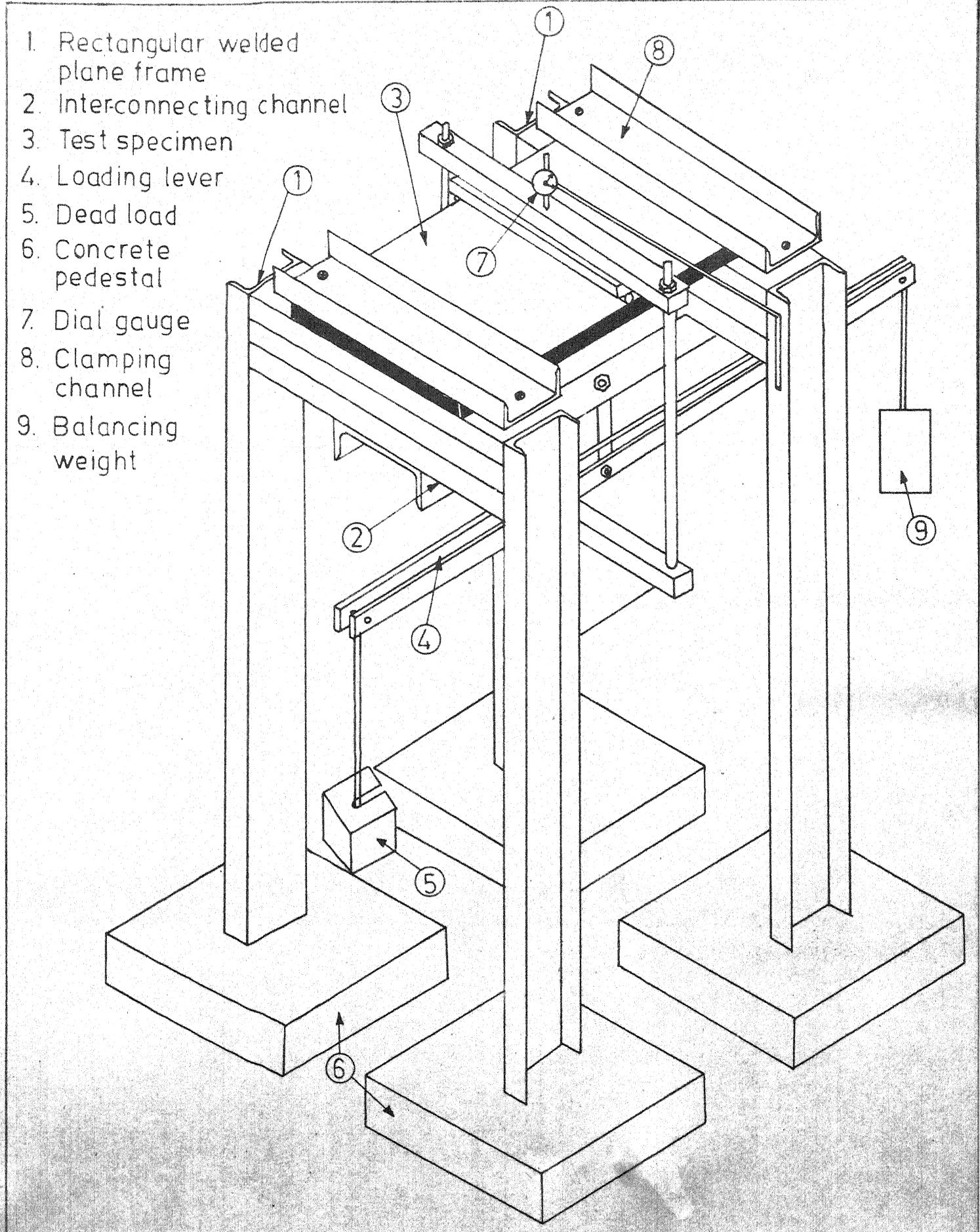

Figure 3.6- Creep setup.

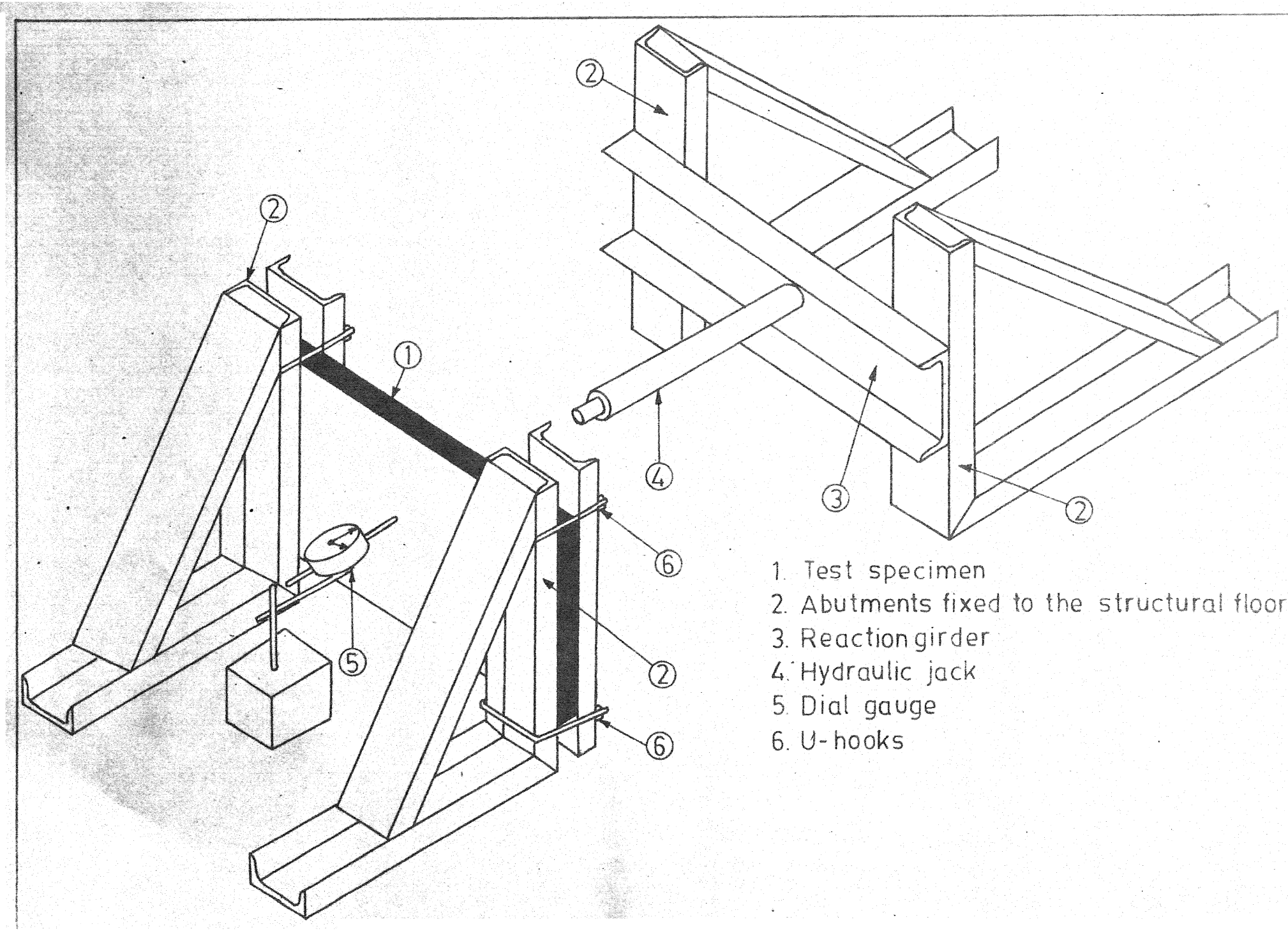
1. Test specimen
2. Abutments fixed to the structural floor
3. Reaction girder
4. Hydraulic jack
5. Dial gauge
6. U-hooks

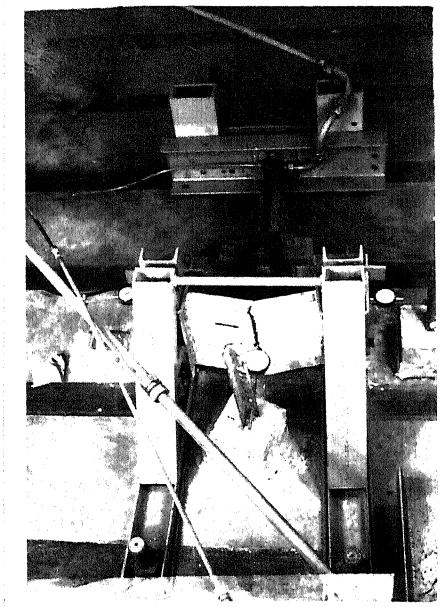

Figure 3.8 Fatigue and Static Test Setup

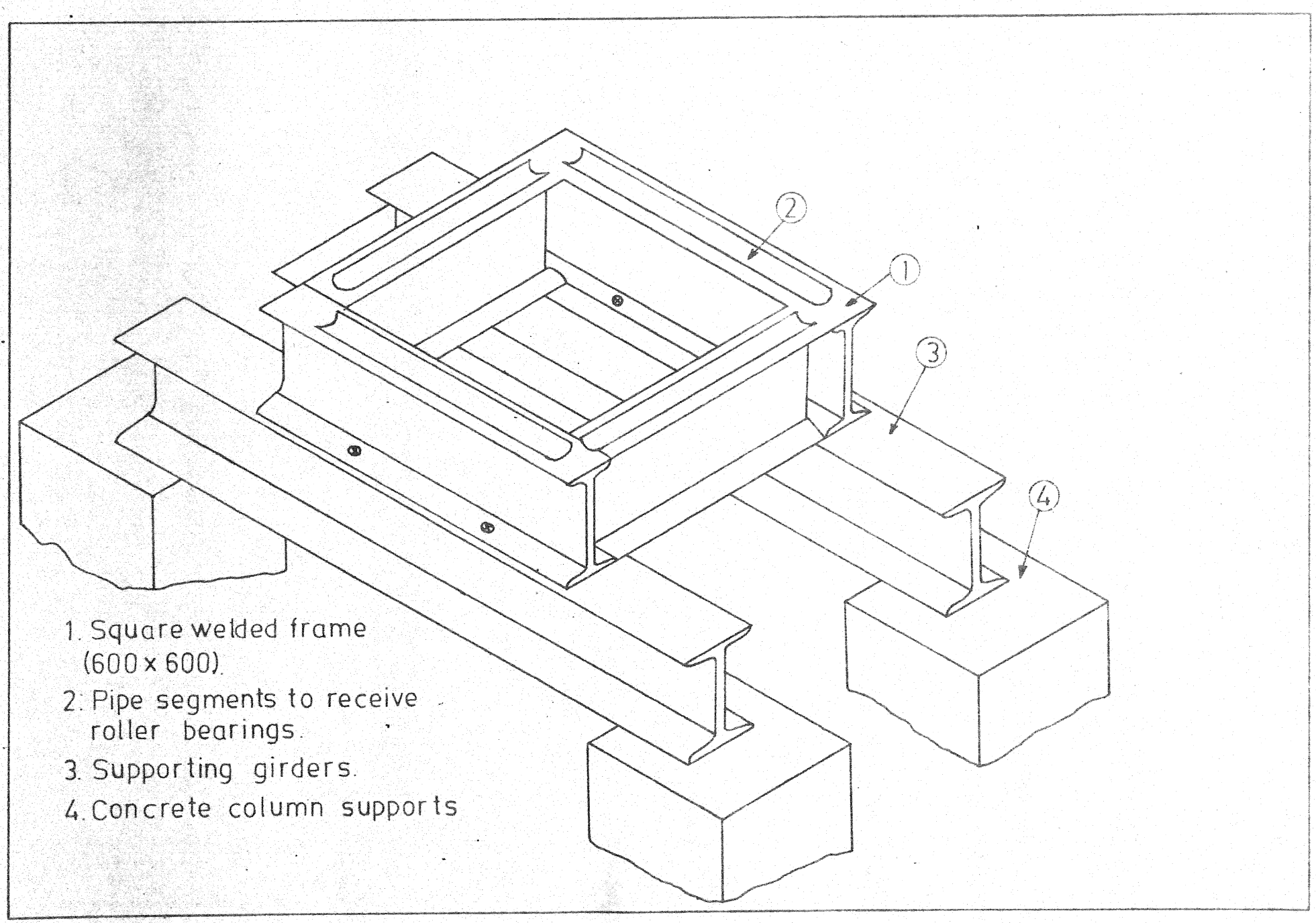

Figure 3.9 - Biaxial End Moment.

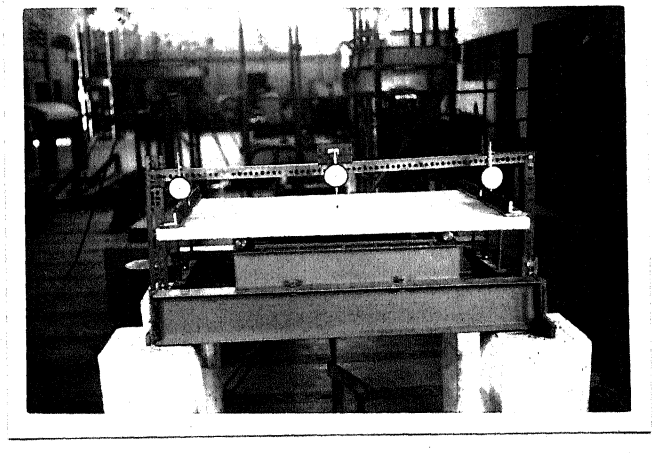

Figure 3.10 Biaxial End Moment Setup with Specimen in Position

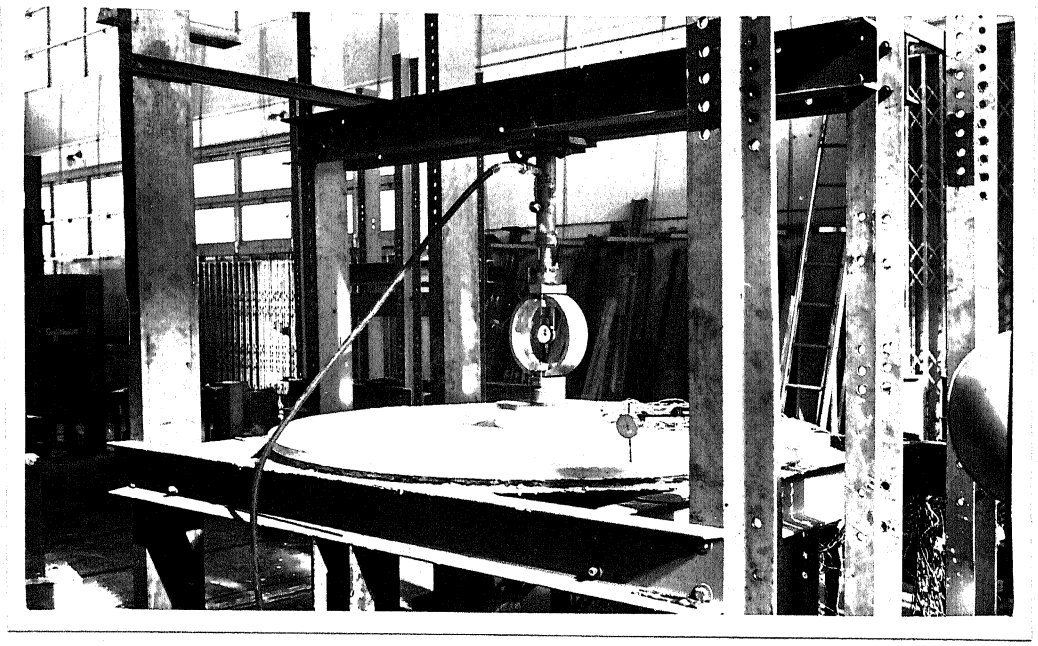

Figure 3.11 Circular Slab Test Setup

CHAPTER IV

CREEP

4.1 General

A material, when subjected to load undergoes deformations. The strains recorded instantaneously during the application of load are termed elastic and those occuring with time are known as creep. Creep can thus be defined as the increase in strain under sustained stress and since this increase can be several times as large as the strain on loading, creep is of considerable importance in structural mechanics and design.

In order to fulfill the basic desiderata of design: safety, serviceability and economy, the influence of creep on the strength and behaviour of entire structure must be clearly understood. To achieve this, the designer should be able to estimate the creep strains fairly accurately. The enhanced interest in design for creep in recent years is due to the use of more advanced concepts which result in shallow structures and to the fact that more complex structures are being designed. Furthermore, use of thin slabs and shells of material like ferrocement in structure may lead to excessive long term deformations and to cracking if time effects in design are not properly taken into account.

4.2 Creep of Ferrocement

Creep is a material property and, hence, its characteristics are greatly influenced by its basic ingredients. Ferrocement, a composite

material, comprises mortar and fine wire mesh as basic materials.

In a strain time curve for mortar, the strain at time zero is primarily elastic, thereafter there are three stages of creep. In the primary range the rate of creep decreases with time. The secondary range designates the range of steady state creep. The tertiary creep may or may not exist. For instance in concrete or mortar, this may arise from an increase in microcracking at high stresses. The creep and elastic deformations have been observed to be essentially proportional upto usual working loads and under over loads this proportionality no longer holds.

A crude estimation of long term deflection is made by assuming the modulus of elasticity as one third of the instantaneous modulus of mortar. For reinforced structures, ACI Building Code (63) recommends that additional long term deflections may be obtained by multiplying the immediate deflection caused by sustained part of the load by 2.0 when A'_s (compressive steel) = 0, 1.2 when $A'_s = 0.5\ A_s$ (tensile steel) and 0.8 when $A'_s = A_s$.

Ferrocement uses high strength rich cement mortar with low water-cement ratio. The influence of various factors on the creep characteristics of mortar is reviewed for a better understanding of creep of ferrocement.

4.3 Factors Influencing Creep of Mortar

In most of the investigations creep has been studied empirically. It is difficult to interpret many of available data due to the fact that in proportioning mortar, it is not possible to change one factor without

altering at least one other. For instance, the richness and the water cement ratio of a mix of given workability may vary at the same time. Certain influences are, however, apparent.

For a given mortar, the lower the relative humidity, creep is higher. The influence of relative humidity is much smaller in the case of specimens which have reached hygral equilibrium with surrounding medium prior to application of load (64).

When microcracking occurs in mortars, the creep behaviour also changes. Since mortars are less grossly heterogenous than concrete, proportionality between creep and stress strength ratio is exhibited in mortars upto a higher limit of 0.85 which in case of concrete is only 0.6. It has been observed that although mortar is a brittle material, a rich mix of mortar has ability to heal up fine cracks which may occur due to loads. When microcracks occur, the incomplete hydrated surface comes in contact with moisture and when the hydration is complete the crack is partly knitted together.

The strength of mortar has significant effect on creep. Creep is observed to be inversely proportional to strength of mortar (65). From the influence of strength on creep it follows, that creep under a given stress is closely related to the water-cement ratio of mix, but for the same stress-strength ratio, creep is sensibly independent of the water-cement ratio.

The magnitude of creep is appreciably influenced by the age at which load is applied. This may be due to increase in strength of mortar with age(66).

Water reducing and set retarding admixtures have been observed to increase the creep of mortar (67) but not in all cases. Usually some workability agents like pozzalona, Plastel II etc. are used in ferrocement, the effect of which on creep should be thoroughly investigated before use.

It has been concluded from experimental results that creep decreases with an increase in the size of the specimen, the reason for which can be attributed to the effects of shrinkage.

Arnstein and Reiner (68) concluded that increasing the aggregate content reduced the rate of creep of mortars but increased that of concrete. L' Hermite (69) reported that the creep of rich mortar is, however, increased. Neither Arnstein and Reiner's nor L' Hermite's statement has been confirmed. Based on the test results, Lorman (70) reported that quantity of cement was not found to be significant factor in creep. Ishai (71) stated that in mortars the magnitude of creep increased with an increase in sand concentration. But it appears that the mix used by Ishai contained a large volume of voids due to lack of cement paste which affected the strength adversely and hence more creep was observed.

de la Pena (72) from a series of tests on mortar specimens found that higher the cement paste content, the higher the creep and that replacing one part of cement by one part of sand decreases creep in direct proportion.

From the foregoing discussions, it is difficult to draw conclusions regarding influence of a few factors on creep of mortar since the findings of different investigators are contradictory. Neville (73), Neville (74)

and Troxell, Davis and Kelly (75) have critically reviewed the studies of various investigators on creep of mortar in their books.

4.4 Influence of Reinforcement on Creep of Ferrocement

It is observed that for reinforced concrete or mortar, without compressive steel, the final deflection is 2.5 to 3.0 times of elastic deflection. In ferrocement reinforcement in the form of mesh is well dispersed inside the matrix, i.e., in compression and tension it is equally reinforced. For such a case as already mentioned in article 4.2, the creep deflection and compressive creep strains are reduced considerably. However, at stresses higher than the cracking strength of ferrocement, the creep is expected to be more due to the presence of fine wire meshes.

4.5 Creep-Time Relationships

The progress of creep with time under load follows a definite pattern. Because of this, various investigators have suggested numerous mathematical expressions relating creep and time. The various empirical relations, viz., hyperbolic, logarithmic, exponential or power functions hold only for concrete/mortars similar to those for which the formulae have been derived. But, however, an approximate estimate of creep for design purposes can be made from experimental data. Only logarithmic and hyperbolic relations were observed to give a better regression fit for the specimens tested under flexural creep.

4.6 Hyperbolic Relation

Ross (76) introduced the relation

$$c = \frac{t}{A + Bt} \qquad \ldots (4.6.1)$$

where c - the creep,

t - the time under load, in days, and

A and B are constants.

The equation (4.6.1) can be rewritten in the form

$$\frac{t}{c} = A + Bt \qquad \ldots (4.6.2)$$

which is a straight line of slope B and intercept A on the t/c axis. A and B are obtained from experimental results. While attempting a straight line fit, the line should be made to pass through the points at later ages, since there is some deviation from the straight line during early period of application of load. Lorman (70) also gave a similar relation.

4.7 Logarithmic Relation

Based on an extensive study of creep, U.S. Bureau of Reclamation (77) has developed a creep expression with the assumption that rate of creep is inversely proportional to time, i.e.,

$$\frac{dc}{dt} = \frac{F(k)}{t + A} \qquad \ldots (4.7.1)$$

where A - a constant to provide for time shift,

k - the age at loading, and

F(k) - a parameter.

F(k) is obtained experimentally and represents ratio of creep with logarithm of time. The solution of equation (4.7.1), after introducing initial conditions of c=0 when t=0 is given by

$$c = F(k) \ln \left(\frac{t}{A} + 1\right) \qquad \ldots (4.7.2)$$

In above expression A is usually taken as 1.

4.8 Test Procedure

The test setups used have been described in Chapter III. Slabs with two opposite edges clamped and other two free were subjected to a central line load parallel to the clamped edges. The loads were applied gradually and deflection readings on the instantaneous application of load taken. Initially the deflection readings were noted at very short intervals for a couple of days and subsequently the same were noted every alternate days. The development of microcracks at the time of application of load and also with time were observed and noted carefully.

The Tables 4.1 through 4.3 summarise the results of the twenty slabs tested under creep. The slabs have been tested for a period of 45 to 90 days. It has been observed that to make a reasonably good estimate of creep strains, experimental studies for a period of 45 to 60 days are bare minimum. The

observed creep-time relationships for twenty slabs tested have been presented in Figures 4.1 through 4.20.

Shrinkage and creep are twin phenomena and principle of superposition does not hold in this case. But if test specimens have attained maturity before putting them to test, strains due to shrinkage are minimised. The effects due to temperature, shrinkage, humidity were corrected for by data from an unloaded control specimen kept under similar conditions.

In order to study the effect of previous load history on creep, loads for a few slabs were increased after a few days of creep. At the end of the test while unloading, the instantaneous elastic recovery and the permanent set of the specimen were noted. These specimens were tested to collapse under similar end conditions as for creep, to compare the load carrying capacity of such specimens with virgin specimens.

4.9 Discussion of the Test Results

Creep-time plots shown in Figures 4.1 through 4.20, indicate that for specimens subjected to sustained stresses less than the cracking stress of ferrocement (35 kg/cm^2), creep increases at a decreasing rate and attains steady state. Whereas for specimens subjected to apparent stresses higher than 35-40 kg/cm^2, steady state is not reached in 45 to 50 days. It is obvious from Figures 4.7 and 4.8 that creep rates are less for specimens which have been subjected initially to sustained loads for 30 to 45 days. This gives an indication that previous load history has an appreciable influence on the creep behaviour of the specimen. The reason for which

may be attributed to the resetting of the molecules under sustained load which results in the compaction of the specimens.

It is obvious from Figures 4.21 in which 15, 30 and 45 days creep for 4c specimens have been drawn against loads, that the load creep relationship is not linear. For concrete specimens this relation has been observed to be linear. The Figure 4.22 shows 30 days creep for 4c, 6c and 8c specimens plotted against apparent tensile stress. It is obvious that at stresses upto cracking stress of ferrocement, the creep is linearly proportional and there is no effect of reinforcement percentage. But for stresses higher than the cracking stress of ferrocement, the creep increases at a faster rate and percentage of reinforcement has an appreciable influence. Creep decreases with increase in percentage of reinforcement.

The hyperbolic and logarithmic fits give a good estimation of creep as shown in Figures 4.23 through 4.27. It is obvious from these figures that the hyperbolic creep expression gives a better fit. The Table 4.4 gives the hyperbolic and logarithmic equations for all the test specimens obtained from least squares fit. The slopes of logarithmic fit have been plotted against stress levels as shown in Figure 4.28, which clearly indicates that creep slopes increase linearly upto cracking stress and thereafter at a faster rate which is obviously due to the development of cracks and creeping of wire mesh. The reasons for wide spectrum of points in Figure 4.28 may be attributed to the percentage of reinforcement, variation in compressive strength, and age at loading which varied from 50 to 150 days as shown in Tables 4.1 through 4.3.

The effect of age at loading on the creep is quite appreciable. This may be attributed to the gain in strength and increase in modulus of elasticity with time. It was observed that control cubes tested 150 days after casting showed an average increase in strength upto 40% over 28 days cube strength.

The strain variations on unloaded control specimen over a period of eight months were observed to be very small with a maximum strain of 10^{-5}. This may be because of the fact that specimen was kept absolutely under dry condition after curing it for 28 days and the age at the time of putting it under test was 150 days approximately.

The creep specimens after unloading were tested to collapse. It was observed that in general they withstood 10-15 percent higher collapse loads compared to their virgin parallels. The reasons for this are attributed to gain in mortar strength with age and also compaction of the specimens at low sustained loads.

It is obvious from the test results that it is practically difficult to study the influence of a particular factor on creep, in isolation. When one factor varies, it affects one or many other factors simultaneously. Further discussion of the test results has been presented in Chapter VIII.

Table 4.1 - An Overview of Creep Test Results for 4c Series

Specimen No.	Average thickness	Load kg	Apparent tensile stress kg/cm^2	Age at loading days	Time under test days	Elastic strain 10^{-3}	Creep strain 10^{-3}	Elastic recovery 10^{-3}	Permanent set 10^{-3}
4c1	25.0	110	16.7	155	45	0.30	0.250	-	-
4c1*	25.0	330	45.4	202	30	1.60	0.70	0.525	0.35
4c2	25.0	440	58.8	70	60	6.20	8.55	10.00	4.75
4c3	25.0	220	35.8	95	45	0.60	1.0	0.600	1.0
4c4	25.0	380	52.6	118	45	2.50	4.35	0.65	6.2
4c5**	25.0	330	50.0	188	60	6.95	7.33	test continued	
4c6	25.0	615	70.50	158	60	6.18	5.44	test continued	

* Same sample under increased load.

** Samples with ~~#~~ 22 gauge wire.

Table 4.2 - An Overview of Creep Test Results for 6c-Series

Specimen No.	Average thickness	Load kg.	Apparent tensile stress kg/cm^2	Age at loading days	Time under test days	Elastic strain 10^{-3}	Creep strain 10^{-3}	Elastic recovery 10^{-3}	Permanent set 10^{-3}
6c1	25.0	110	16.7	155	75	0.475	0.350	0.30	0.525
6c2	25.0	220	33.4	155	47	0.625	0.375	-	-
6c2*	25.0	515	66.0	202	43	2.55	1.480	-	-
6c3	25.0	220	33.4	155	75	0.475	0.490	0.413	0.550
6c4	28.0	515	55.3	79	60	3.2	4.60	2.24	5.45
6c5	28.0	585	61.2	87	45	1.90	2.95	1.425	3.14
6c6	28.0	380	46.0	119	45	1.00	3.60	2.04	2.54
6c7	28.0	700	69.0	150	53	3.62	2.25	test continued	
6c8**	28.0	485	60.0	137	60	2.35	4.25	test continued	

* Same sample under increased load.

** Samples with +/- 22 gauge wires.

Table 4.3 - An Overview of Creep Test Results for 8c-Series

Specimen No.	Average thickness	Load kg.	Apparent tensile stress kg/cm^2	Age at loading days	Time under test days	Elastic strain 10^{-3}	Creep strain 10^{-3}	Elastic recovery 10^{-3}	Permanent set 10^{-3}
8c1	25.0	220	33.4	153	45	0.35	0.425	-	-
8c1*	25.0	440	59.4	198	30	2.25	0.30	-	-
8c2	30.0	590	56.5	79	50	1.96	2.275	1.91	2.32
8c3	30.0	330	37.4	70	13	0.725	1.125	-	-
8c3*	30.0	700	65.8	83	47	2.70	5.77	2.98	5.48
8c4	30.0	545	53.0	110	45	1.80	2.68	1.62	2.92
8c5	30.0	424	45.0	123	45	2.48	3.375	3.750	1.925
8c6**	30.0	670	60.0	140	60	6.82	6.0 test continued		

* Same sample under increased load.

** Samples with #/= 22 gauge wires.

Table 4.4 - Logarithmic and Hyperbolic Creep Fits

Specimen No.	Load kg	Equations $c = C + D \ln(t+1)$	Equations $t/c = A + Bt$
4C1	110	$c = 0.002 + 0.020 \ln(t+1)$	$t/c = 100.217 + 9.77t$
4c1*	330	$c = 0.046 + 0.062 \ln(t+1)$	$t/c = 13.8 + 3.58t$
4c2	440	$c = -0.23 + 0.810 \ln(t+1)$	$t/c = 3.28 + 0.26t$
4c3	220	$c = 0.04 + 0.090 \ln(t+1)$	$t/c = 14.52 + 2.28t$
4c4	380	$c = -0.12 + 0.470 \ln(t+1)$	$t/c = 4\,4.90 + 0.48t$
6c1	110	$c = 0.055 + 0.027 \ln(t+1)$	$t/c = 78.6 + 7.0\,t$
6c2	220	$c = 0.030 + 0.027 \ln(t+1)$	$t/c = 36.8 + 6.10t$
6c2*	515	$c = 0.048 + 0.13 \ln(t+1)$	$t/c = 11.38 + 1.55t$
6c3	220	$c = -0.024 + 0.049 \ln(t+1+$	$t/c = 68.55 + 4.29t$
6c4	515	$c = -0.37 + 0.48 \ln(t+1)$	$t/c = 10.1 + 0.41t$
6c5	585	$c = 0.03 + 0.28 \ln(t+1)$	$t/c = .6.5 + 0.75t$
6c6	380	$c = 0.035 + 0.35 \ln(t+1)$	$t/c = 4.9 + 0.61t$
8c1	220	$c = 0.088 + 0.04 \ln(t+1)$	$t/c = 38.0 + 5.06t$
8c1*	440	$c = 0.008 + 0.02 \ln(t+1)$	$t/c = 39.0 + 8.04t$
8c2	590	$c = 0.058 + 0.20 \ln(t+1)$	$t/c = 7.9 + 1.01t$
8c3	330	$c = 0.05 + 0.14 \ln(t+1)$	$t/c = 6.71 + 1.86t$
8c3*	700	$c = -0.064 + 0.43 \ln(t+1)$	$t/c = 5.65 + 0.48t$
8c4	545	$c = 0.1 + 0.25 \ln(t+1)$	$t/c = 5.27 + 0.83t$
8c5	424	$c = 0.003 + 0.33 \ln(t+1)$	$t/c = 5.6 + 0.65t$

* Same sample under increased load.

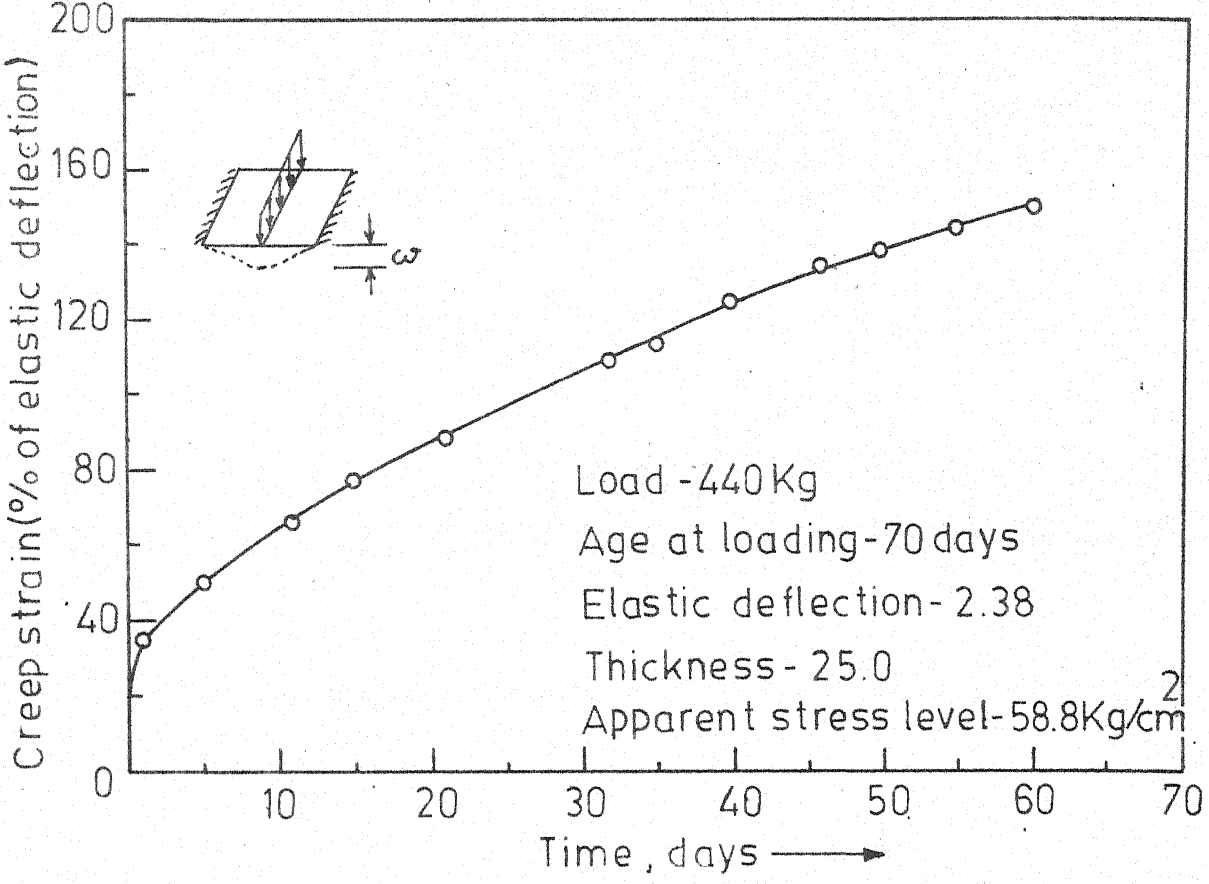

Figure 4.1 - Creep - Time Relationship for 4C2.

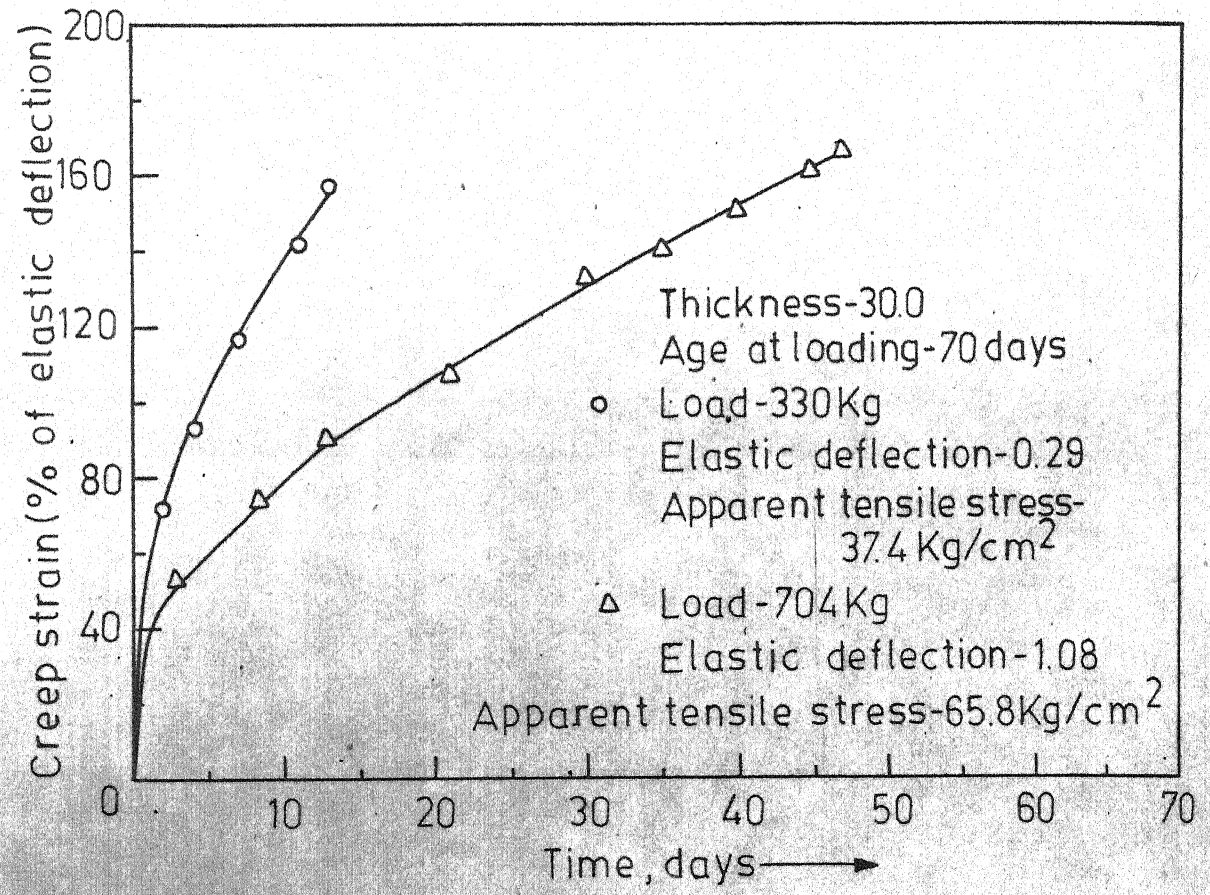

Figure 4.2 - Creep - Time Relationship for 8C3.

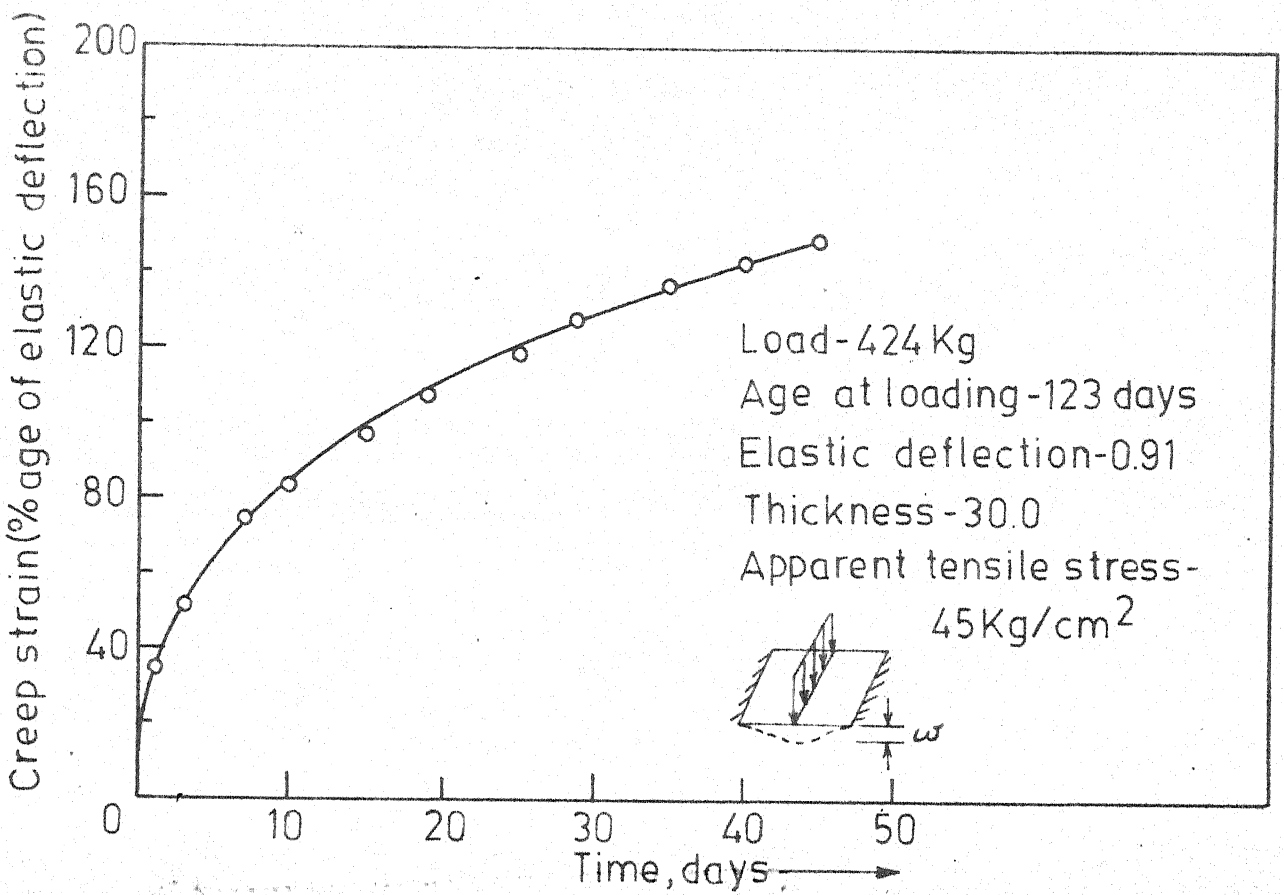

Figure 4.3 - Creep-Time Relationship 8C5.

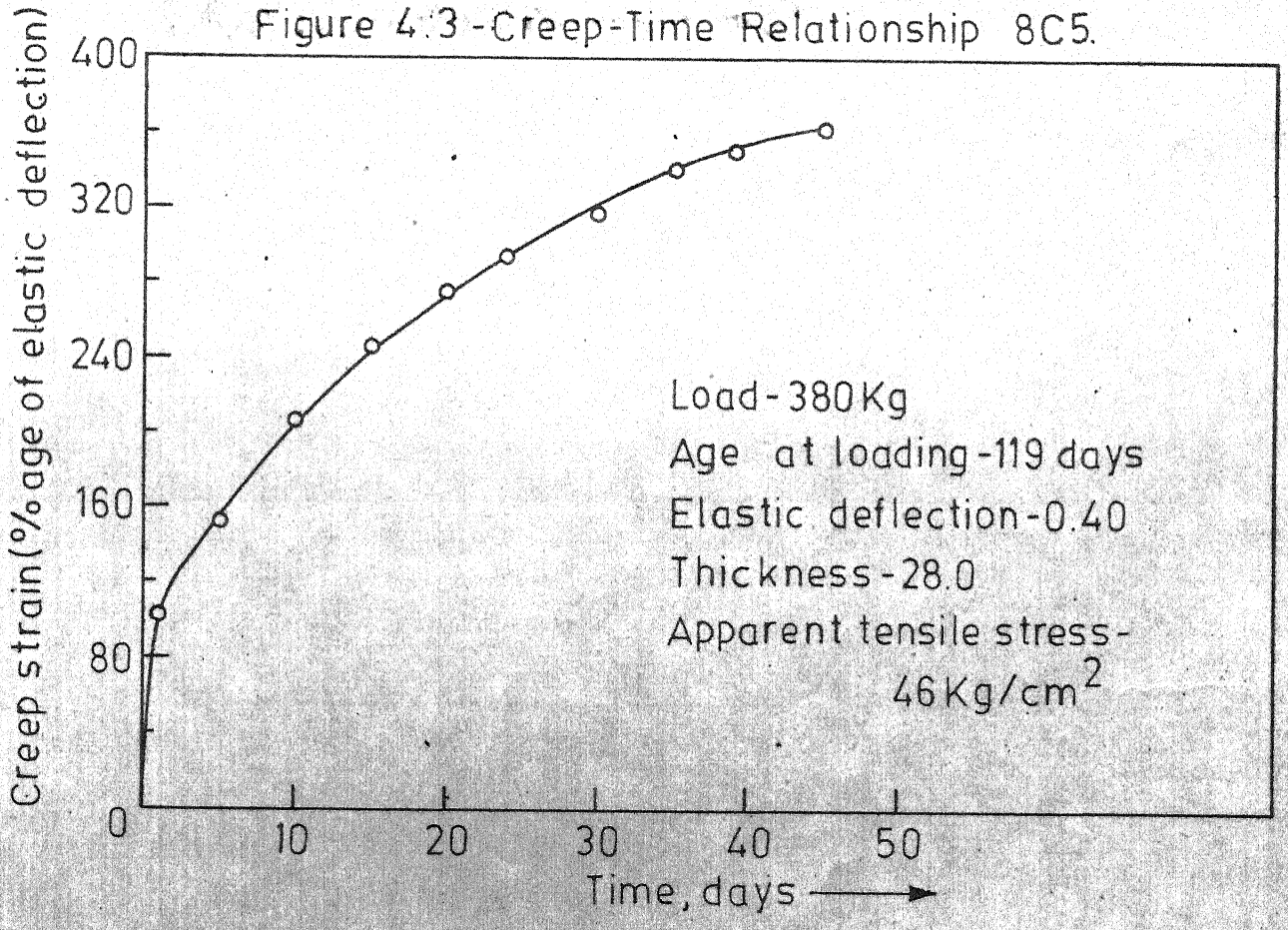

Figure 4.4 - Creep-Time Relationship 6C6.

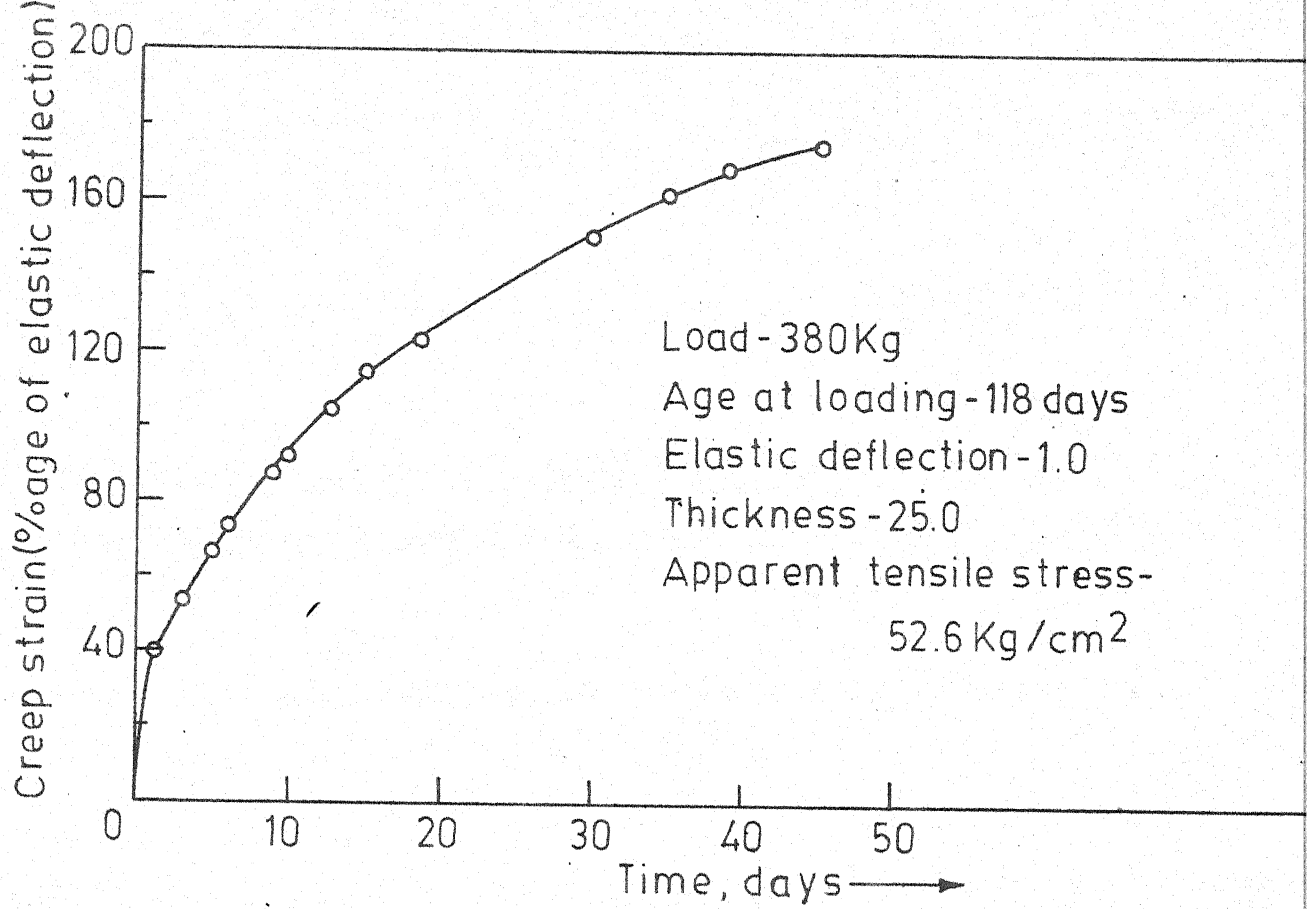

Figure 4.5 - Creep - Time Relationship for 4C4.

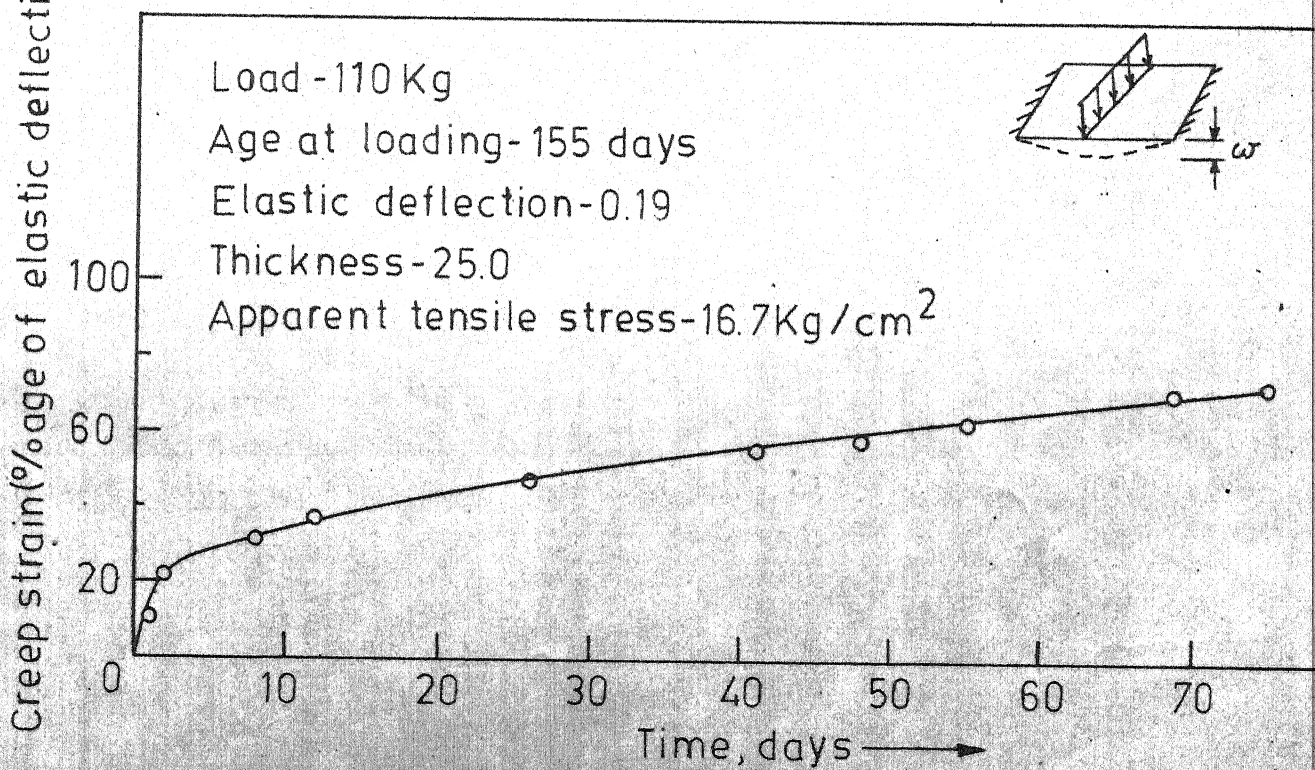

Figure 4.6 - Creep - Time Relationship for 6C1.

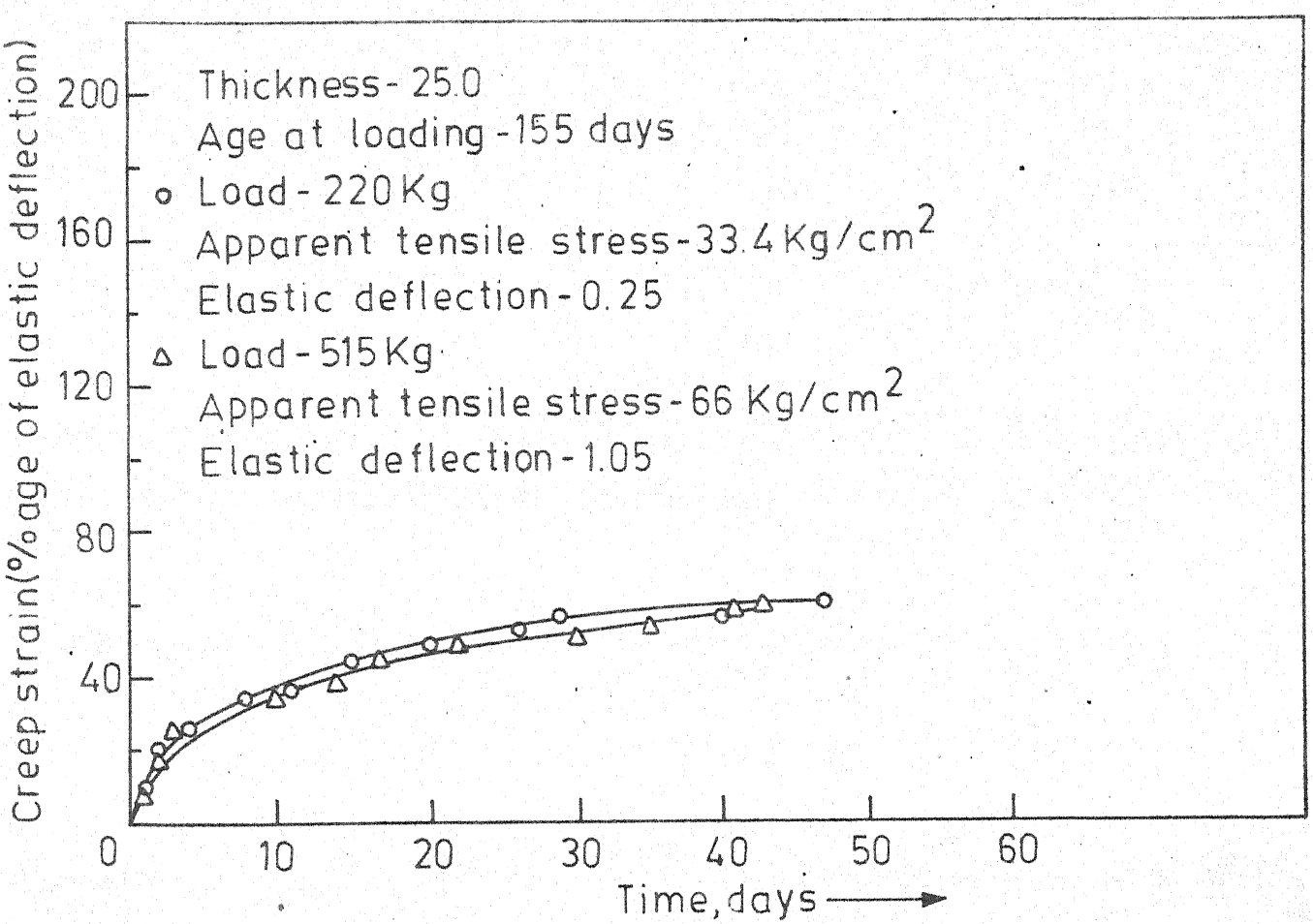

Figure 4.7 - Creep-Time Relationship for 6C2.

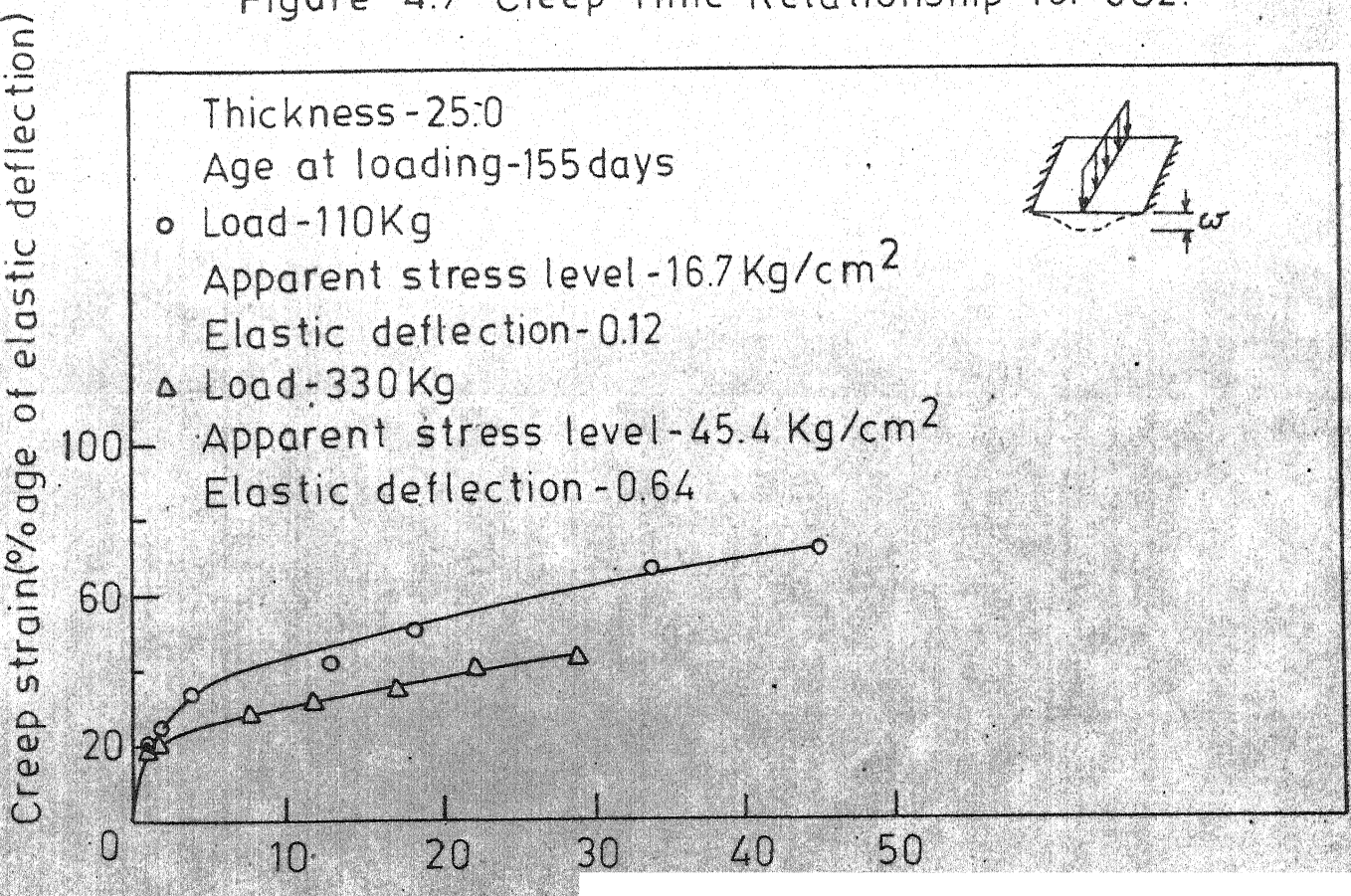

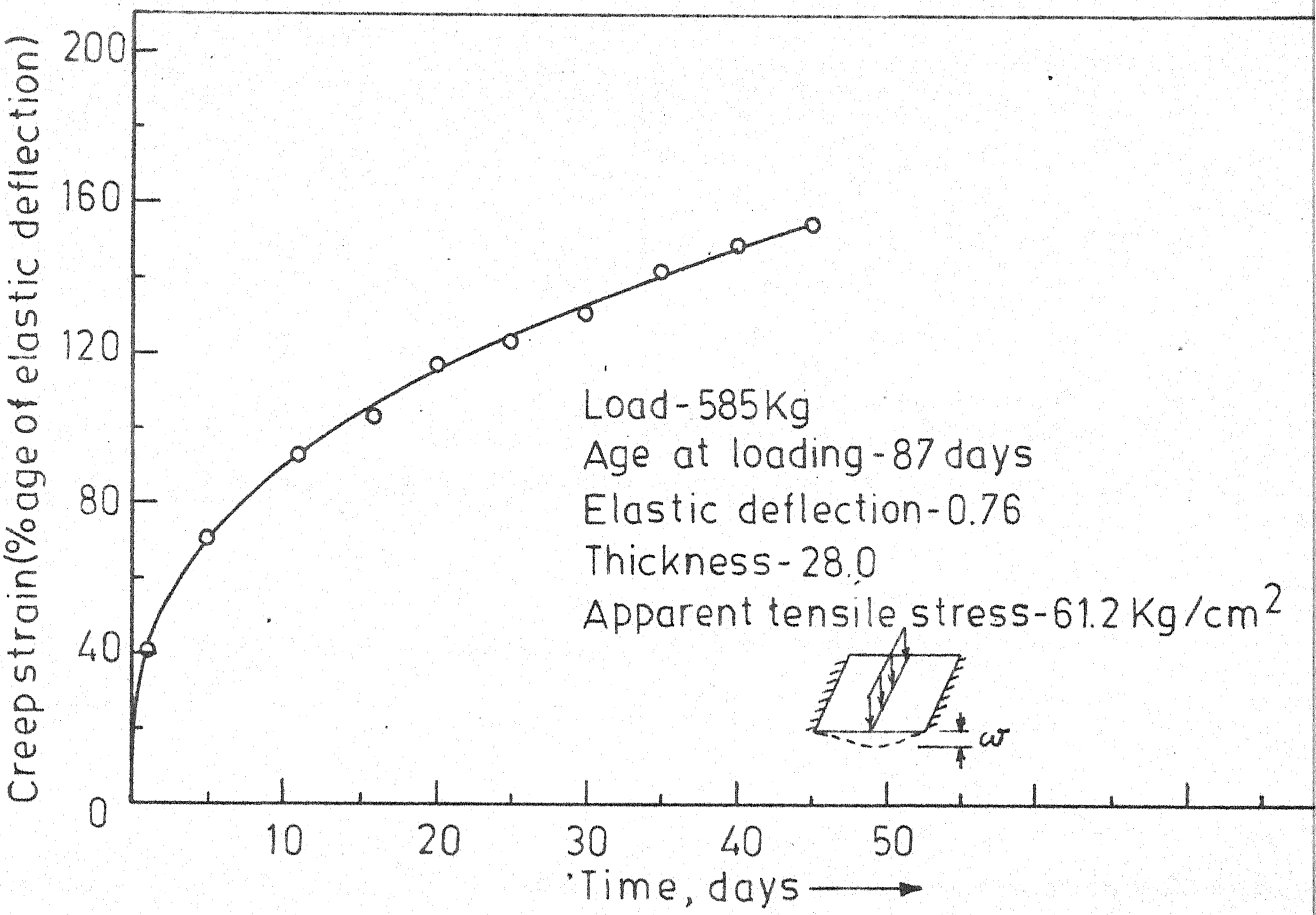

Figure 4.9 -Creep-Time Relationship for 6C5.

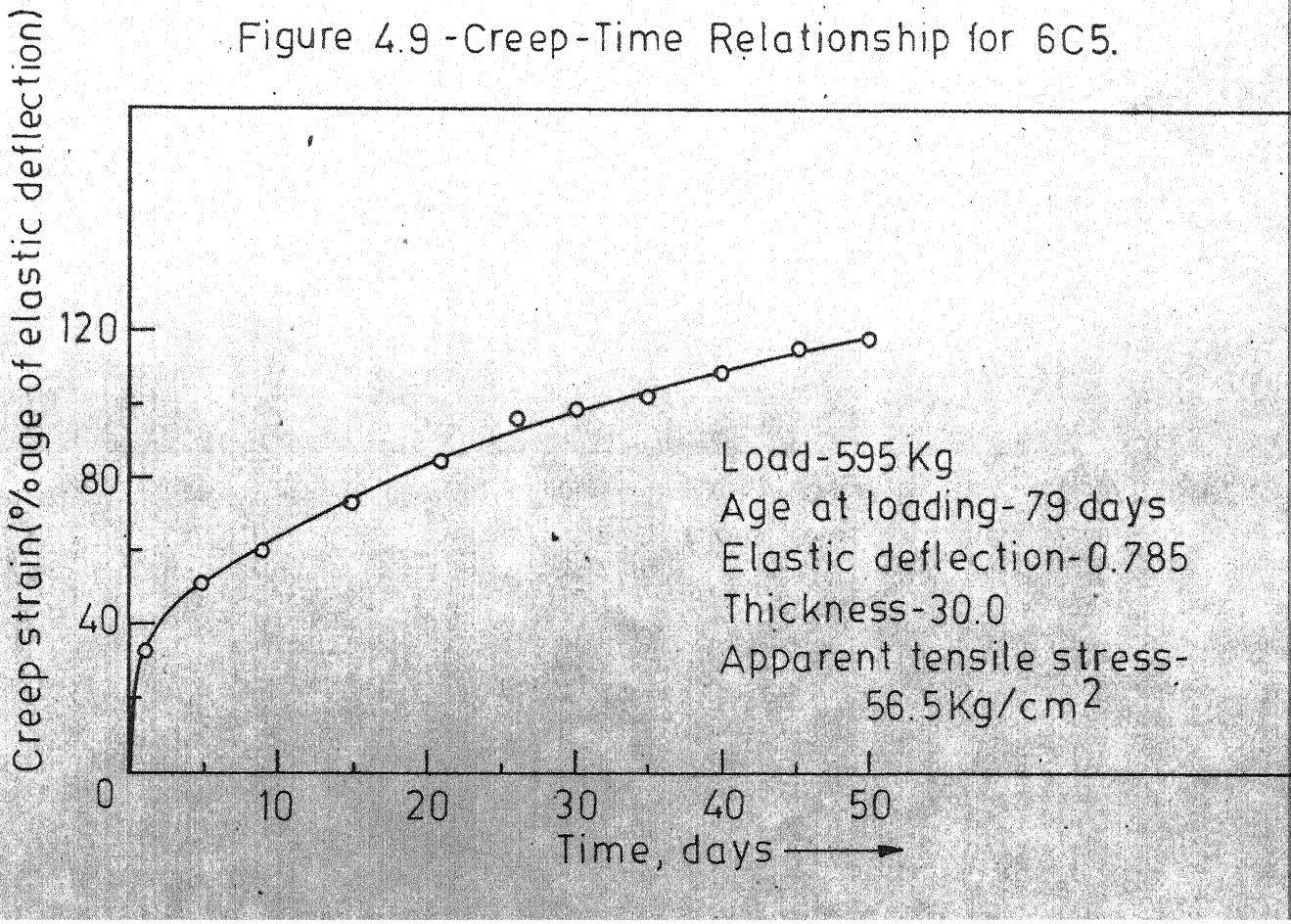

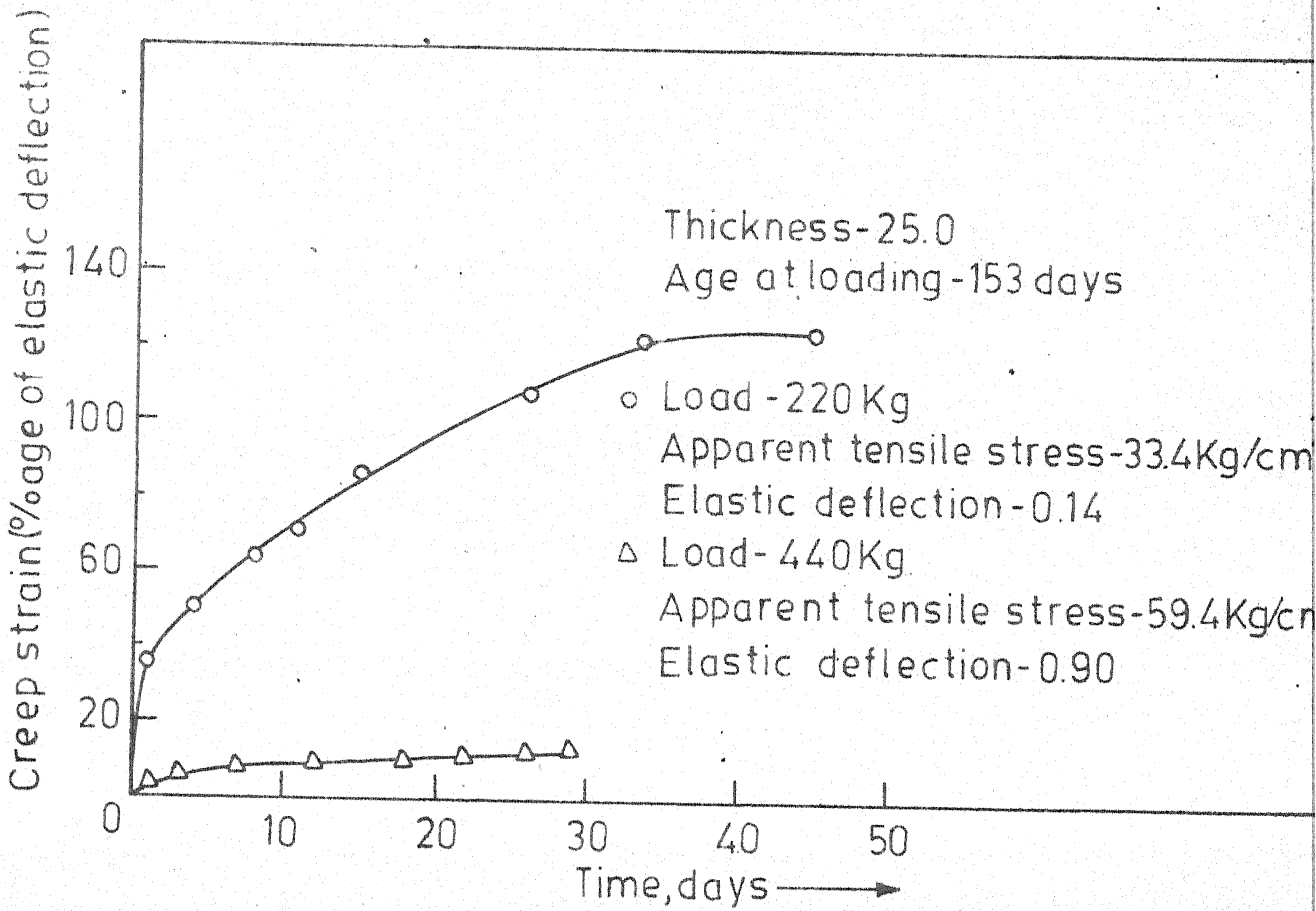

Figure 4.11 - Creep - Time Relationship for 8C1.

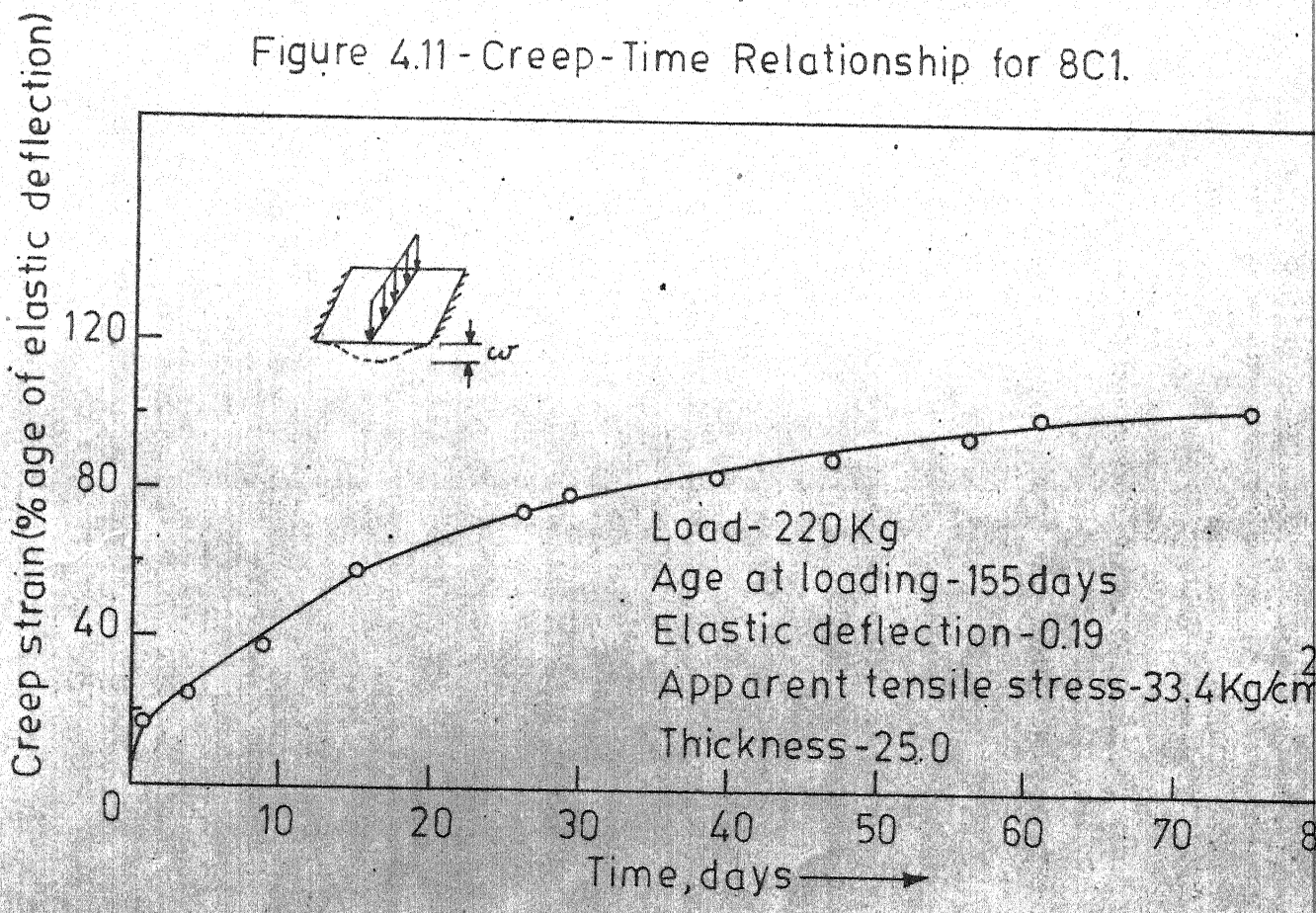

Figure 4.12 - Creep - Time Relationship for 6C3.

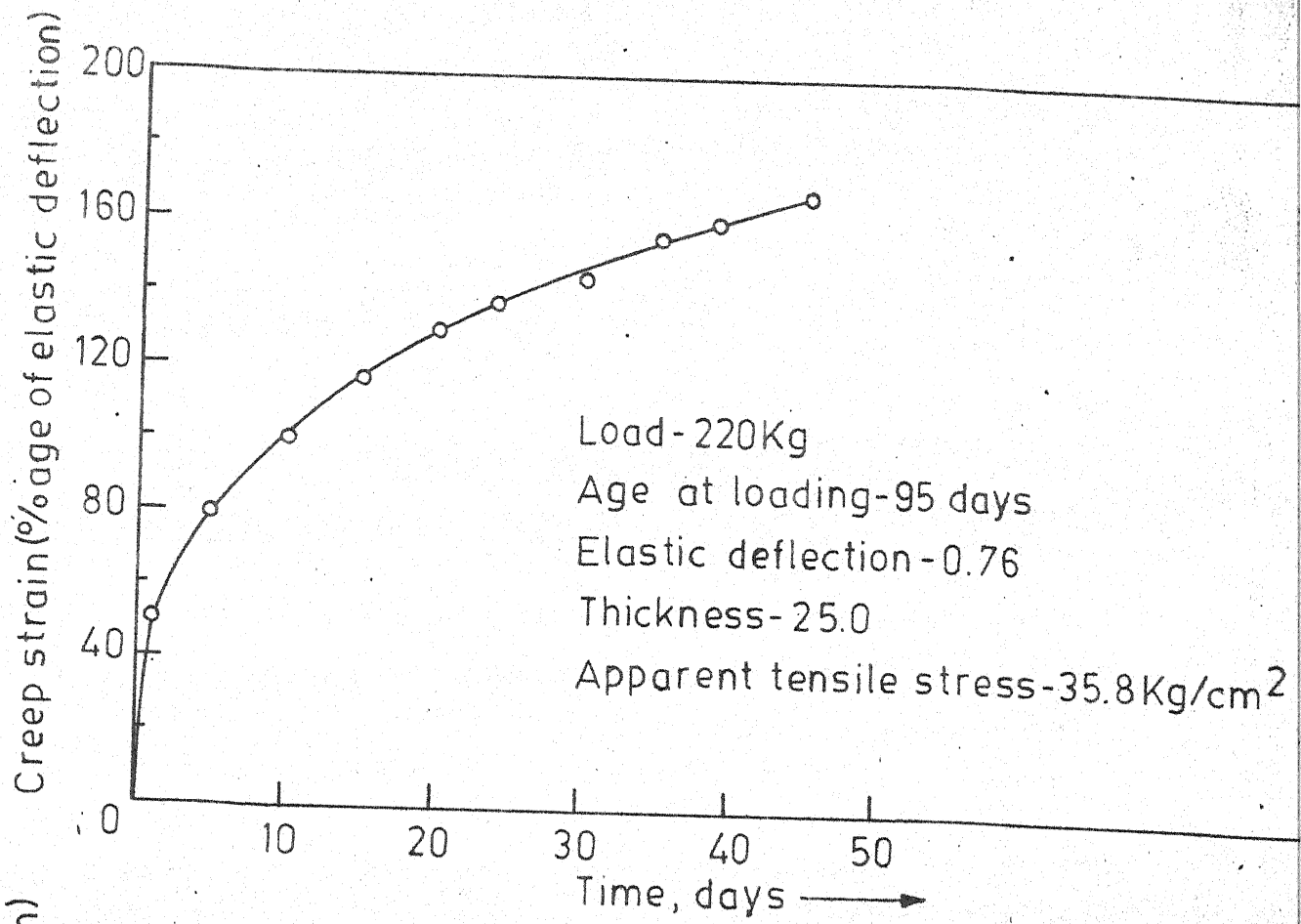

Figure 4.13 - Creep - Time Relationship for 4C3.

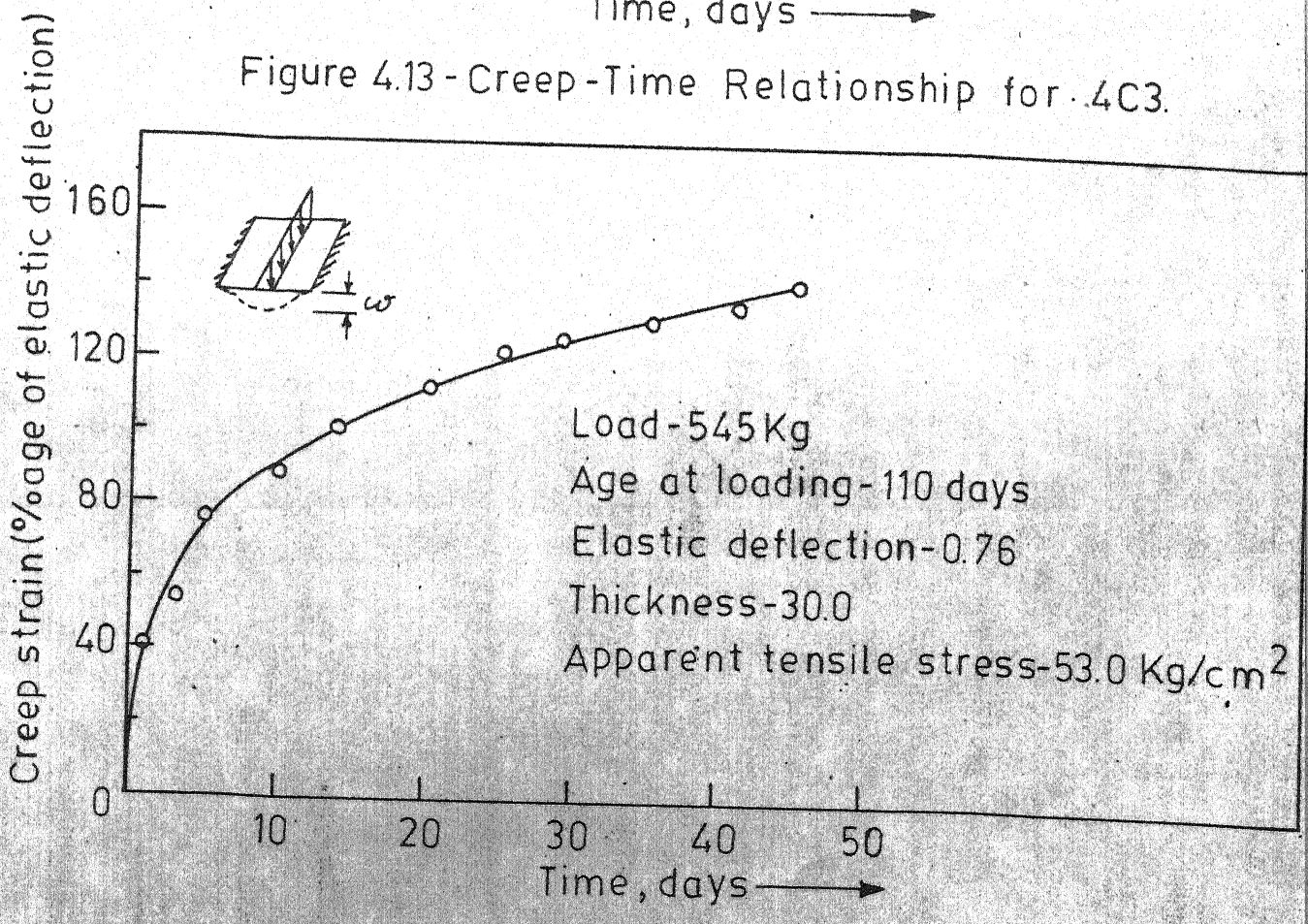

Figure 4.14 - Creep - Time Relationship for 8C4.

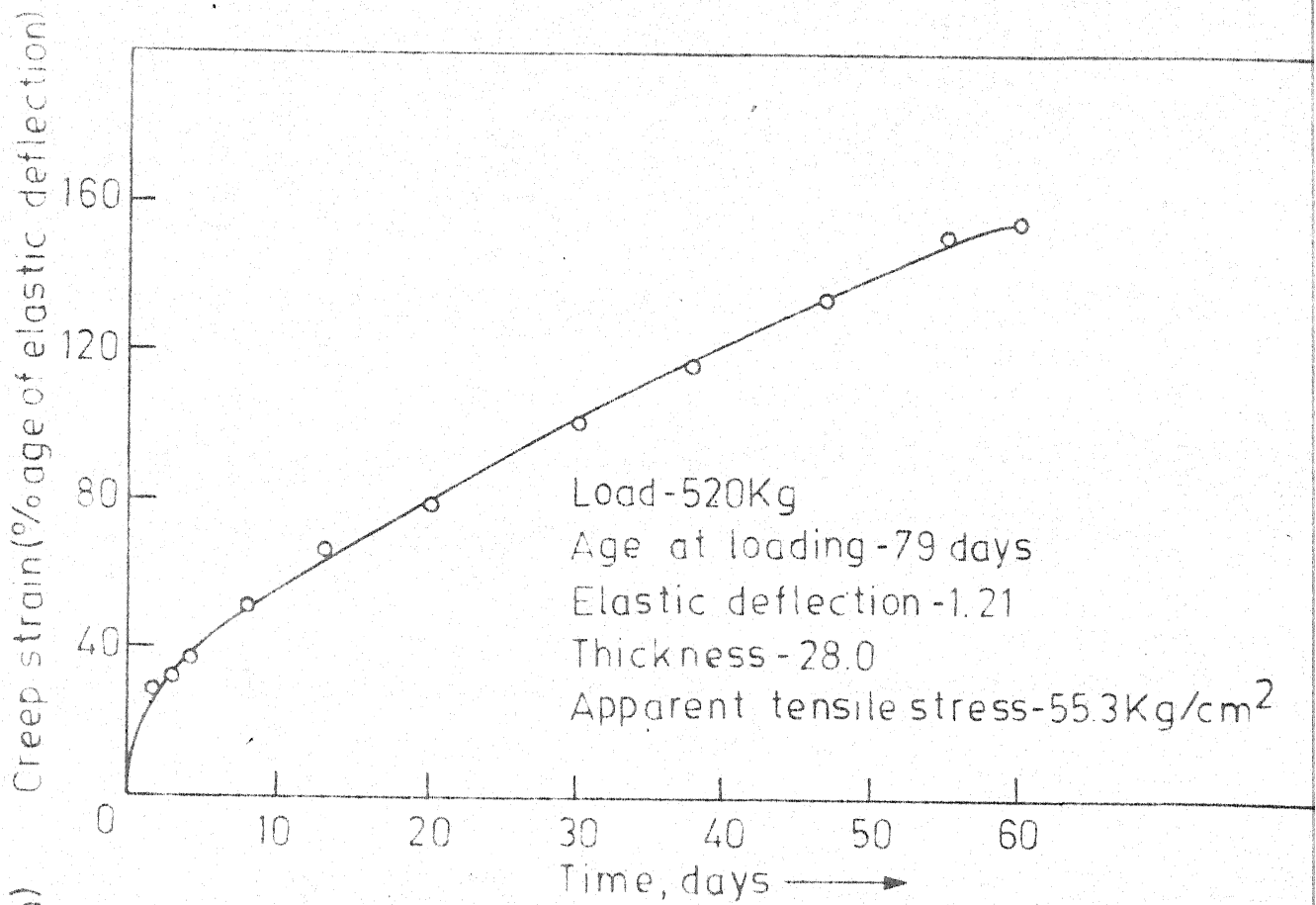

Figure 4.15 - Creep-Time Relationship for 6C4.

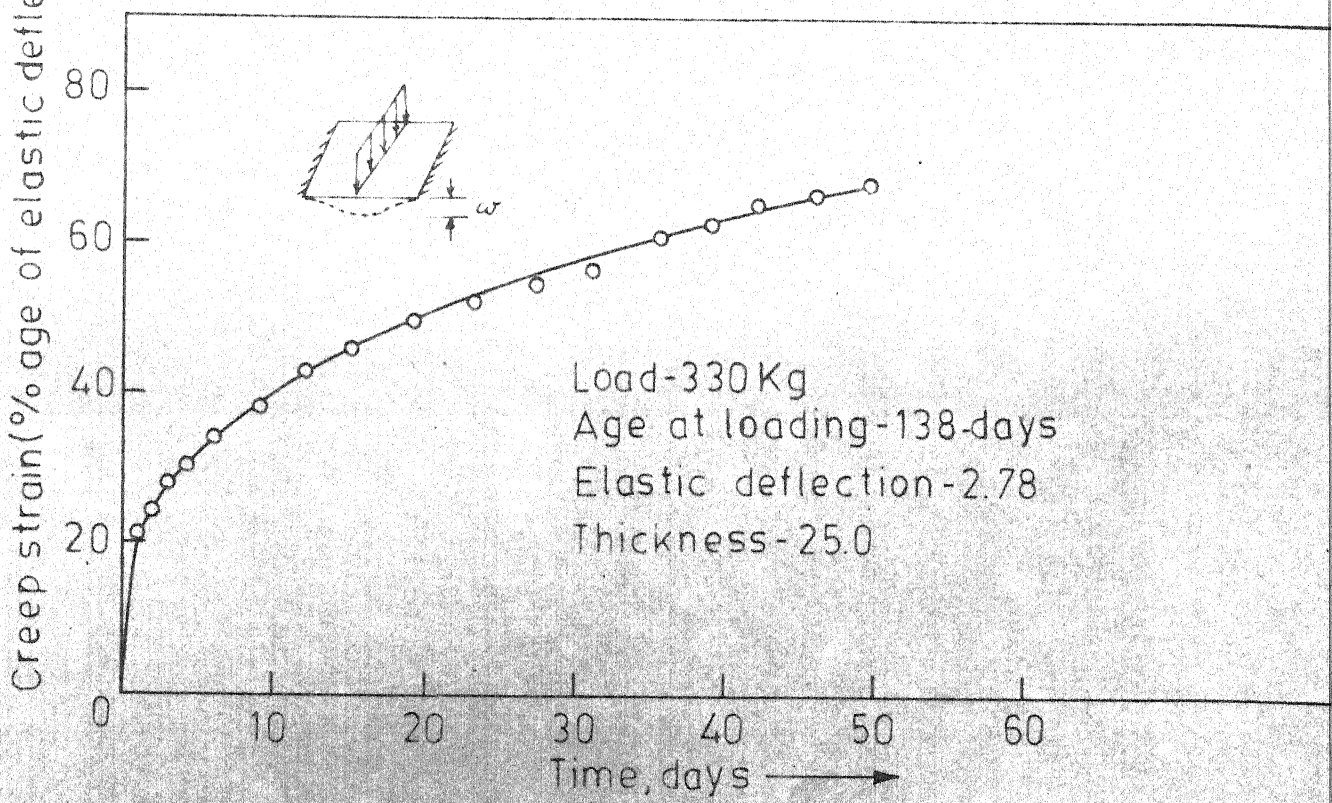

Figure 4.16 - Creep-Time Relationship for 4C5.

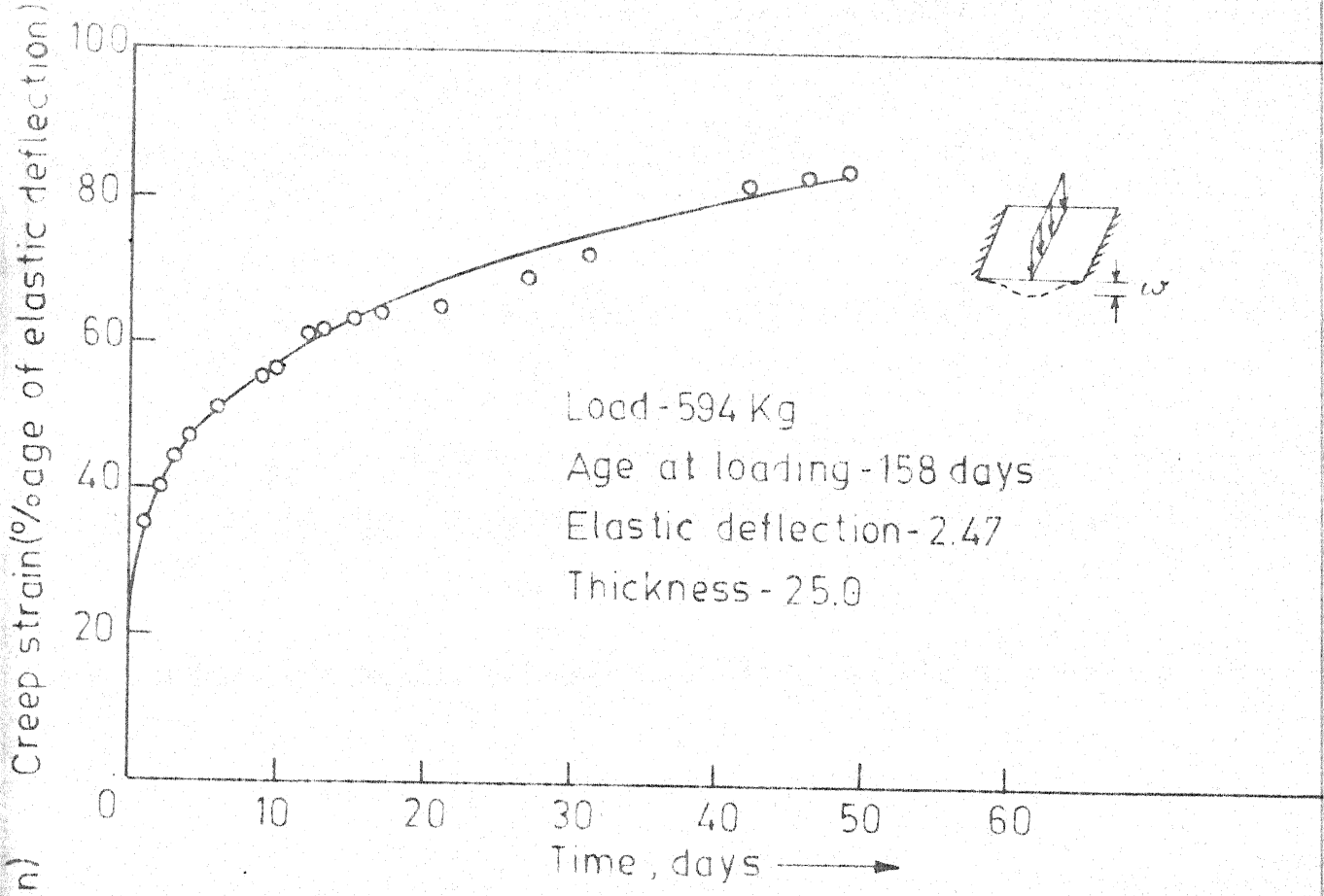

Figure 4.17 - Creep - Time Relationship for 4C6.

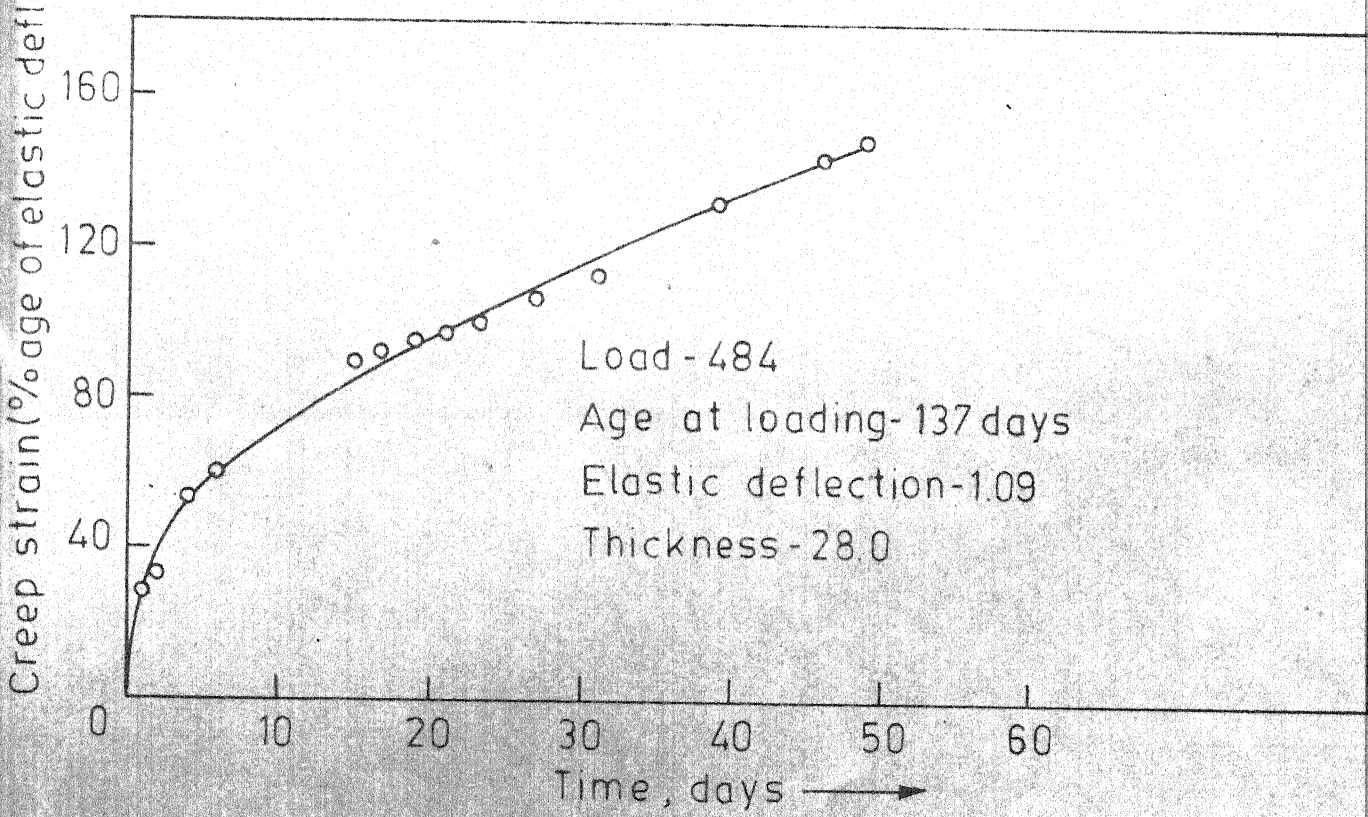

Figure 4.18 - Creep - Time Relationship for 6C8.

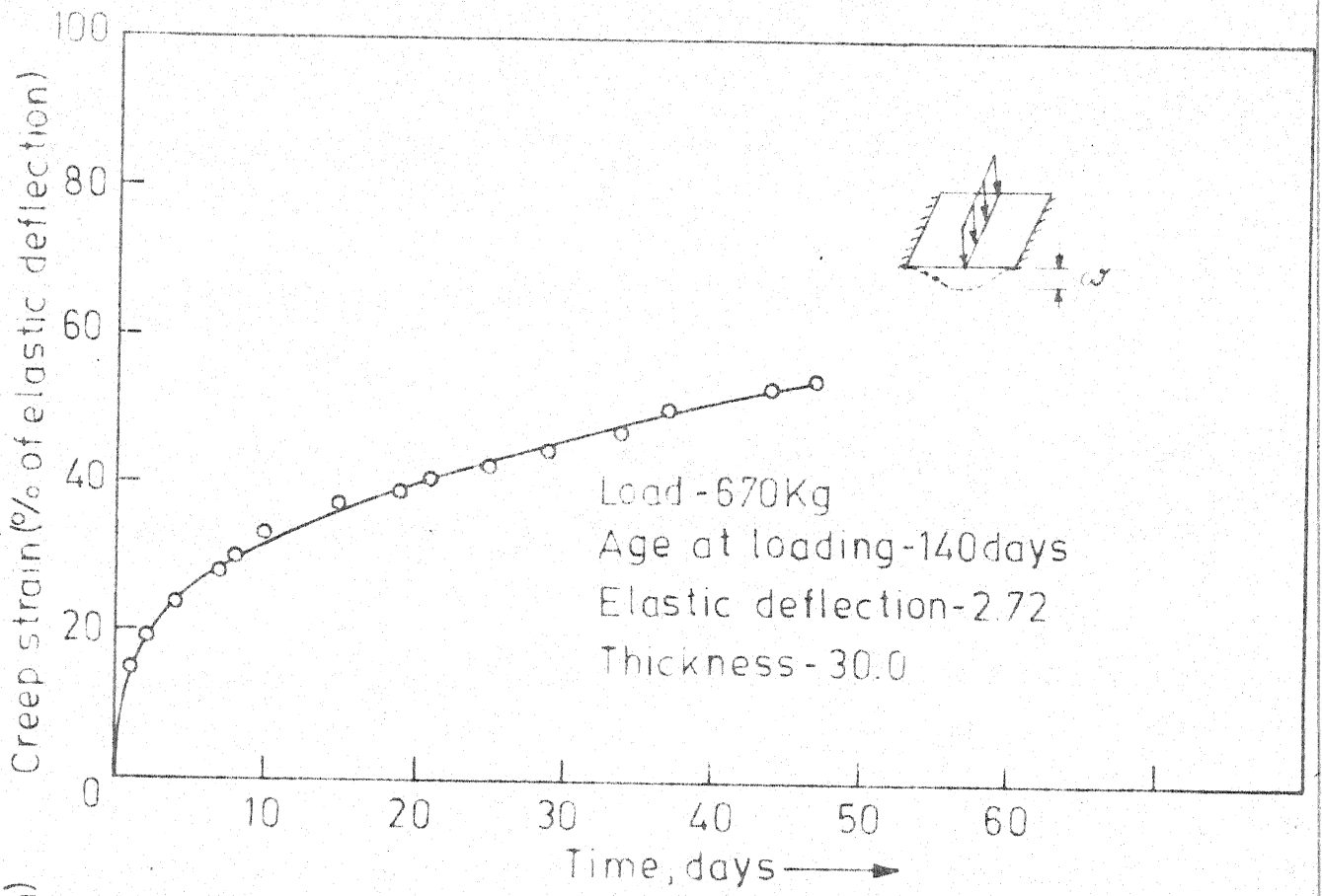

Figure 4.19 - Creep - Time Relationship for 8C6.

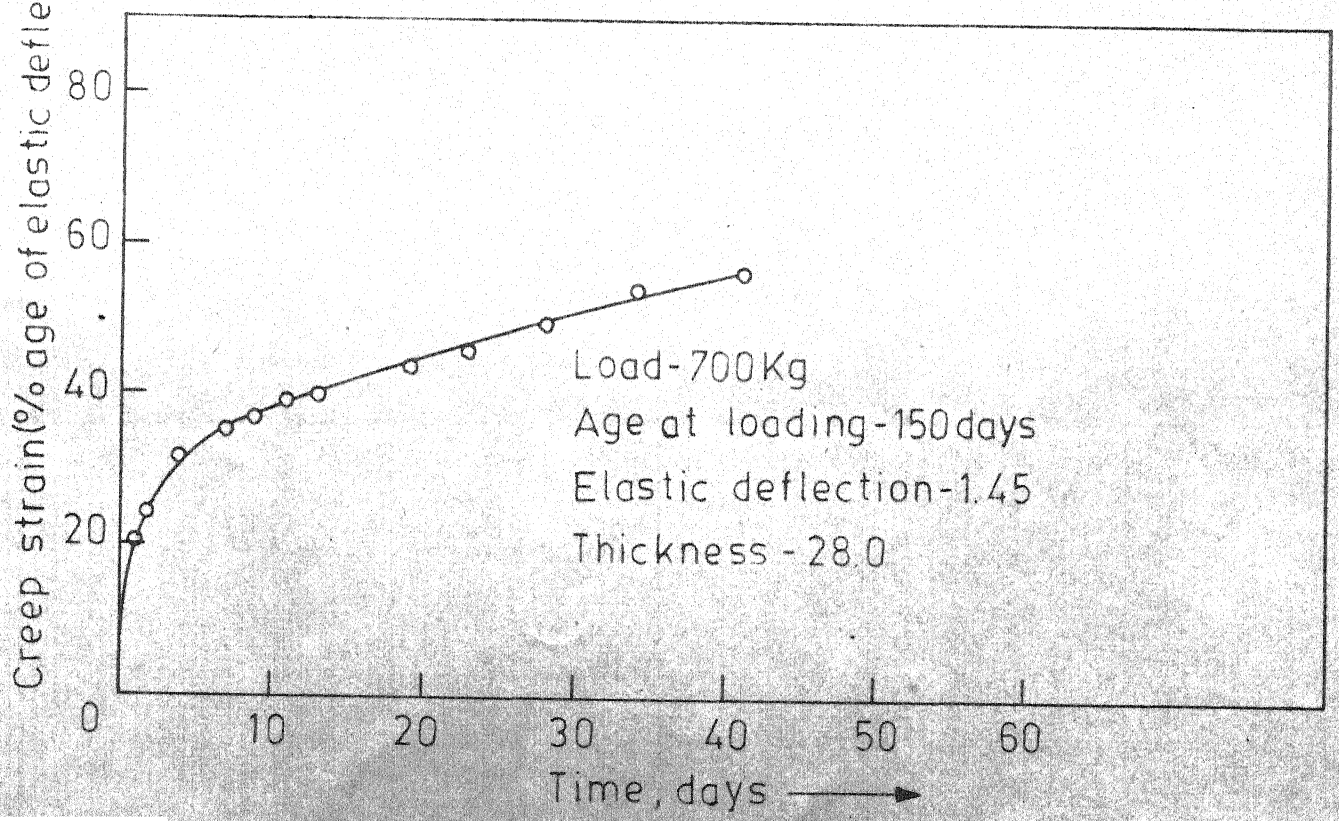

Figure 4.20 - Creep-Time Relationship for 6C7.

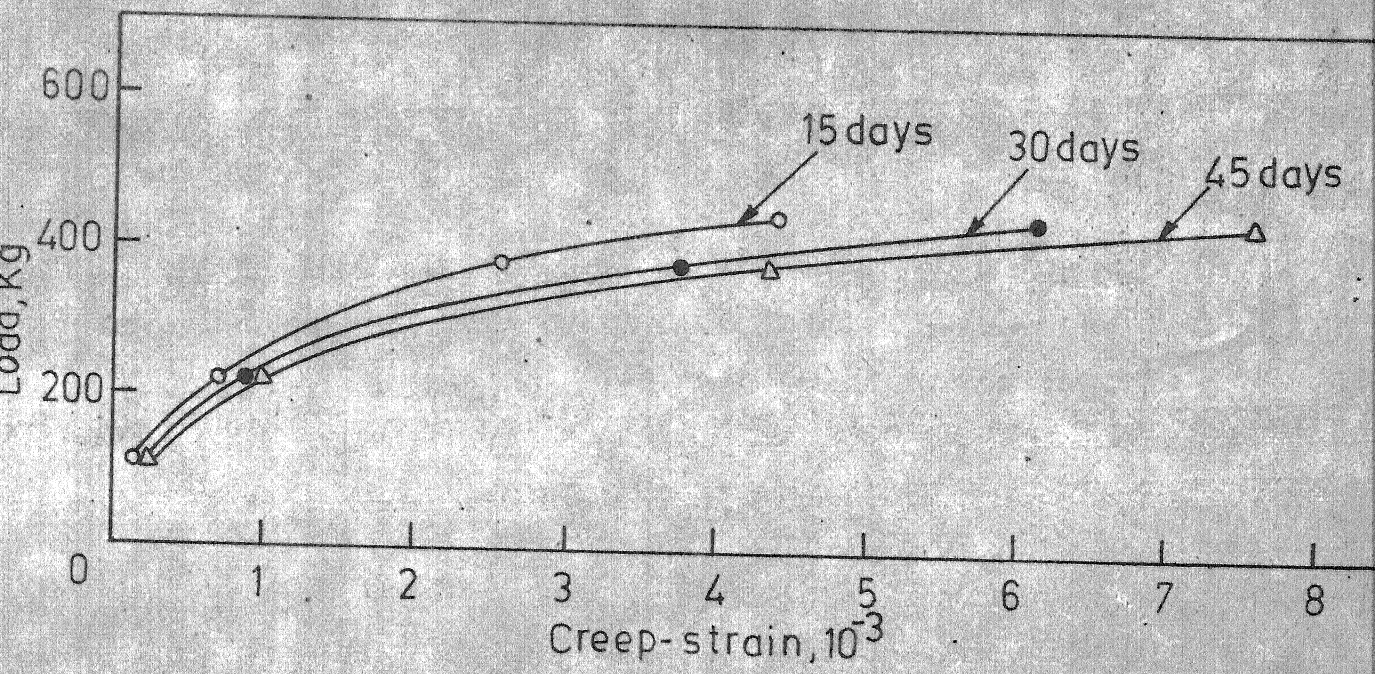

Figure 4.21 - Load - Creep Relationship for 4 C specimens.

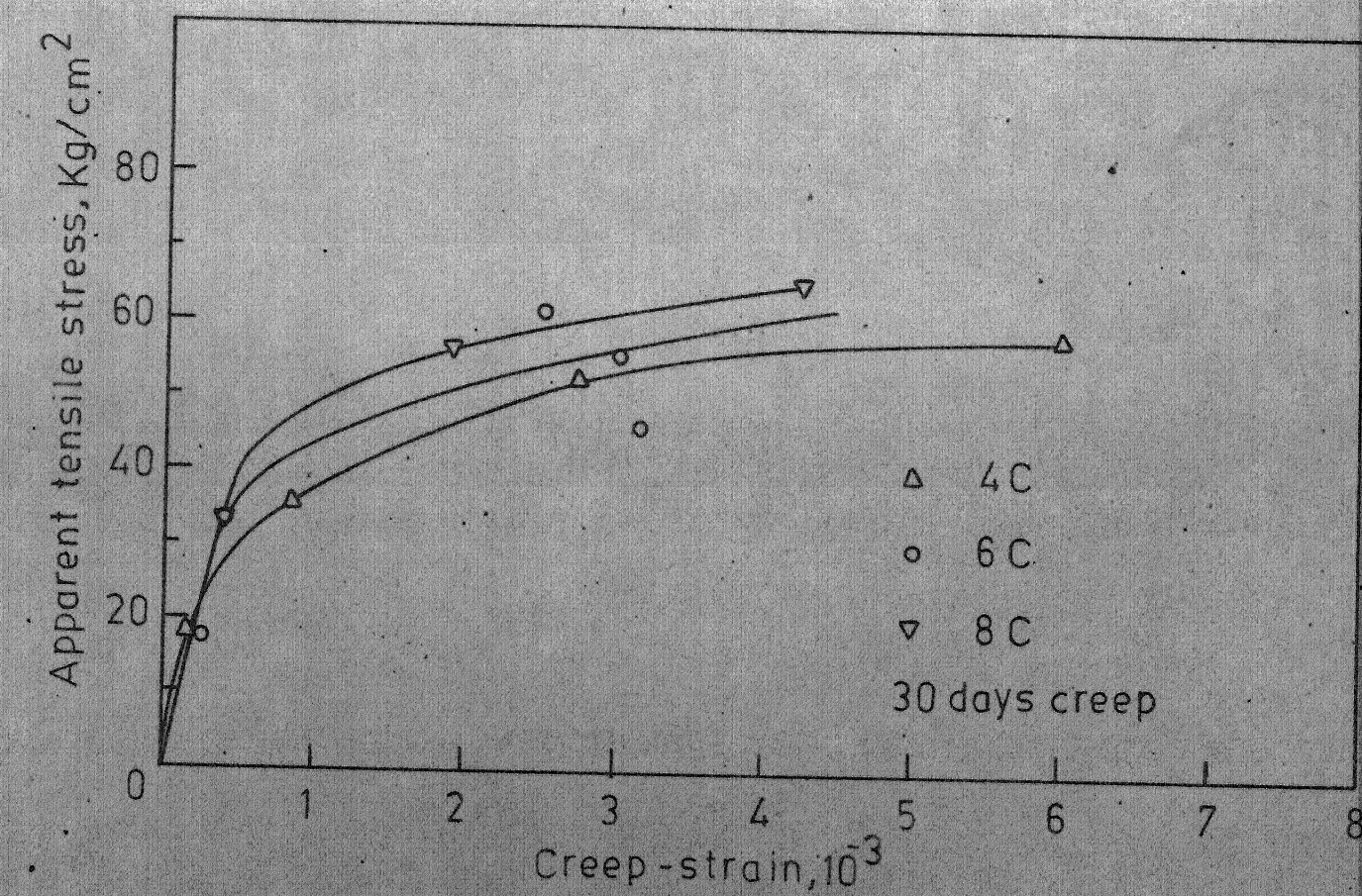

Figure 4.22 - Stress - Creep Relationship.

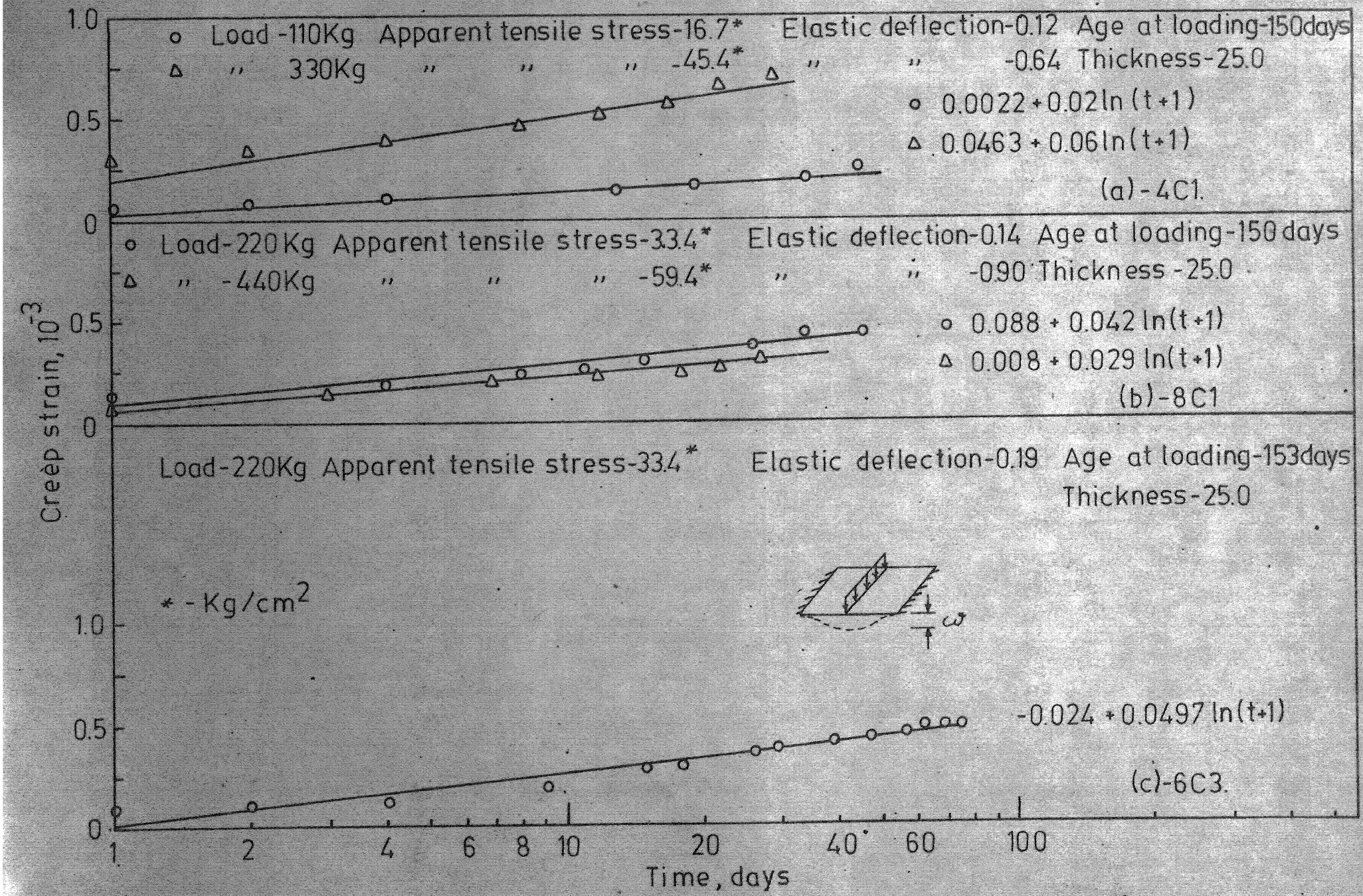

Figure 4.23-Creep-Ln(t+1) Relationship.

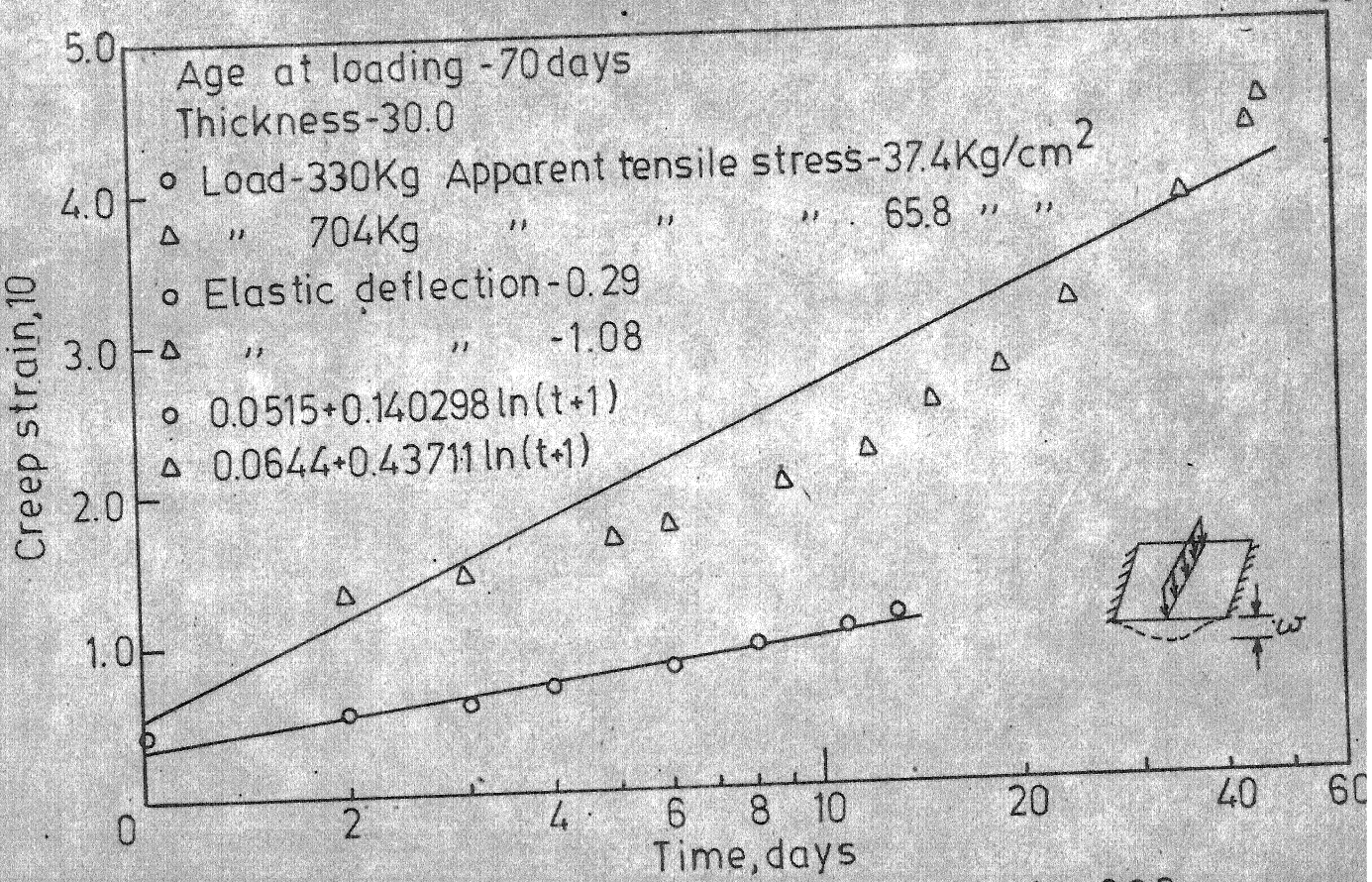

Figure 4.24-Creep-Ln(t+1) Relationship for 8C3.

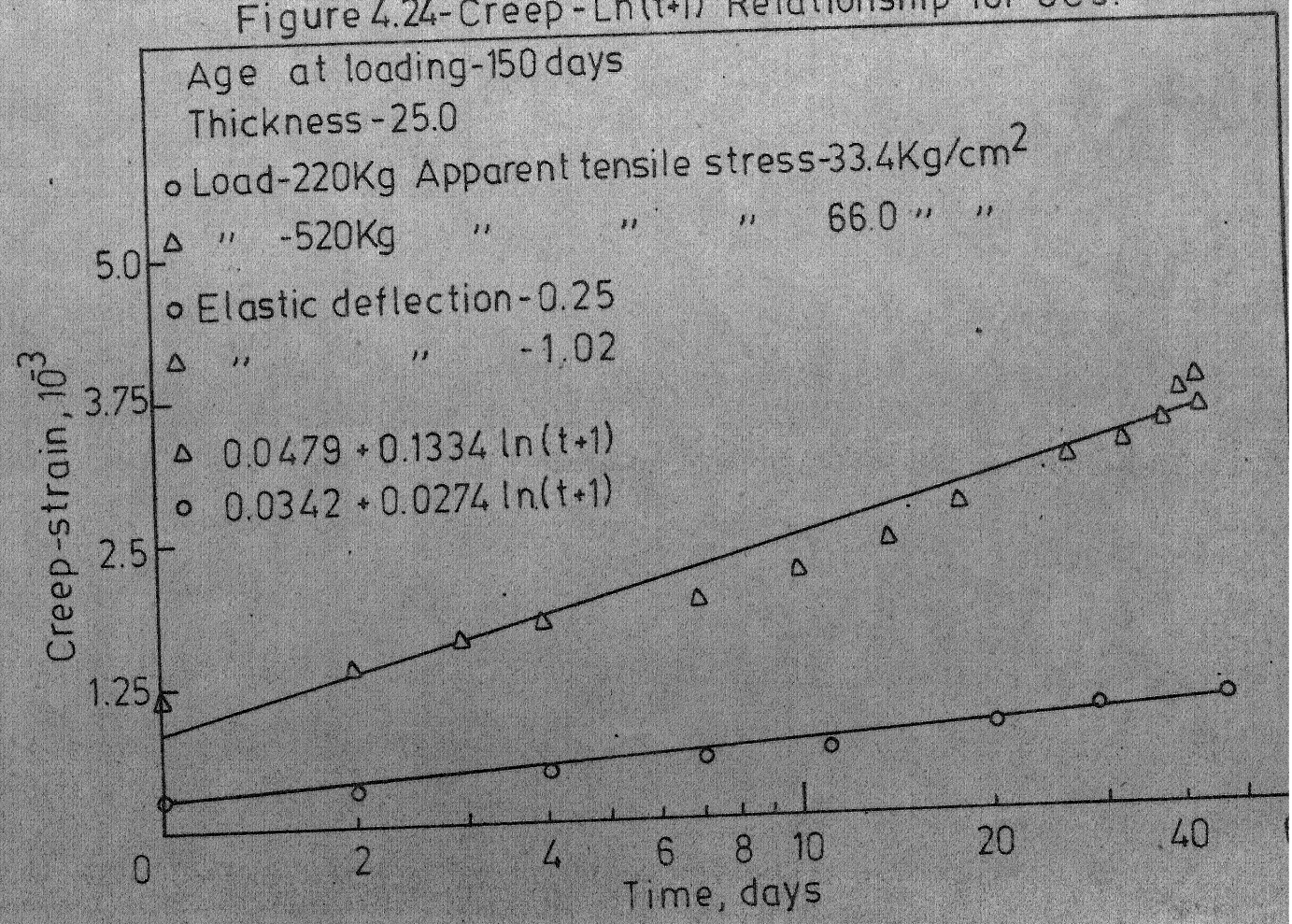

Figure 4.25-Creep-Ln(t+1) Relationship for 6C2.

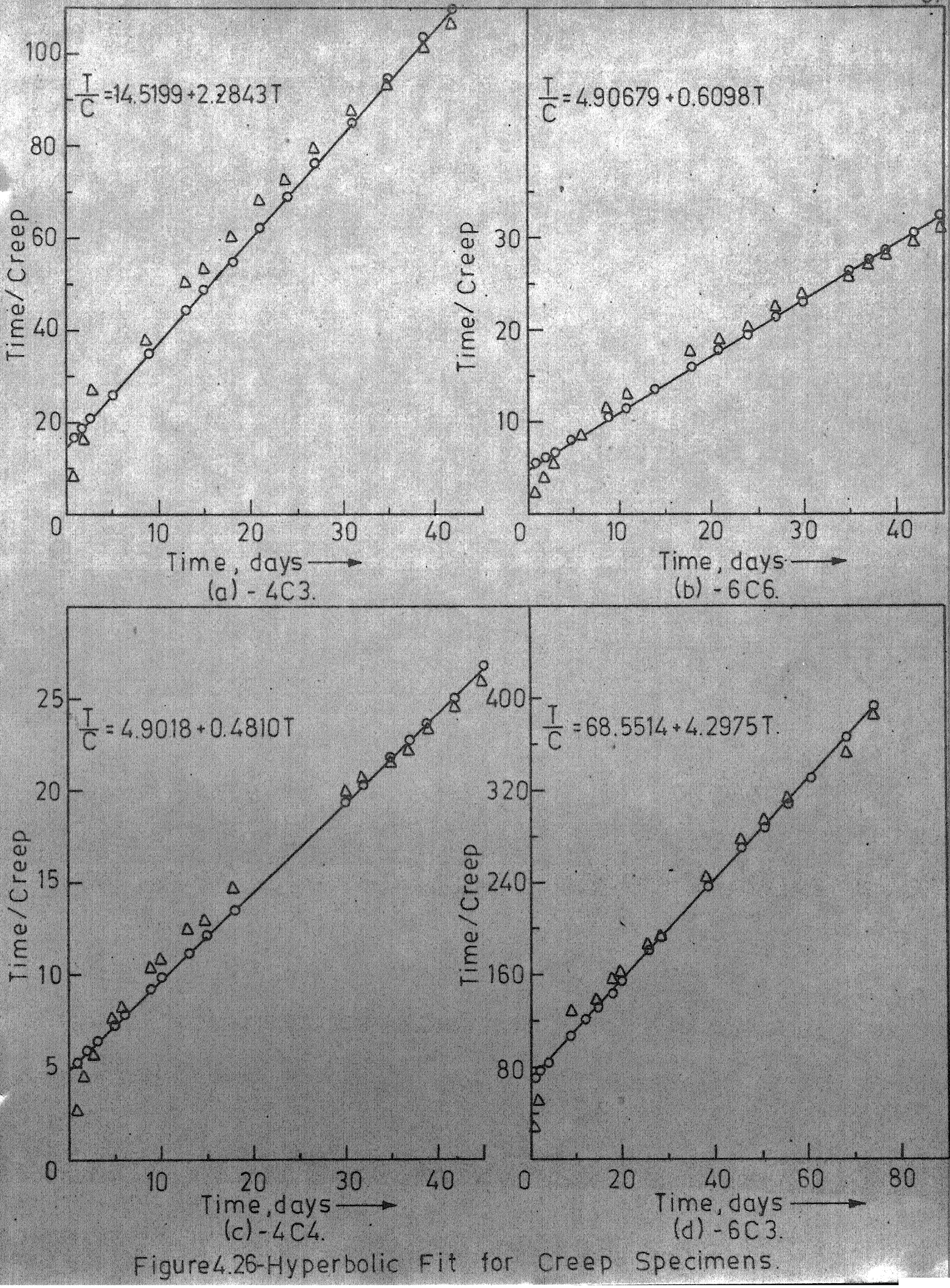

Figure 4.26 - Hyperbolic Fit for Creep Specimens.

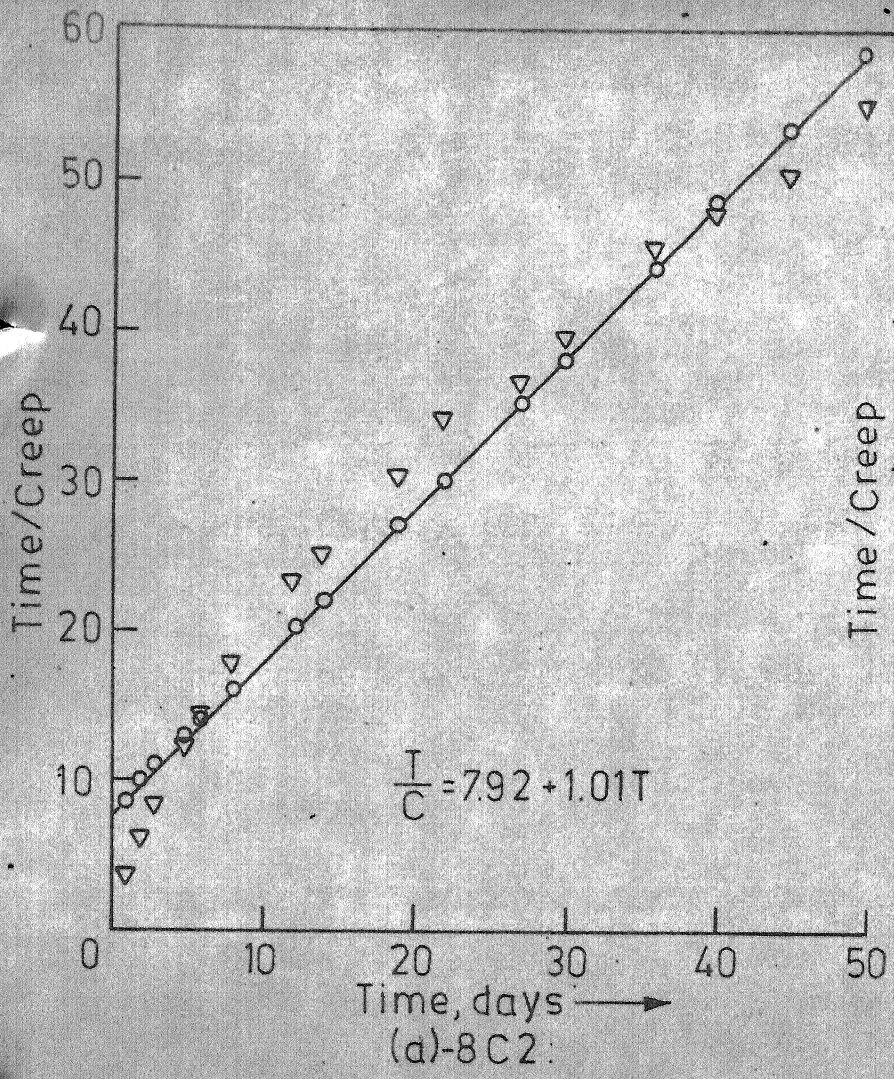

(a)-8C2.

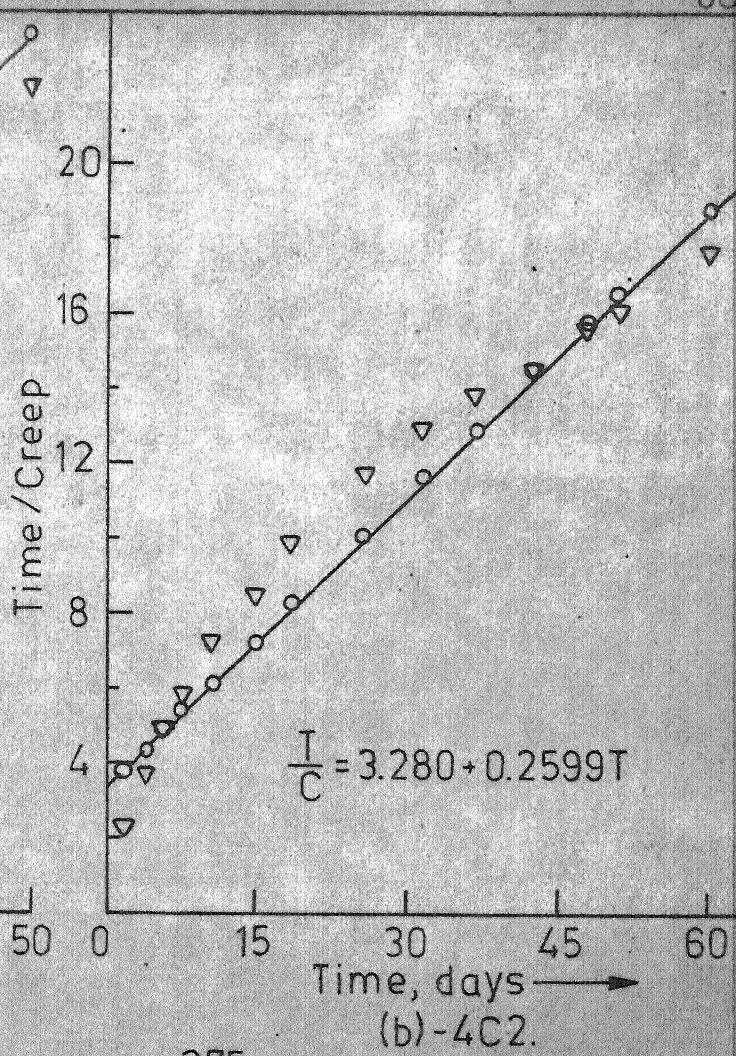

(b)-4C2.

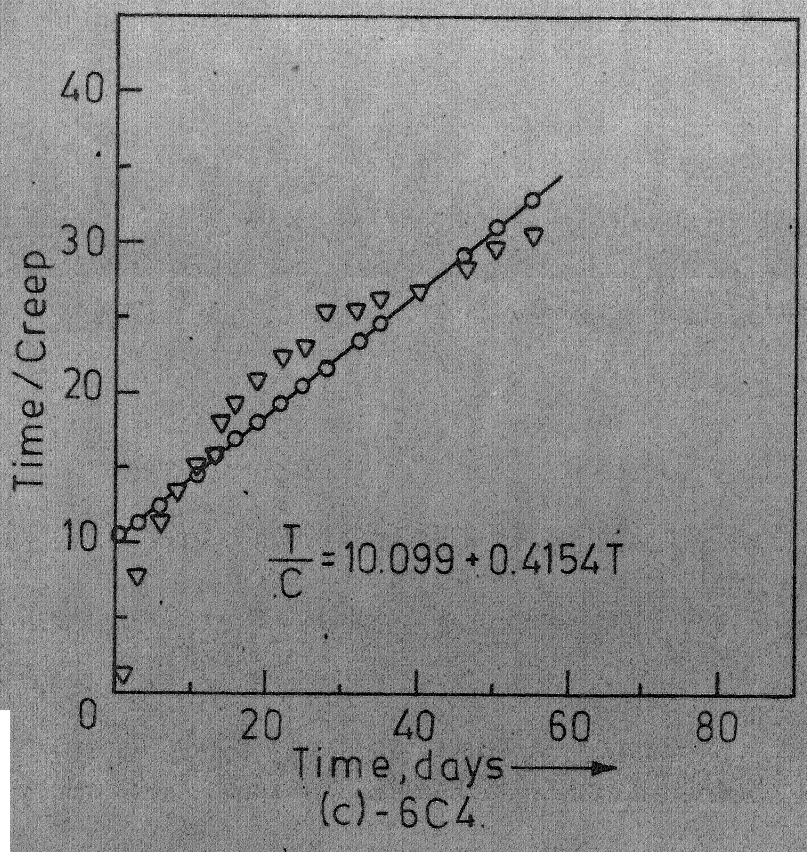

(c)-6C4.

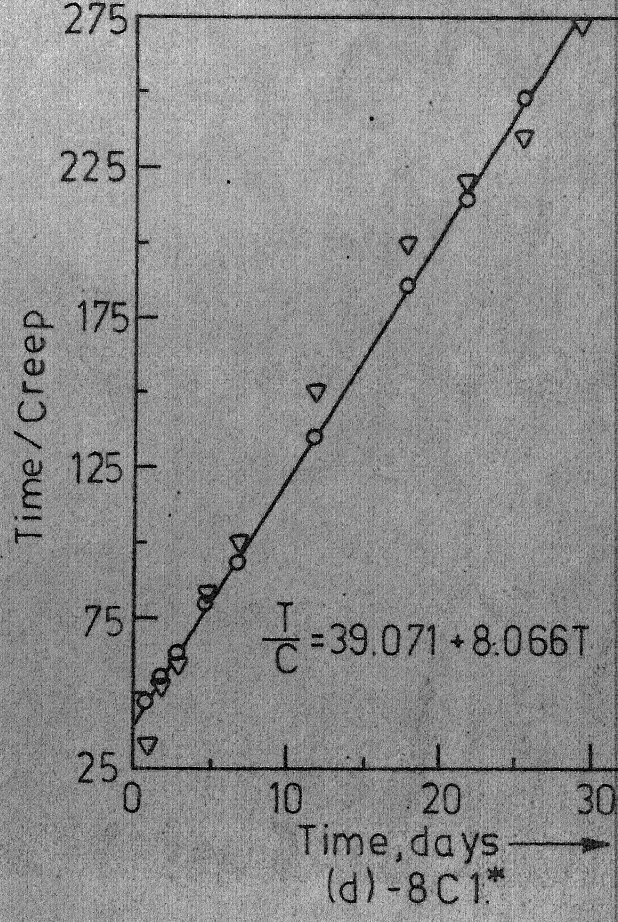

(d)-8C1.*

Figure4.27-Hyperbolic Fit for Creep Specimens.

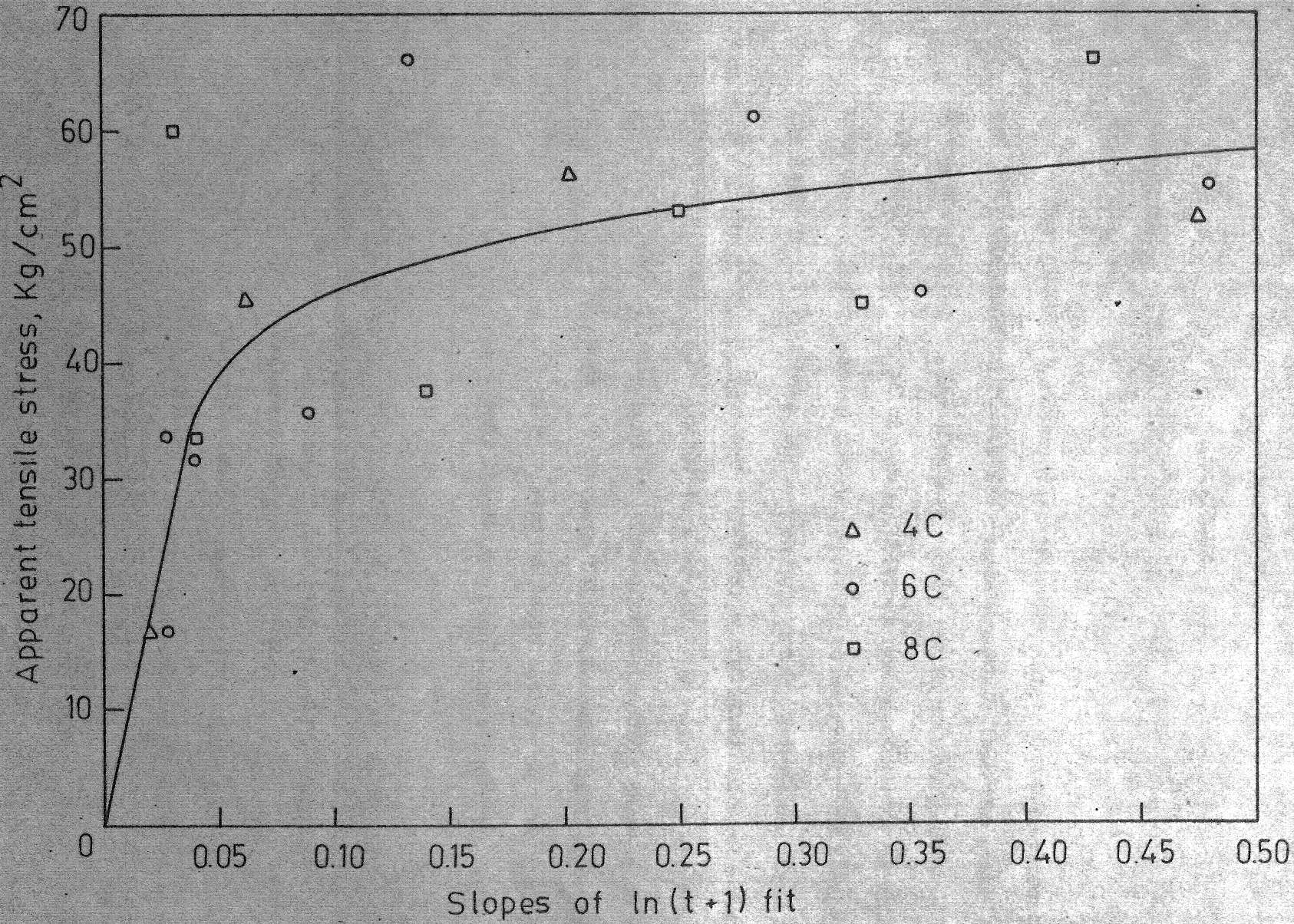

Figure 4.28 - Apparent Tensile Stress - Slope of Ln(t+1) Fit.

CHAPTER V

FATIGUE

5.1 General

Fatigue is a process of progressive permanent internal change in material subjected to repetitive stresses smaller than the static strength. These changes may be damaging and result in progressive growth of cracks and complete failure if stress repetitions are sufficiently large. Fatigue strength is influenced by the range, rate, eccentricity and history of loading besides material property and environmental conditions. Even for metals, experiments indicate that some crystals in a stressed element reach their limit of elastic action sooner than others, and eventually after many repetitions of stress, some minute elements rupture. This phenomenon results in progressive fracture and complete failure.Somewhat similar conditions occur in concrete. It appears reasonable to explain fatigue through fracture mechanics as it is an energy absorbing phenomenon which accumulates with each cycle of loading.

5.2 Griffith's Criterion for Rupture

Griffith (6) attacked the problem of rupture of elastic solids from energy approach. The criterion for rupture of linearly elastic brittle material in which crack exists prior to the application of load states that the crack will propagate spontaneously if the elastic energy release due to unit increase in the crack area is at least equal to the surface energy absorbed by the newly formed surfaces of the crack. Mathematically the

hypothesis states that

$$\frac{\partial U}{\partial a} \geq \frac{\partial W}{\partial a} \qquad \ldots (5.2.1)$$

where $2a$ - the length of existing crack or flow,

U - the strain energy due to crack and

W - the surface energy absorbed by the surfaces of the crack.

For a plane stress problem with an infinite plate of unit thickness subjected to uniform tensile stress σ, with an elliptic crack length 2a existing, as shown in Figure 5.1, the elastic energy is given by

$$U = \frac{\pi \sigma^2 a^2}{E} \qquad \ldots (5.2.2)$$

where E - the Young's modulus of the material.

The surface energy is given by

$$W = 4Sa \qquad \ldots (5.2.3)$$

where S - the specific surface energy of the material.

In view of equation (5.2.1), equations (5.2.2) and (5.2.3) yield

$$S = \frac{\pi \sigma^2 a}{2E} \qquad \ldots (5.2.4)$$

A plot of equations (5.2.2) and (5.2.3) against crack length is shown in Figure 5.2 in which the slope of strain energy at X is equal to the slope

of the surface energy. It is obvious that for point beyond X, the crack is unstable, since increase in the released strain energy due to increase in crack length will be more than the increase in the surface energy for the crack length. It is obvious from equation (5.2.4) that if crack or flaw length is very small, the strength of material will be very high. But the relation has its limitations since, for zero flaw length, the theoretical strength is infinity, which is not true. However, equation (5.2.4) suggests that if a brittle material like concrete has no flaws, its tensile strength would be equal to compressive strength. For convenience the left hand side of equation (5.2.2) is designated by G and the critical value of G for which unstable crack extension takes place is denoted by G_c. In view of the fore-mentioned notations

$$G \geq G_c \qquad \ldots (5.2.5)$$

G_c is also termed as the 'fracture toughness' of the material.

Irwin (78) and Orwan (79) extended the Griffith criterion for crack extension in the brittle materials to ductile materials by considering work associated with the plastic flow at the tip of the crack. The criterion for the crack extension in the ductile material may be given by

$$\frac{\partial U}{\partial a} = \frac{\partial}{\partial a}(W + V) \qquad \ldots (5.2.6)$$

where V - the work done due to plastic deformation.

The second term of the right hand side of equation (5.2.6) is much larger

than the other term for ductile materials and hence the length of crack required for unstable propagation is much more when compared to brittle materials. Narayan Swamy (80) advanced a very general form of energy balance criterion for crack propagation written as follows

$$\Delta U = \Delta [f_1(a) + f_2(a, \sigma, t, \delta) + f_3(a^2, \sigma^2, E^2, \dot{a}^2) - f_4(a) - f_5(a^2, \sigma^2)] \quad \ldots (5.2.7)$$

where f_1 - the surface energy, function of crack length,

f_2 - the time-dependent irrecoverable deformation, function of crack length a, stress level σ, time t and other parameter δ,

f_3 - the kinetic energy of crack propagation dependant on $\dot{a}$, the crack velocity,

f_4 - the energy at stress concentration and

f_5 - the energy of the applied stress field.

Sneddon (81) considered the elastic analysis and then related the Griffith problem of a penny shaped crack and helped to disclose the fact that the elastic stress field in the neighbourhood of a crack can be represented by

$$\sigma_{ij} = \frac{1}{\sqrt{r}} \left[K_1 f^1_{ij}(\theta) + K_2 f^2_{ij}(\theta) + K_3 f^3_{ij}(\theta) \right] + \ldots \text{ other non-singular terms} \quad \ldots (5.2.8)$$

where σ_{ij} - the stress components,

K_1, K_2, K_3 - the stress intensity factors of the dimensions psi $\sqrt{in}$,

r, θ - the coordinates characterising the location of the point at which stress field is sought and

$f_{ij}^1, f_{ij}^2, f_{ij}^3$ - the scalar functions of θ.

The equation (5.2.8) reflects readily the so called crack tip singularity and K_1, K_2 and K_3 are consequently known as stress intensity factors which are dependent on the Young's modulus and crack length. The evaluation of K_1, K_2 and K_3 in any particular problem is adequate to characterize the stress field around the crack tip as far as fracture problems are concerned. The literature on fracture mechanics has been critically reviewed by Rao (82).

5.3 Concrete - Fracture Mechanics

The concept of largest flaw size for determination of tensile strength of concrete appears to be reasonable since the concrete of rich mixes and better composition gives much improved tensile strength. Since the fracture toughness, G_c of concrete is very low, concrete is a very flaw sensitive material. The crack length required for its unstable propagation under a given stress condition is very small. Microcracks or flaws do exist in concrete or mortar even at no loads. These facts give strong hold for the application of fracture mechanics to study the important properties of concrete like tensile strength, fatigue strength etc., as the Griffith

theory assumes an initial crack for the material failure. However, due to the nonhomogeneity of concrete/mortar, the theory is to be modified. Glucklish (83) suggested a nonlinear energy absorption curve, as shown in Figure 5.3, for concrete to account for its nonhomogeneous nature. The propagation of cracks in this case is intermittent. As shown in Figure 5.3, when the stress is sufficiently large for a crack a_0 to propagate, it extends to a_1, where the energy requirement is changed and thus the structural element can take more stress with crack length a_1 and it continues till the stress level is sufficient to make the strain energy release rate at least equal to the rate of the surface energy at that particular crack length.

5.4 Fracture Toughness of Concrete

Kaplan (84) applied the fracture mechanics to concrete with great success assuming that there is no plastic flow around the tip of the crack. Two independent analytical methods for determination of G_c were developed. It is reported that the values of G_c so found differ considerably from the experimental values reported by Romualdi and Batson (10). Kaplan reported the value of G_c equal to 0.1 in lb/in^2 by one method and 0.01 in lb/in^2 by other method, whereas value reported by Romualdi and Batson was 0.03 to 0.07 in lb/in^2.

5.5 Application of Fracture Mechanics to Ferrocement

Romualdi and Batson (85) were perhaps the first to apply fracture mechanics concepts to study the improved behaviour of concrete under tensile

loads. They observed similarity between riveted stiffness in a plate and reinforcing bars in concrete. This has already been explained in Chapter I. The application of fracture mechanics to concrete shows the need for its improving fracture toughness. This is achieved by reinforcing concrete with very closely spaced thin wires of high modulus dispersed throughout the matrix. This not only improves the fracture toughness, but also the crack arrest mechanism. The thin wires located normal to the plane of crack create a differential strain between two materials. Consequently, shear force along the stiffer element will tend to prevent the crack opening as far as bond force forces along stiffer elements are not exceeded. These forces produce a stress intensity factor of magnitude K_b which has an opposite sense to the stress intensity factor K_σ due to uniform tensile stress σ. Thus the total intensity factor is given by

$$K_t = K_\sigma - K_b \qquad \ldots (5.5.1)$$

The reformulated crack propagation condition is now

$$K_t \not< K_c \qquad \ldots (5.5.2)$$

where K_d, the critical intensity factor is a material property of the ferrocement composite to be determined experimentally.

The inelastic behaviour of a specimen under pulsating loads is due to the presence of cracks. Also the inelastic strains increases with increase in crack width. With increasing number of load cycles, extra elastic energy

is stored. Thus, the criterion for the fatigue failure can be laid similar to the Griffith criterion for tensile stress field as the strain energy stored during a fatigue test, in specified number of load cycles, for unit increase in crack length must be at least equal to the surface energy of the newly formed surfaces. It is very difficult to measure the surfaces formed by microcracks in concrete or mortar. The inelastic strain due to this increase in crack length may be very small, but the cumulative effect of this additional small amount of strain energy at each cycle will be large enough for small loads to cause failure. It is also obvious that more the G_c greater will be the fatigue strength.

5.6 Fatigue Strength of Concrete

The influence of various factors on the fatigue strength of concrete/mortar is briefly reviewed here. The detailed descriptions are given in Recommendations of ACI Committee (86), Neville (74) etc. The fatigue strength under compressive, tensile or flexural load for 10^7 cycles is observed to be 55 percent of the static strength. The frequency of loading between 70 to 1000 cycles per minute has little effect on the fatigue strength. Most of the permanent deformation takes place in the early stages of test, usually the first few thousand cycles. The secant modulus of elasticity decreases with repeated loads. It is reported that as the range of stress is decreased, the upper limit of stress is increased substantially.

The design for fatigue is facilitated by use of modified Goodman (87) diagram as illustrated in Figure 5.4. It is based on the observations that

fatigue strength of concrete is same whether the mode of loading is tensile, compressive or flexural. The range of loading has definite effect on the strength as indicated in Figure 5.4. For zero minimum stress level, the maximum stress the concrete can support for one million cycles is 50% of the static strength. As the minimum stress level is increased, the stress range that concrete can support decreases.

Cyclic loading below the fatigue limit improves the fatigue strength of concrete and it is observed that it exhibits higher static strength. The fatigue strength of concrete is increased by rest period. The increase is proportional in first 1 to 5 minutes, beyond which there is no increase.

For specimens subjected to random cyclic loads, Miner's hypothesis (88) states that

$$\sum \left(\frac{n_r}{N_r}\right) = 1 \qquad \ldots (5.6.1)$$

where n_r - the number of cycles applied at a particular stress condition and

N_r - the number of cycles which cause fatigue failure at the same stress condition.

If the upper stress level is below the fatigue limit, the stress-strain curve indefinitely remains straight and failure does not take place within the specified limit.

5.7 Test Procedure

The fatigue strength of slabs, clamped along two opposite edges with the other two free, were determined from central pulsating line loads applied parallel to the clamped edges. The details of the test setup and fatigue testing machine are described briefly in Chapter III. The loads were applied to test specimens in monotonically increasing order in increments of 80 kg to a predetermined upper load level for each specimen and the midspan deflection reading noted for each increment of load. The upper load limit of the pulsating loads for different test specimens varied between 60-90% of the ultimate load carrying capacity of the slabs tested under similar conditions. The load levels at the first visible cracks were noted carefully. The lower load limit of the pulsating loads for all thirty six slabs tested was kept at 440 kg due to the machine constraints as laid down in the operating manual. The machine was operated six to eight hours a day. The increase in the fatigue strength, if any, due to rest period is assumed to be uniform for all the specimens. All the specimens were tested at a load pulsating frequency of 500 cycles/minute. For the first thirty minutes, at the start of the pulsator, the frequency was maintained at 220 cycles/minute.

The incremental fatigue deflections at the end of each day and recovery in deflection over the next day were noted carefully. A few specimens were subjected to pulsating peaks, equivalent to 10-15% of the ultimate load, every six hours for a period of 60-120 seconds. Those specimens, which did not fail under pulsating loads upto prefixed number of cycles, were tested to collapse under static load.

The Tables 5.1 through 5.3 summarise the results of the fatigue test series. The deflection-load cycle relationships for some typical test specimens are shown in Figures 5.5 through 5.10. The single cycle load-deflection curves and load-deflection hysteresis loops for a few typical specimens have been presented in Figures 5.11 through 5.15 and mid-span deflection -log cycle plots for a few typical specimens in Figure 5.16.

5.8 Discussion of the Test Results

It was observed that although, the change in linearity in load-deformation curve occurred at load levels of 250-400 kg, the visible crack at the midspan or along the clamped edges was observed between 480 to 640 kg. This delayed appearance of cracks is attributed to the effective crack arrest mechanism of ferrocement.

The Figures 5.5 through 5.8 indicate that the residual deformation grows with the number of cycles until it reaches a stable condition and again it is observed to increase with load cycles till the failure occurs. This peculiarity was observed for the specimens subjected to low upper loads which caused endurance limit in the range of 1 to 3 million load cycles. Those specimens which failed within 10^6 cycles, exhibited a continuous increase in the residual deformation and also in deformation at upper load level. The residual deformation is termed as fatigue creep in the literature. The specimens were observed to recover some percentage of the residual deformation over the rest period. The fatigue deformations under pulsating loads decreased with an increase in the age at which load was first applied.

This characteristic was observed to be similar to the behaviour of specimens under sustained loadings presented in Chapter IV. The increase in total fatigue creep was greater for the specimens subjected to higher ranges of load. The kinks in the fatigue creep curves of Figure 5.16 are due to change in upper load levels or formation of additional microcracks. The deflection-cycles relationships are observed to be linear for slabs subjected to load levels less than the one that causes fatigue failure (2×10^6 cycles).

The test results demonstrate that ferrocement has high resistance to repeated loading. It is of interest to note that the lower load limit of 440 kg for all the specimens was approximately 180, 150 and 130% of cracking load and approximately 40, 31 and 25% of ultimate loads for 4F, 6F and 8F series (with # 19 gauge wire mesh), respectively. The slabs were observed to develop quite wide cracks at upper load levels of 680 kg to 1200 kg under single cycle of loads. Even under these severe cracks, the specimens withstood upto 2×10^6 load cycles, clearly indicating that the closely spaced thin wires arrest crack propagation efficiently.

The load-deformation curves, shown in Figures 5.11 and 5.12, become linear with increasing number of cyclic loading. The concavity of the load-deformation curves towards the load axis indicates how near to failure the specimen is. The Figure 5.12(d) shows load-deformation curve for specimen 8F3 at 1.708×10^6 load cycles. The specimen finally failed at 2.12×10^6 cycles. The stiffness of the specimens is observed to decrease, to a limited extent, due to repeated loads, but it stablizes after several repetitions as shown in Figure 5.11(c) and 5.15.

The Figures 5.13 through 5.15 demonstrate that the areas under hysteresis loops decrease with the number of load cycles. The areas stabilise after several load cycles, in case of those specimens which are not near the fatigue limit. The hysteresis loop areas again increase for those specimens which fail under pulsating loads. The difference between energy stored during loading and the energy given up during unloading is dissipated in some manner during each cycle. Part of this energy causes microcracks to nucleate and macrocracks to feed on small surrounding cracks.

A few specimens were subjected to peak loads of short durations (60 to 120 seconds) to study the effect of the same on the fatigue loads. These peak loads were in general 15% of the upper load levels. It was observed that if the upper load level was sufficiently high to cause failure within 2×10^6 cycles of load, the peak loads at intervals of 6 hours accelerated the failure. No appreciable effect of peak loads on the endurance limit or fatigue creep was observed, if upper load level was quite small.

From the limited data, an attempt has been made to draw S-N curves which are shown in Figure 5.17. The apparent tensile stress levels have been calculated by making use of relations shown in Appendix A. The tests reported here are preliminary in nature. The characteristics of the ferrocement slab under pulsating loads at lower stress levels are not studied. These may be quite different and hence no extrapolation of the S-N curves is possible.

The failure of a specimen under repeated loading was distinctly different from a failure under static test. Those specimens which failed

under pulsating loads underwent larger deformations, indicating that ferrocement has ability to deform plastically through microcracking mechanism. A close observation of the specimens failing under repeated flexural fatigue showed that the fracture of wire was in the plane of the mortar. Whereas, the broken wires in the specimens tested under static loads were characteristically tensile. At the collapse, very clear yield lines, one at the mid-span and two along the clamped edges were noticed as shown in Figure 5.18. The static flexure tests performed on the specimens, not failed in fatigue, yielded results within the limits of their virgin parallels.

Great variation in fatigue life is observed in spite of the fact that 'identical' specimens are run under 'identical' conditions. Hence for interpretation of the fatigue experiments, the use of statistical methods is a necessity in modern technology. However, the statistical methods are not attempted here due to lack of compatible sample size. The most convenient method of treating fatigue test data is Weibull distribution.

From the foregoing discussion it is quite clear that ferrocement has a tremendous potential for use wherein high resistance to fatigue is required.

Table 5.1 - Summary of Flexural Fatigue Tests on 4F Series

S.No.	Average thickness mm	Age at testing days	Upper load kg	Change in load		Peak every six hours kg	Cycles 10^6	Sample failed	ultimate load kg
				to kg	at cycles 10^6				
4F1	25.0	72	720	-	-	-	0.282	Yes	-
4F2	25.0	139	880	-	-	-	2.075	Yes	-
4F3	25.0	37	720	-	-		1.40	Yes	-
4F4	25.0	68	720			1040	2.43	Yes	-
4F5	25.0	125	800	-	-	920	1.914	No	1120
4F6	25.0	119	960	-	-	-	0.010	Yes	-
4F7	25.0	138	880	-	-	-	0.740	Yes	-
4F8	25.0	169	880	-	-	-	0.073	Yes	-
4F9*	25.0	125	680	-	-	-	0.666	Yes	-
4F10*	25.0	145	720	-	-	-	0.414	Yes	-

* With 22 gauge wire

Table 5.2 - Summary of Flexural Fatigue Tests on 6F Series

S.No.	Average thickness mm	Age at testing days	Upper load kg	Change in load		Peak every six hours kg	Cycles 10^6	Sample failed	Ultimate load kg
				to kg	at cycles 10^6				
6F1	25.0	55	680	760,800 840,880	1.7, 2.9,3.0	-	3.02	Yes	-
6F2	25.0	89	800	-	-	-	2.05	No	1040
6F3	25.0	104	800	-	-	-	2.05	No	1080
6F4	25.0	118	800	-	-	-	0.30	Yes	-
6F5	25.0	124	800	-	-	-	2.145	No	1200
6F6	28.0	44	800	880,960 1040	2.0,2.3 2.6	-	2.66	No	1440
6F7	28.0	62	920	-	-	-	1.14	Yes	-
6F8	28.0	89	1000	-	-	1120	0.707	Yes	-
6F9	28.0	103	960	-	-	1120	0.537	Yes	-
6F10	28.0	141	1000	-	-	-	1.06	Yes	-
6F11	28.0	154	1000	-	-	-	1.11	Yes	-
6F12*	28.0	133	800	-	-	-	0.731	Yes	-
6F13*	28.0	143	800	-	-	-	1.14	NO	1080

* With ~~//~~ 22 gauge wire

Table 5.3 - Summary of Flexual Fatigue Tests on 8F Series

S.No.	Average thickness mm	Age at testing days	Upper load	Change in load		Peak every six hours	cycles 10^6	Sample failed	Ultimate load kg
				to kg	at cycles 10^6				
8F1	30.0	57	1000	-	-	-	2.45	Yes	-
8F2	30.0	82	920	1000	0.761	1200	2.78	No	1760
8F3	30.0	72	1080	-	-	1240	2.12	Yes	-
8F4	30.0	106	960	-	-	1120	2.00	No	1440
8F5	30.0	134	1200	-	-	-	0.120	Yes	-
8F6	30.0	153	1120	-	-	-	0.165	Yes	-
8F7	30.0	142	1120	-	-	-	0.592	Yes	-
8F8	30.0	156	1120	-	-	-	0.311	Yes	-
8F9*	30.0	128	800	880	1.46	-	1.60	No	1120 kg
8F10	30.0	155	1120	-	-	-	0.292	Yes	-
8F11*	30.0	146	1000	-	-	-	0.010	Yes	-

* With 22 gauge wire

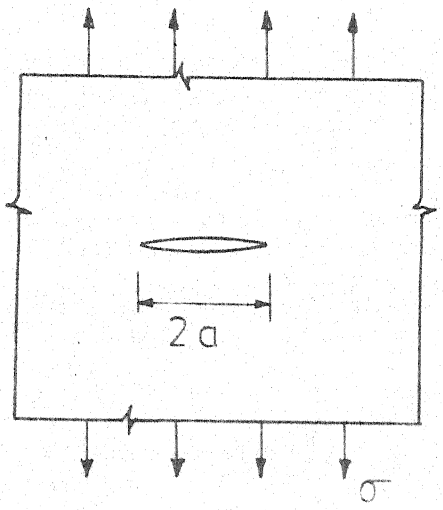

Figure 5.1 - Uniaxial Tension in the Presence of a Crack.

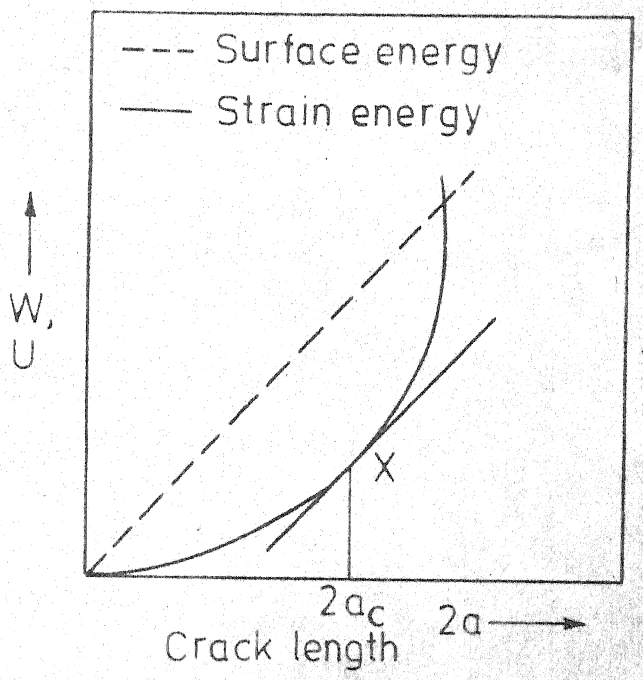

Figure 5.2 - Griffith's Fracture Criterion.

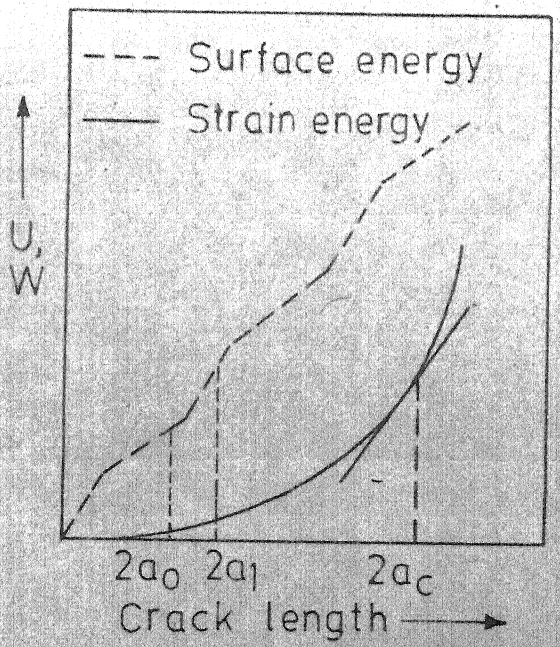

Figure 5.3 - Griffith's Criterion Applied to Non-homogeneous Concrete.

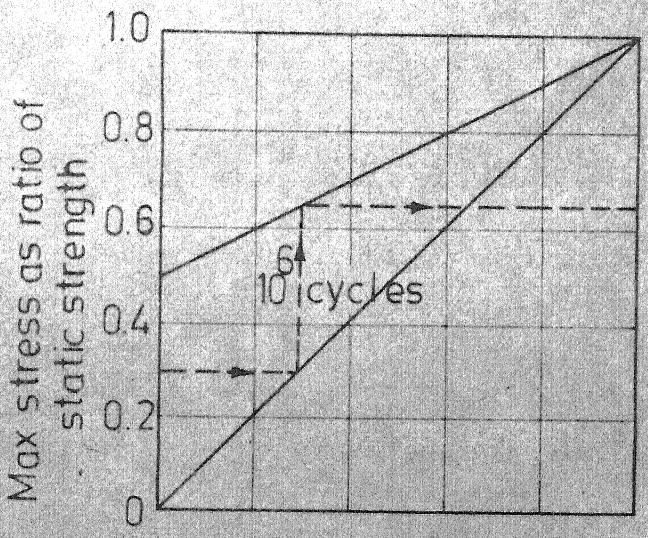

Figure 5.4 - Modified Goodman Diagram for Concrete.

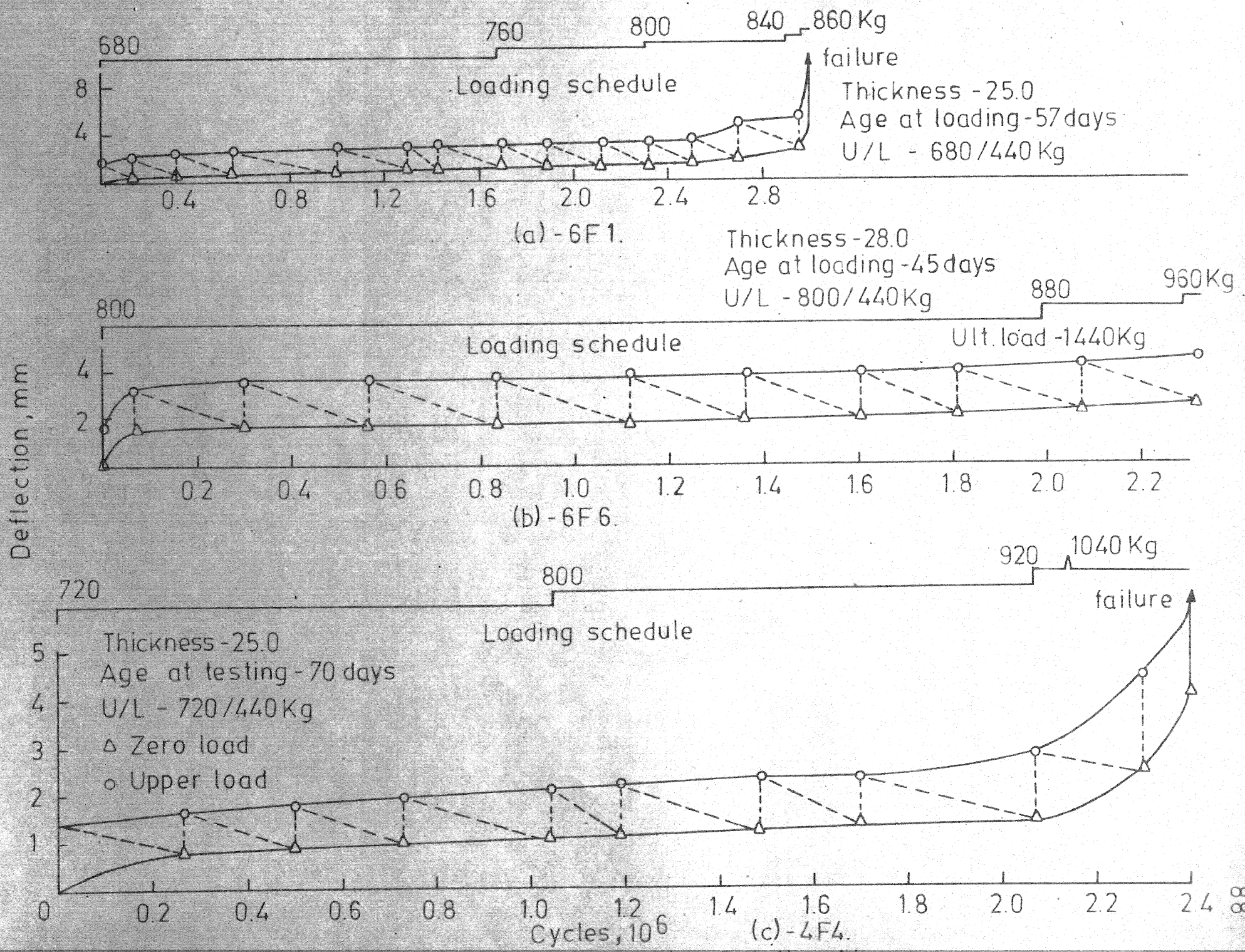
680
760
800
840
860 Kg
failure
Loading schedule
Thickness - 25.0
Age at loading - 57 days
U/L - 680/440 Kg
8
4
0.4
0.8
1.2
1.6
2.0
2.4
2.8
(a) - 6F 1.
Thickness - 28.0
Age at loading - 45 days
U/L - 800/440 Kg
880
960 Kg
800
Loading schedule
Ult. load - 1440 Kg
Deflection, mm
4
2
0.2
0.4
0.6
0.8
1.0
1.2
1.4
1.6
1.8
2.0
2.2
(b) - 6F 6.
920
1040 Kg
720
800
failure
Loading schedule
Thickness - 25.0
Age at testing - 70 days
U/L - 720/440 Kg
△ Zero load
○ Upper load
5
4
3
2
1
0
0.2
0.4
0.6
0.8
1.0
1.2
1.4
1.6
1.8
2.0
2.2
2.4
Cycles, 10^6
(c) - 4F4.

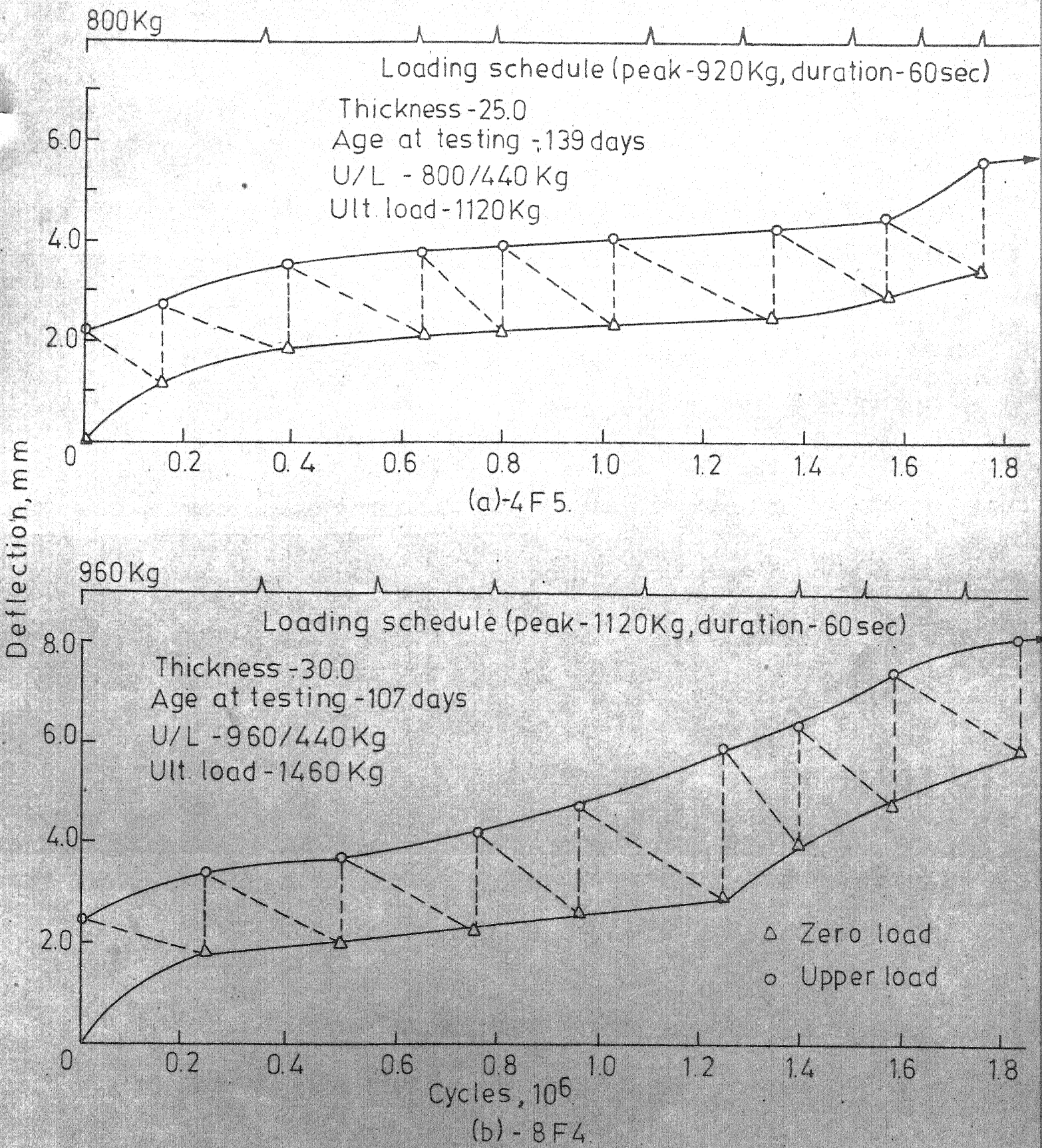

Figure 5.6 - Deflection - Cycle Relationship.

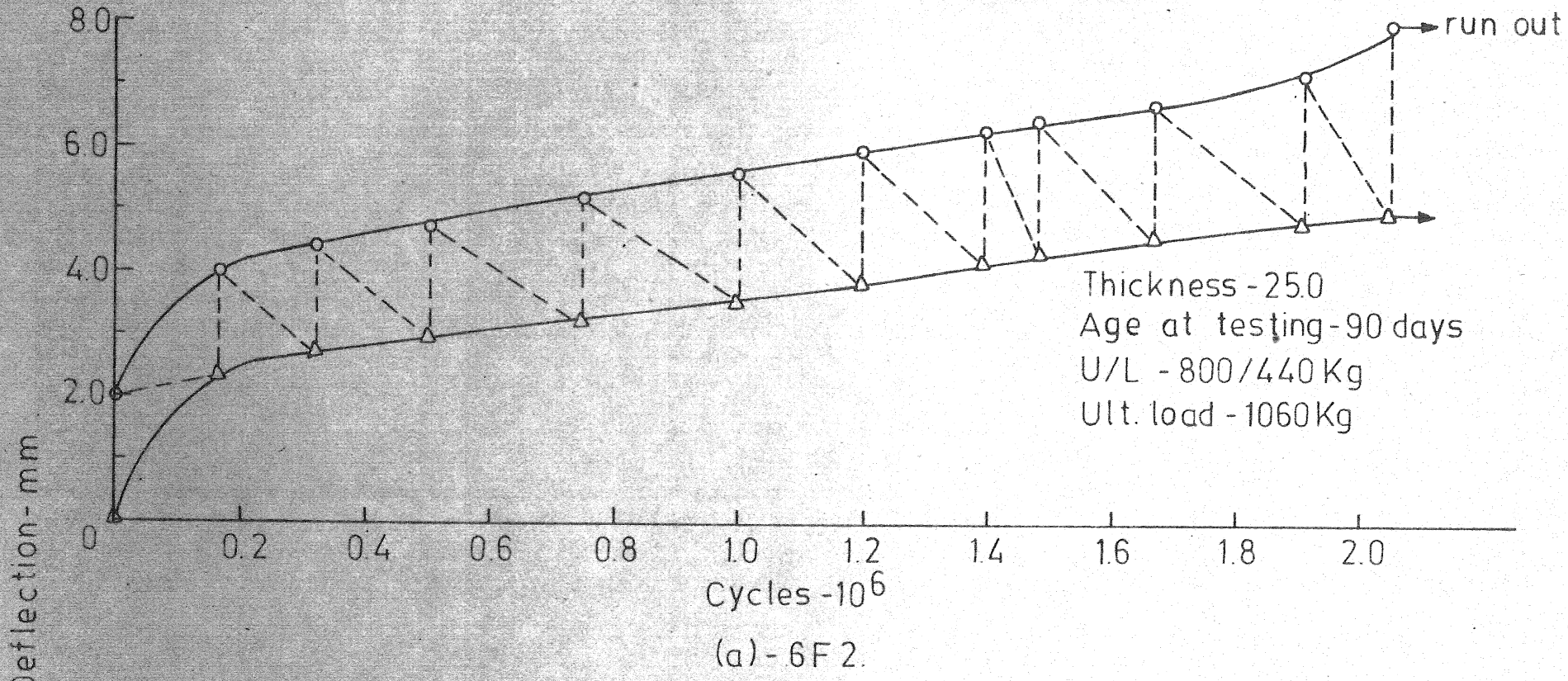

(a) - 6F 2.

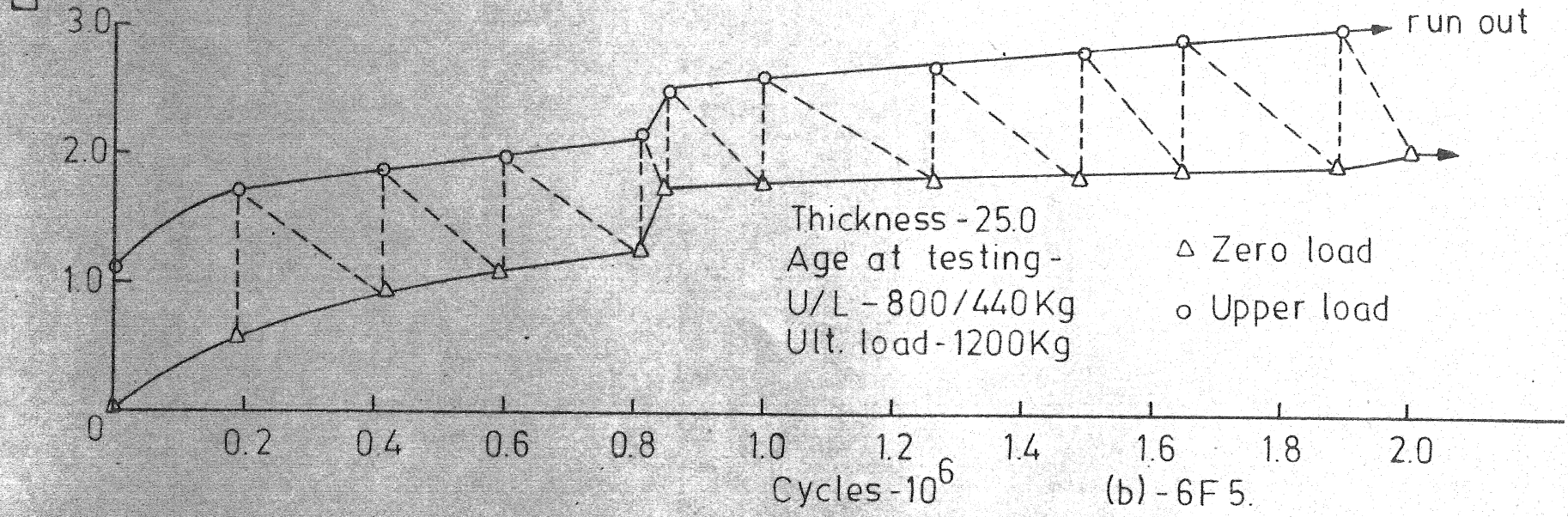

(b) - 6F 5.

Figure 5.7 - Deflection - Cycles Relationship.

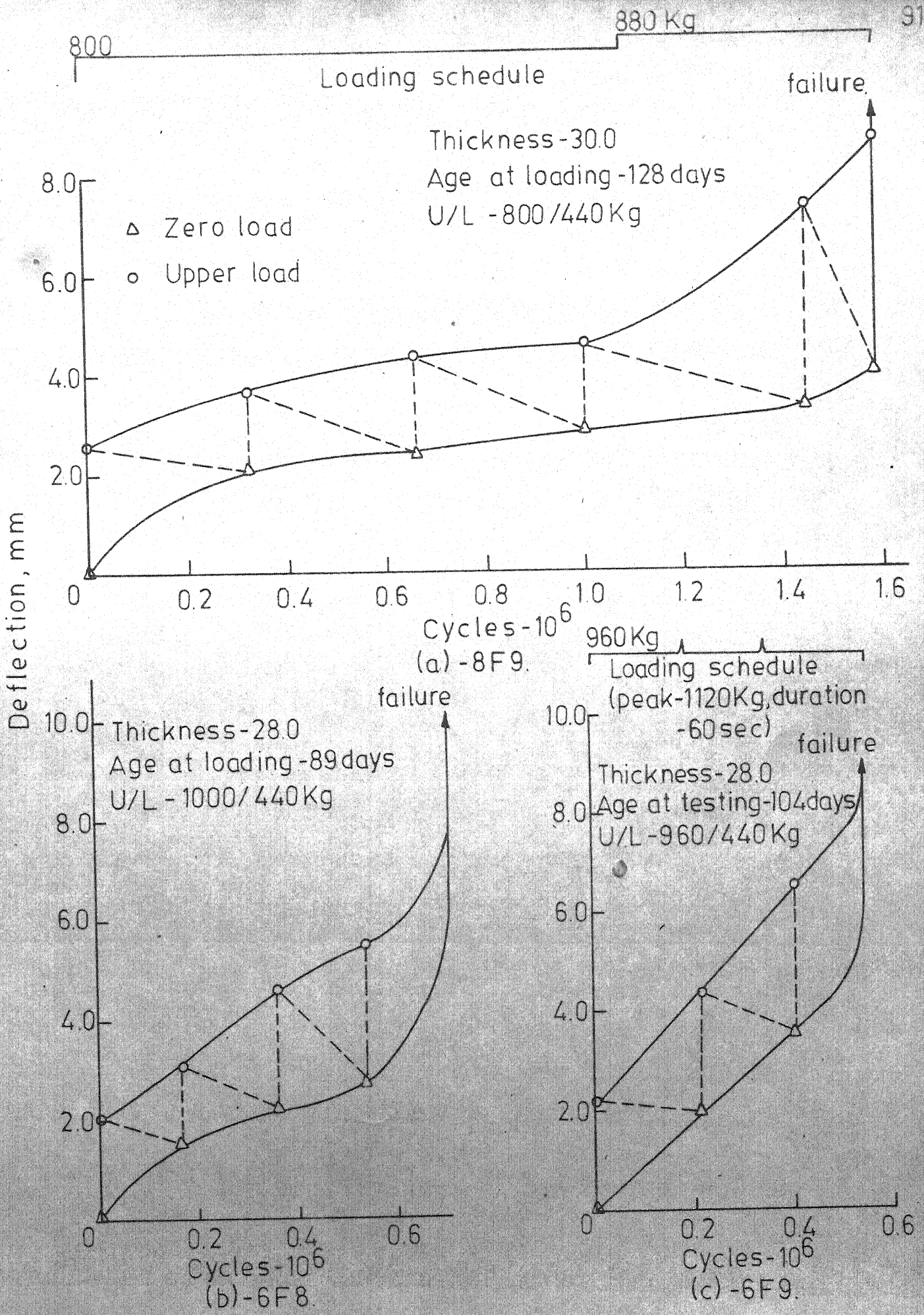

Figure 5.8 - Deflection - Cycle Relationship

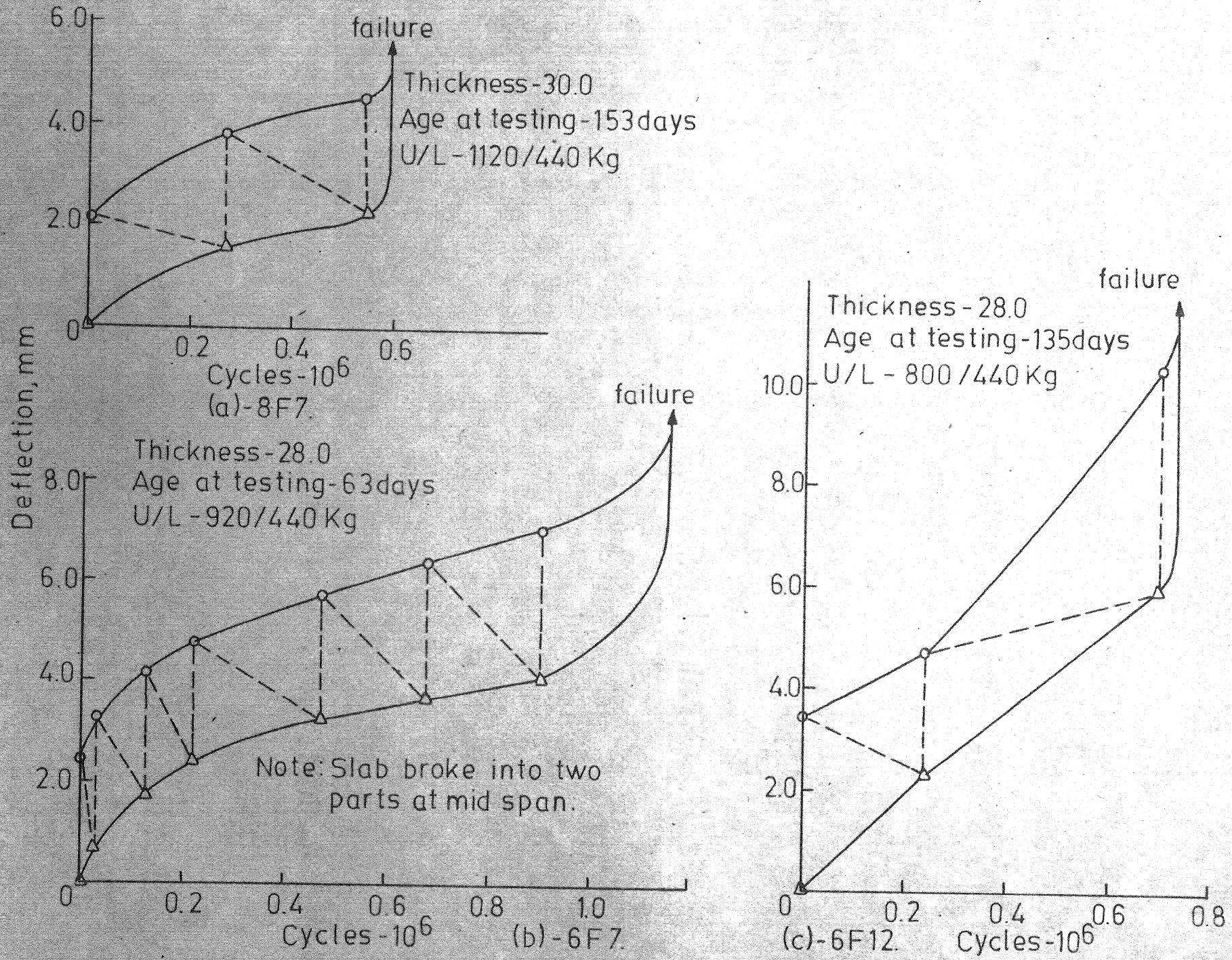

Figure 5.9 -Deflection -Cycles Relationship.

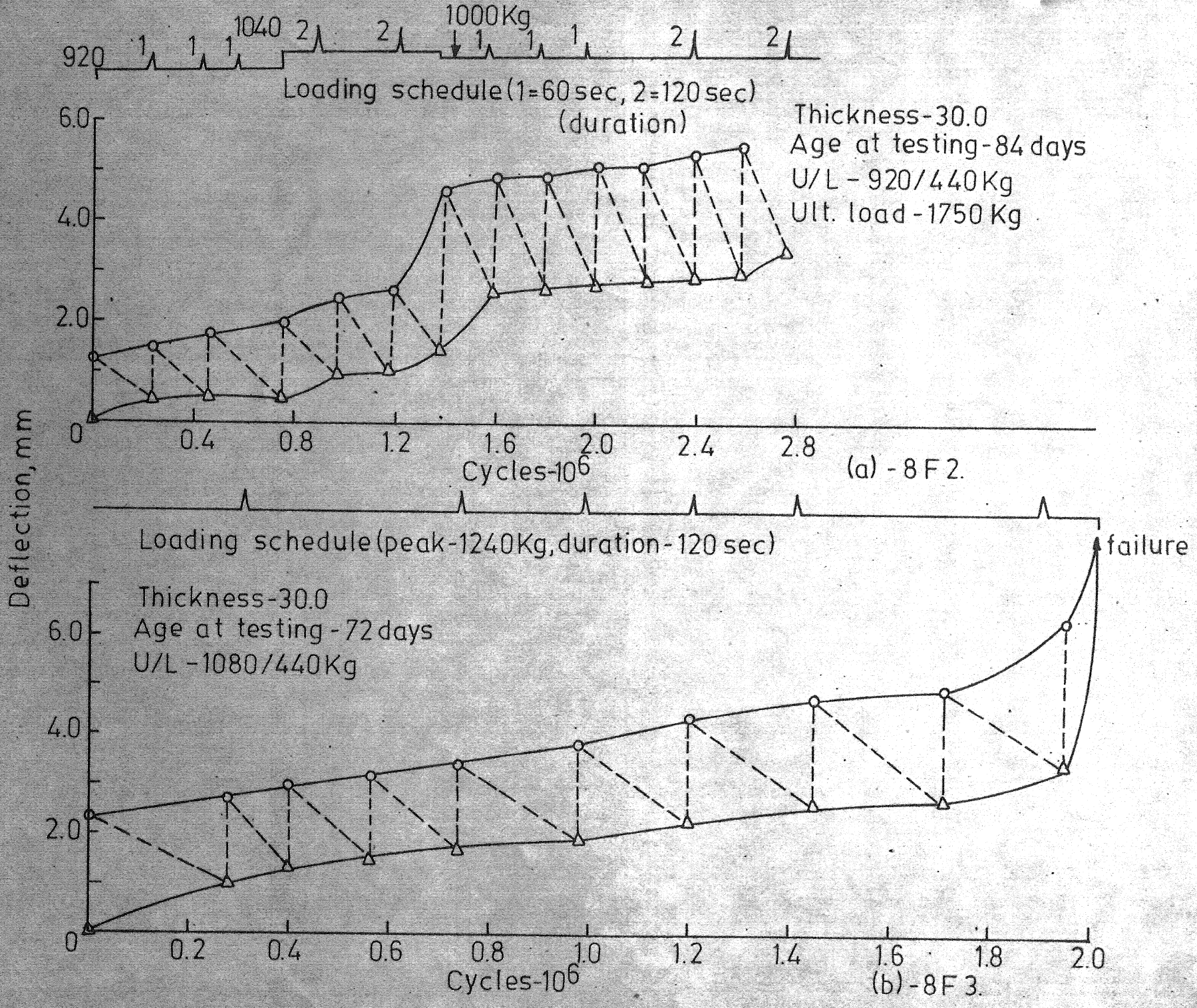

Figure 5.10 - Deflection - Cycles Relationship.

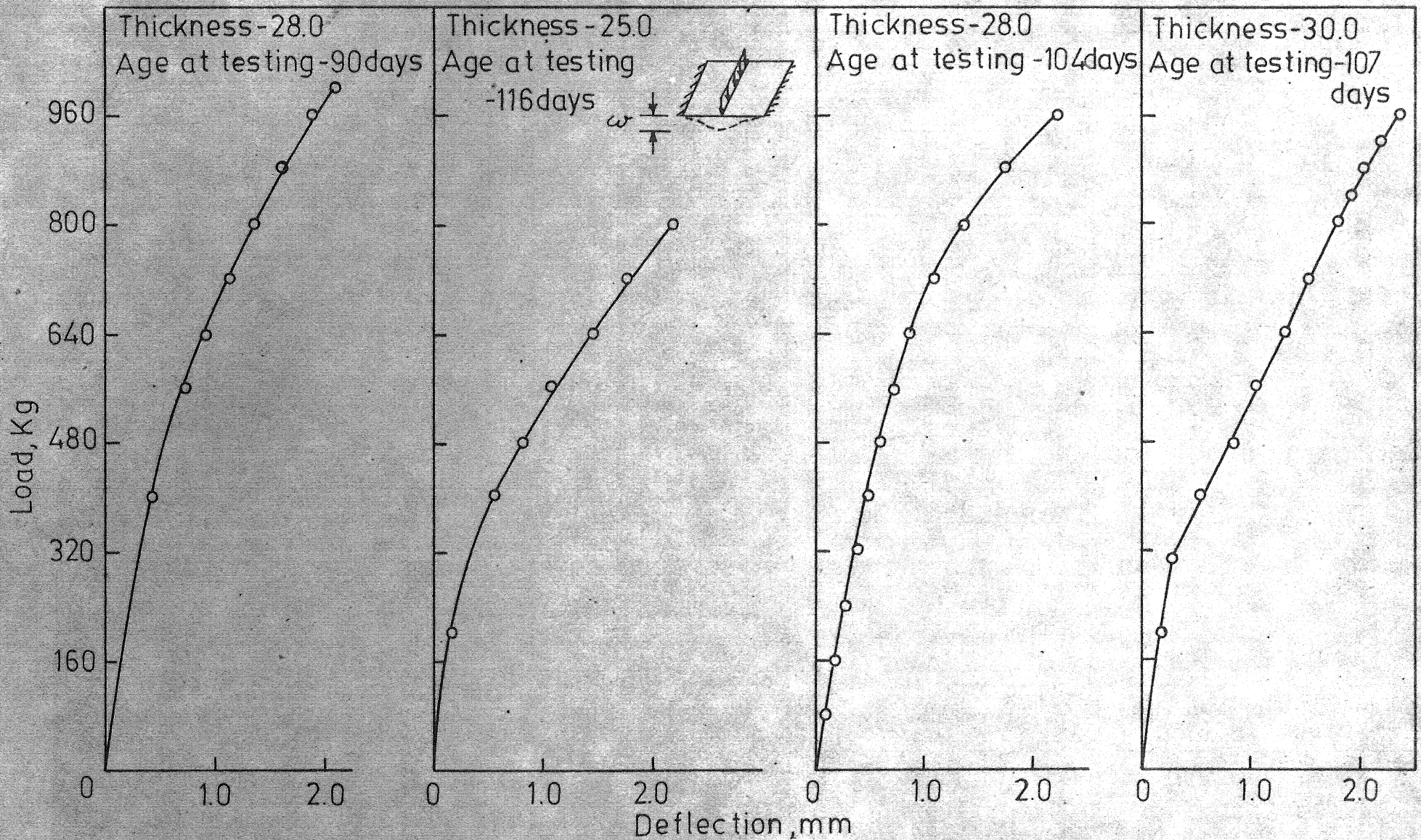

Figure 5.11 - Load - Deflection Relationship for Fatigue Series.

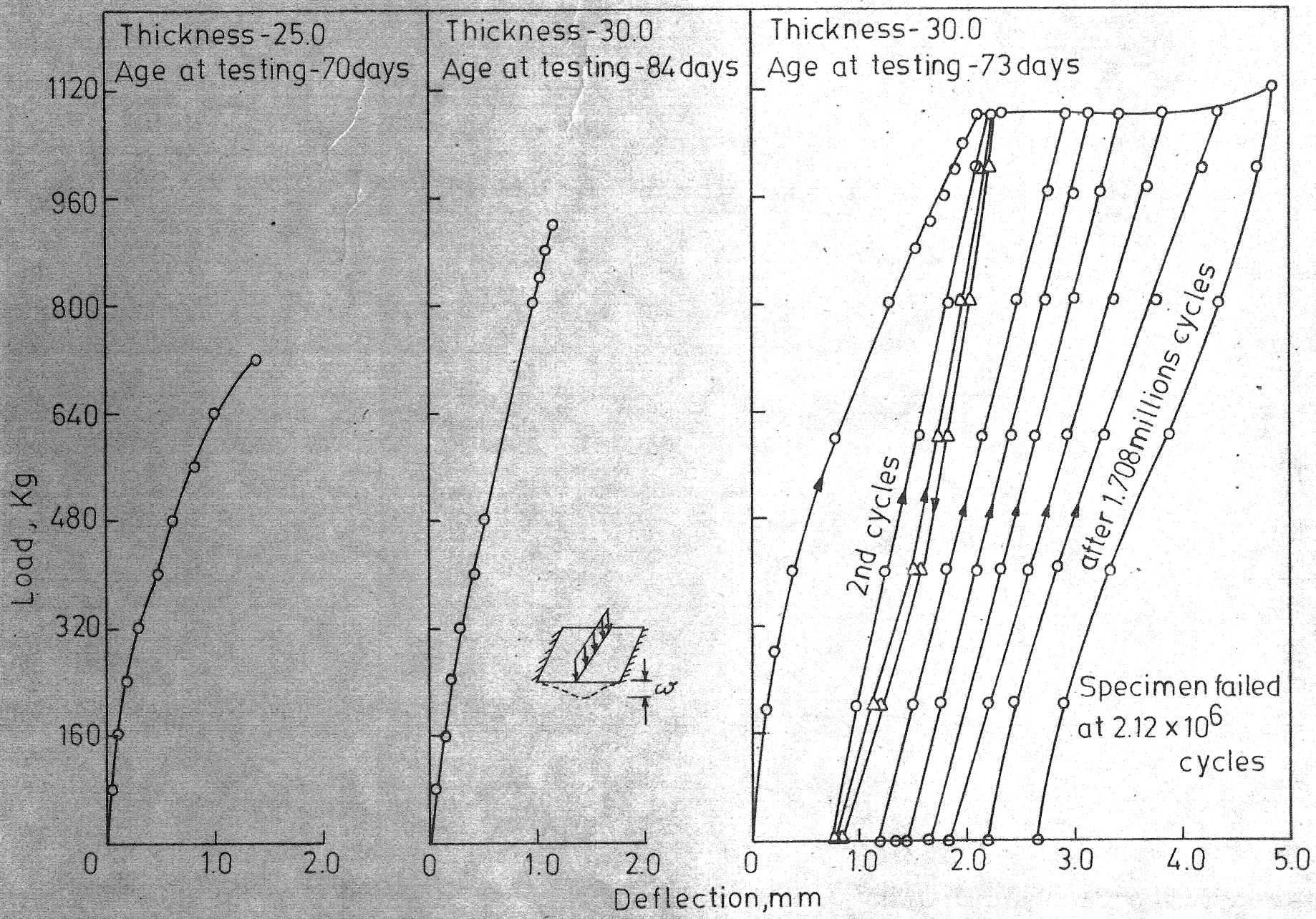

Figure 5.12 - Load - Deflection Relationship for Fatigue Series.

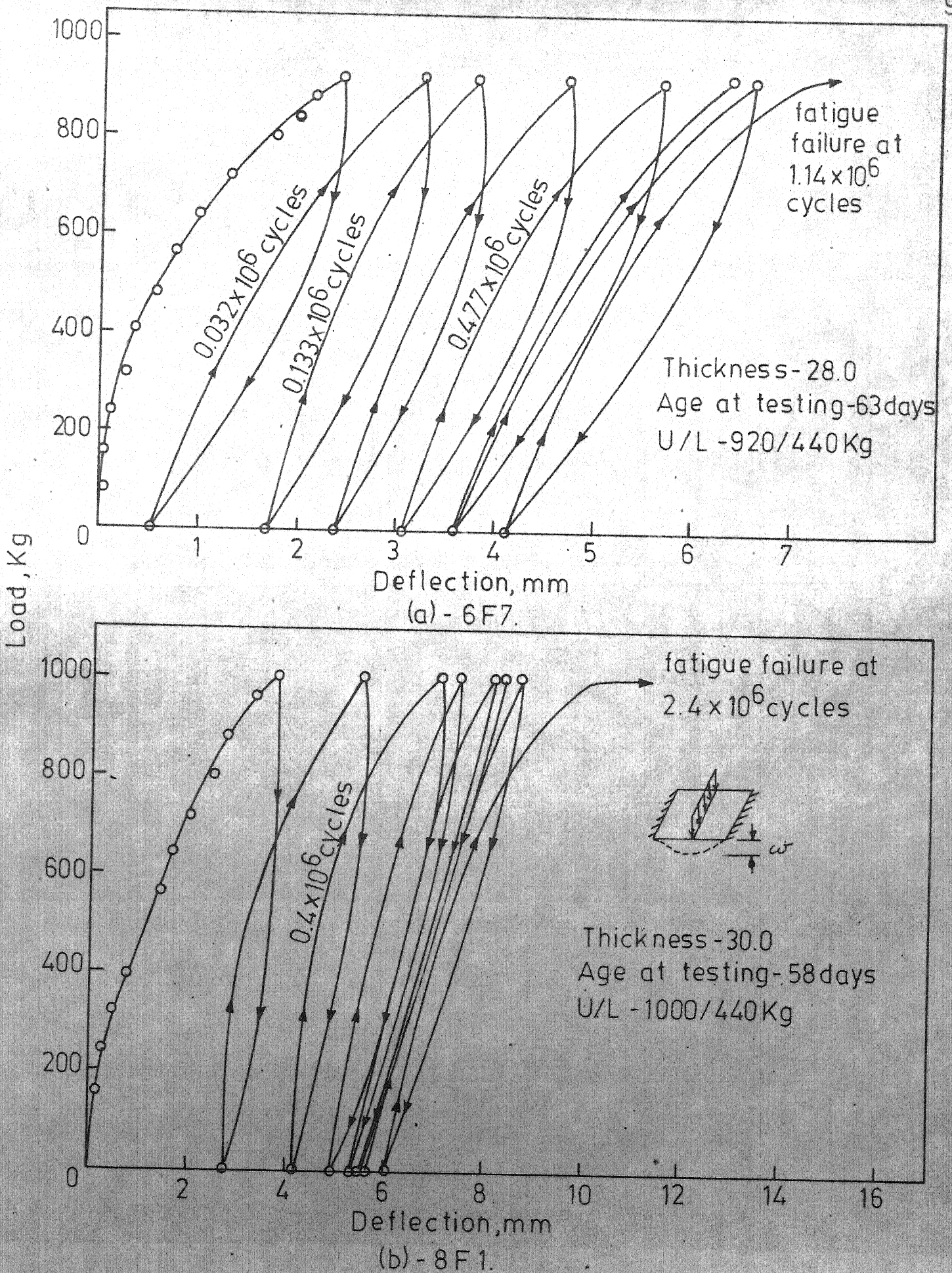

Figure 5.13 - Load - Deflection Hysteresis Loops.

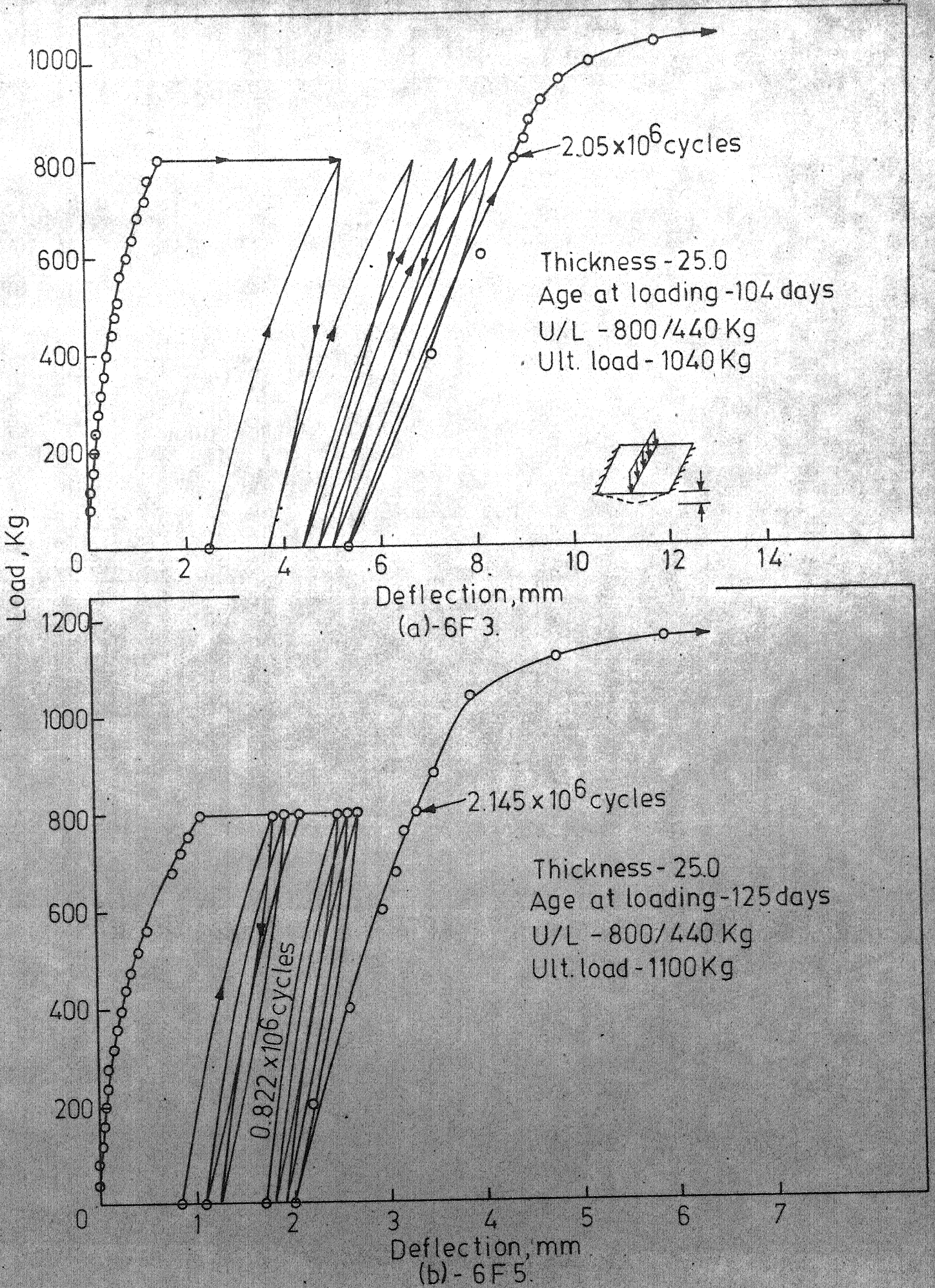

Figure 5.14 - Load - Deflection Hysteresis Loops.

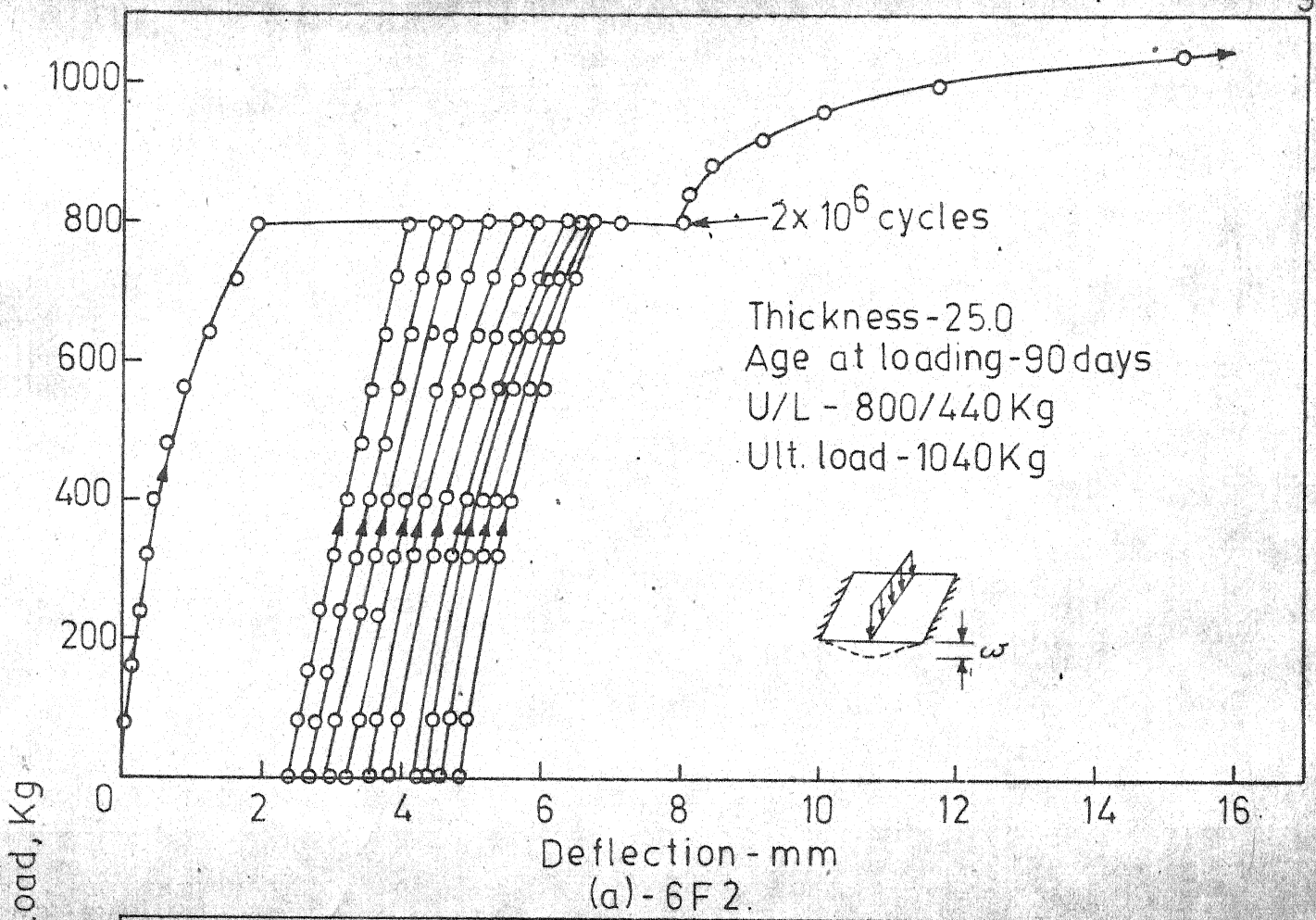

(a) - 6F2.

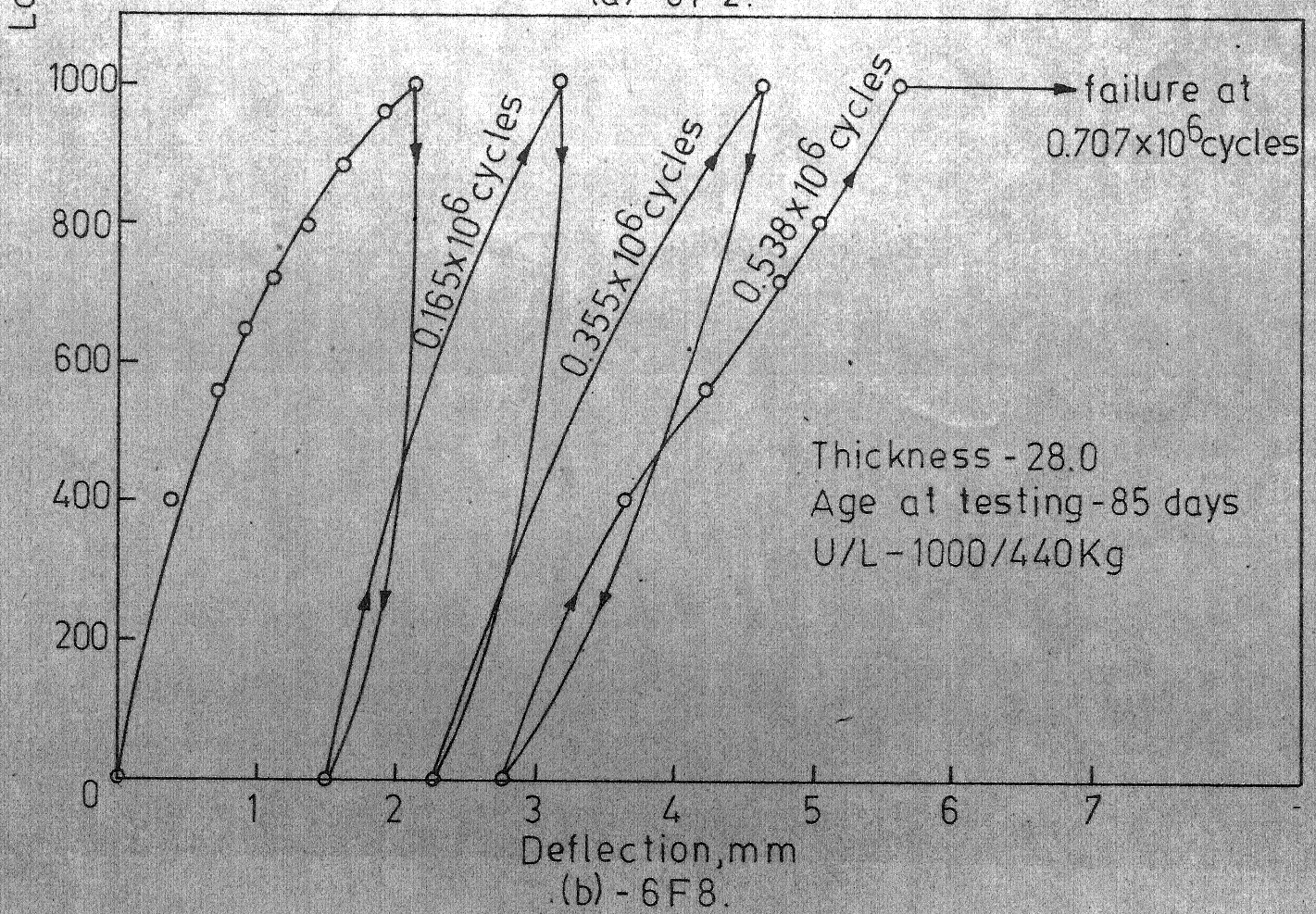

(b) - 6F8.

Figure 5.15 - Load - Deflection Hysteresis Loops.

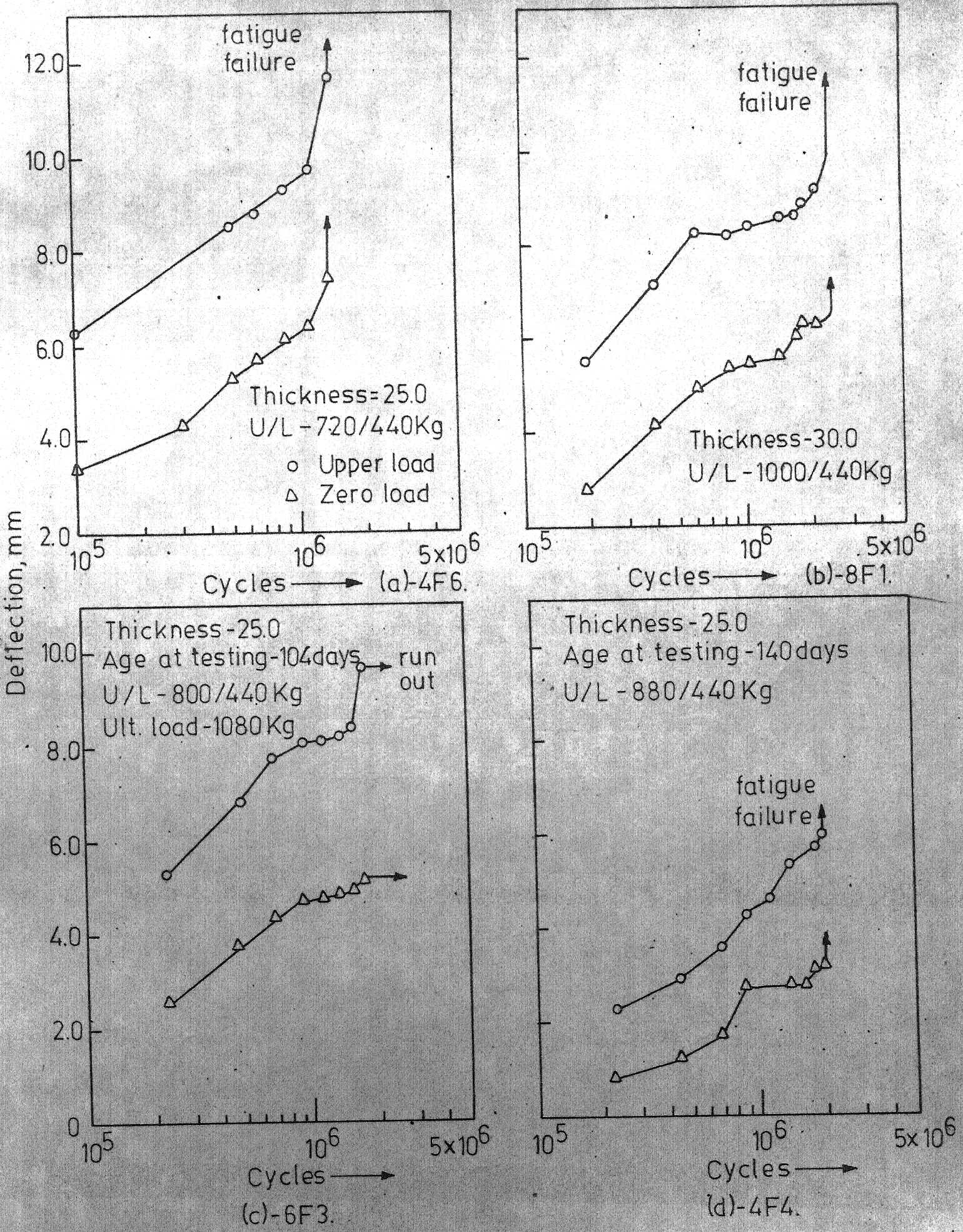

Figure 5.16-Deflection-Log Cycle Relationship.

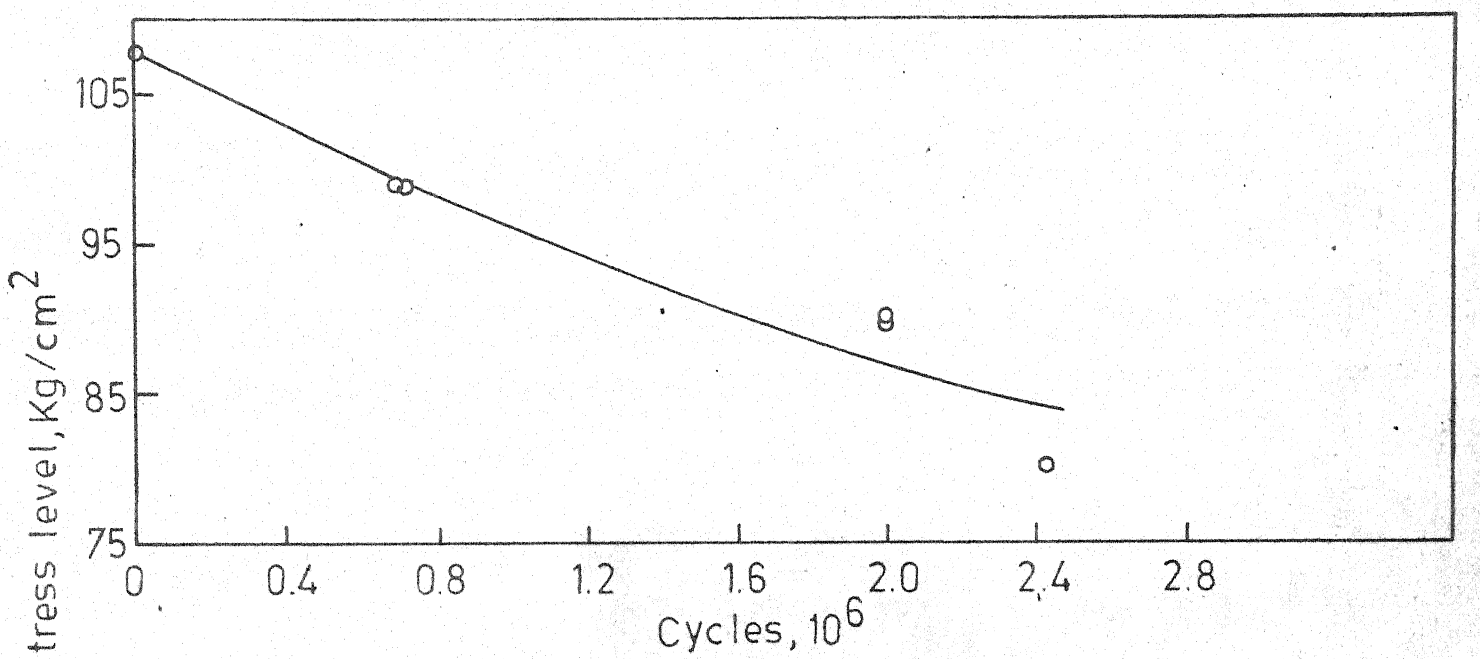

(a)- 4F series.

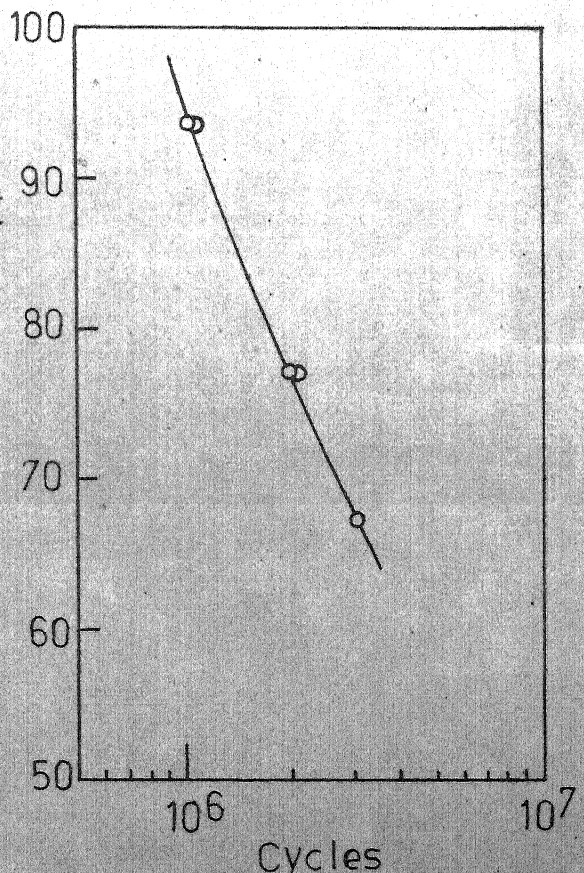

(b)- 6F series.

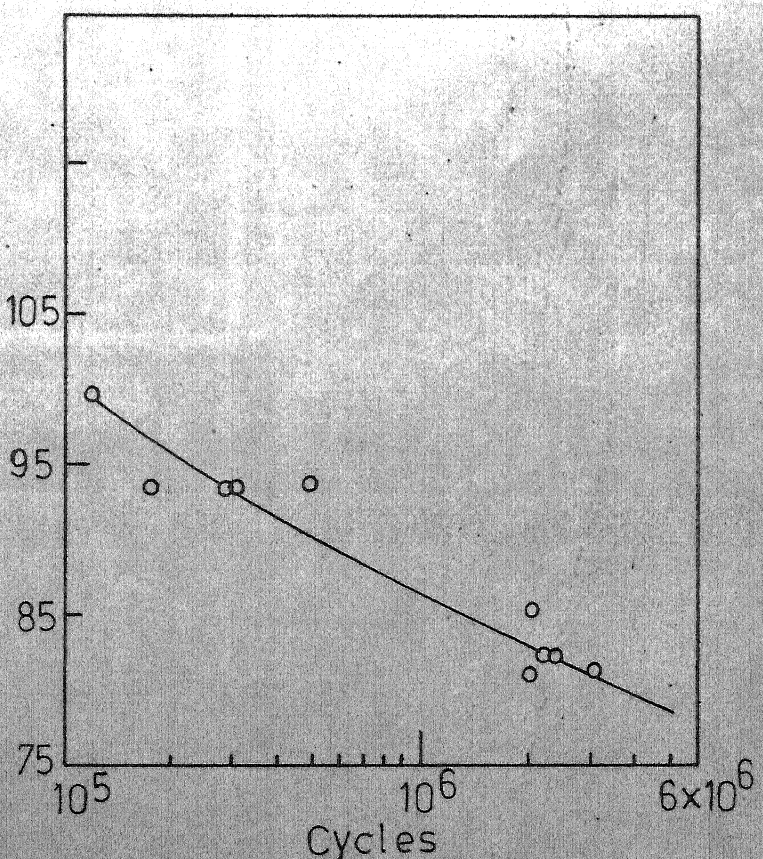

(c)-8F series.

Figure 5.17-S - N Curves from Flexural Fatigue Tests.

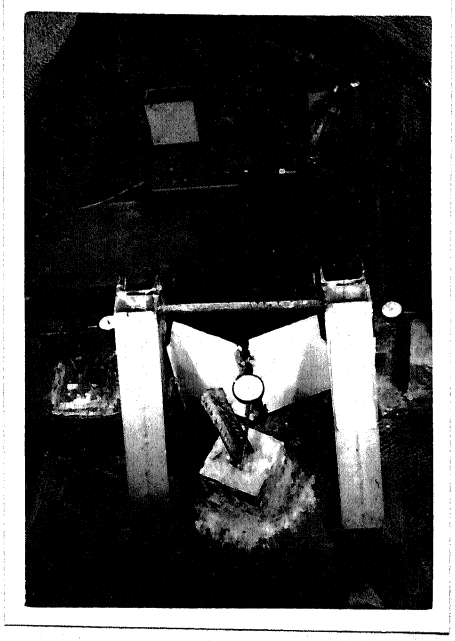

Figure 5.18 Yield Lines in a Specimen After Fatigue Failure

CHAPTER VI

YIELD CRITERION

6.1 General

Plastic analysis is a branch of structural analysis dealing with structures loaded into plastic range. The object of plastic limit analysis is the calculation of collapse loads, at which the structures continue to deform while the loads remain constant. In other words unrestricted plastic flow occurs in structures. The constitutive equations in theory of plasticity are defined by the yield condition and the associated flow rule.

6.2 The Yield Condition and Flow Rule

The yield cohdition is a function of stress components which relates the generalised stresses at yield and is given by

$$Y(Q_i) = 0 \qquad \ldots (6.2.1)$$

where Q_i - the generalised stress, i = 1,2,3,...n.

The equation 6.2.1 represents a surface in the stress space. The stress distributions are elastic if

$$Y(Q_i) < 0$$

The stress distributions for which this function vanishes are plastic. The condition

$$Y(Q_i) > 0 \qquad \ldots (6.2.3)$$

is ~~intolerable by the material~~ inadmissible.

The point, curve or surface corresponding to equation (6.2.1) is known as the yield point, the yield curve or the yield surface respectively in one - , two - and n - ($n \geq 3$) dimensional stress space represented by the components of the stress vector Q_i. If $n > 3$, the surface is a hyper surface. The yield surface was shown to be convex always (Prager (45)).

For any state of stress at the yield limit, the flow rule gives the ratio between the increments of plastic strain. Therefore, the plastic flow law can be expressed as

$$q_i = \eta \frac{\partial Y}{\partial Q_i} \qquad i = 1,2,3.....n. \qquad (6.2.4)$$

where η is an arbitrary positive scalar. The equation 6.2.4 implies that the strain vector is normal to the yield surface given by equation 6.2.4 and hence the flow rule sometimes referred to as the normality flow rule.

6.3 Yield Criteria

In this section, the yield criteria which are commonly used in the determination of the collapse loads are described and also a brief review of the development of the other yield criterion applicable to conventional reinforced concrete, fibre reinforced concrete and ferrocement are presented.

6.3.1 The Tresca Yield Criterion

This is also known as the Coulomb - Tresca yield criterion. For a two dimensional structure, loaded transversely, the yield criterion is given by

$$\max \left(|M_1| , |M_2| , |M_1 - M_2| \right) = M_0 \qquad \ldots \quad (6.3.1)$$

where M_1 and M_2 - the principal moments and

M_0 - the yield moment of the material in uniaxial bending.

The yield condition and the strain vectors are shown in Figure 6.1(b).

6.3.2 The Mises Yield Criterion

This is also referred to in the literature as Huber, Hencky and Mises yield criterion. In terms of principal moments of a plate loaded laterally, it is given by

$$M_1^2 + M_2^2 - M_1 . M_2 = M_0^2 \qquad \ldots \quad (6.3.2.1)$$

The Figure 6.1(a) shows the yield curve and the flow rule.

6.3.3 Square Yield Criterion

This yield criterion was intuitively adopted by Johansen (57) in the plastic analysis of reinforced concrete plates. For any isotropically reinforced plate the yield criterion is shown graphically in Figure 6.1(c).

Mathematically, it is given by

$$|M_i| = M_0 \qquad i = 1,2.. \qquad \ldots \quad (6.3.3.1)$$

It states that the ultimate moment in one direction is independent of the moment in the perpendicular direction. The extension of yield criterion to an orthotropic yield surface was discussed by Wood and Armer (89) and Clyde (90). Other yield criteria for orthotropically reinforced plates are shown in Figure 6.2.

6.3.4 Various Yield Criteria: Development and Application

Kao, Mura and Lee (91) presented the analysis of load carrying capacity of square orthotropic plates on simple supports using the yield criterion suggested by Hill (92).

Nielsen (93) formulated yield condition for both isotropic and orthotropic slabs based on the characteristics of concrete and the reinforcement and presented a number of upper and lower bound solutions for different types of slabs.

Kemp (94) showed that the true yield criterion is a normal moment criterion while the tangential and the twisting moments on the yield line may vary. He noted that only the normal moments contributed to the dissipation of the energy and concluded that the yield line theory was built on the basis of the normal moment yield criterion.

Sawczuk (95) studied the influence of membrane action on the limit load of rigid perfectly plastic plates.

Kwiecinski (96) formulated a yield criterion for quasi-isotropic reinforced slabs. He analysed the yield moment as a plastic hinge taking into account the possibility of kinking of the reinforcement on the open fracture line. The theory proposed is a partial kinking theory whose limiting cases are the square yield criterion (stepped yield criterion) and the theory based on perfect kinking of the reinforcement. The ultimate moment in an initially isotropic slab is shown to be on the inclination of the plastic hinge.

Kwiecinski (56) formulated the yield criterion for an orthotropically reinforced slab with a rigid-plastic behaviour, taking the partial kinking of the reinforcement on the yield hinge.

Flügge and Nakamura (97) presented a general theory to furnish complete solutions for shells of revolution based on an approximate yield condition derived from the Tresca criterion. The bounds are determined for a shallow truncated conical shell subjected to a line load.

Kwiecinski (98) considered the partial kinking of the reinforcement at yield and derived a yield condition for an orthotropically reinforced slab. He pointed out that the concept of stepped yield line loads to a kinematically inadmissible mechanism, while the present criterion is permissible.

Massonet (99) obtained complete analytical solution for the exact limit load of isotropic and orthotropic slabs using Hopkins (100) and Schumann's (101) general results and developed a criterion for the kinematically admissible mechanism and the statically admissible stress field.

Zawidzki and Sawczuk (102) presented a set of complete solutions for plastic flexure of fibre-reinforced plates under rotationally symmetric conditions of loading and supports.

Prince and Kemp (103) developed a yield criterion for isotropically reinforced concrete slabs based upon strain compatibility requirements across the crack along a yield line. A generalised yield criterion incorporating the expression for normal moment of resistance was presented. The square yield criterion was shown to be a lower bound of the generalized yield criterion. The experimental results show good agreement with the theory.

Beckett (104) introduced the concepts of multiple limit states (limit states of collapse, local damage, deflection etc.) and applied to the analysis of reinforced concrete beam and slab system.

Prager (105) investigated the plastic failure of matrix-reinforced composite sheet.

Biron (106) considered an open cantilever cylindrical shell with longitudinal rib reinforcement and computed the collapse pressure (load). The yield surface was derived using the strain mapping method for the Tresca yield criterion.

McLanghlin and Batterman (107) studied the limit behaviour of fibrous materials composed of planar arrays of long elastic perfectly plastic fibres, site bonded or imbedded, in a strengthless matrix. The equations of limit surfaces obtained are based on the lower and upper bound theorems of limit

analysis. The effects of fibre orientation geometry, fibre yielding, fibre buckling and pull-out of fibres from the structures are included in the theory.

McLaughlin and Batterman (108) determined the limiting values of a concentrated force acting on simply supported circular plates or arbitrarily shaped clamped plates obeying an arbitrary yield condition symmetric about certain lines in a simple and straight forward manner by applying extended limit design theorems, thus encompassing all the previous results of Hopkins and Prager (109), Drucker and Hopkins (110), Hopkins and Wang (111), Haythornthwaite and Shield (112), Zaid (113) and Schumann (99). It is also shown that Zaid's (113) results apply to materials other than those obeying the Tresca yield condition.

Wasti (114) obtained a yield criterion for anisotropic plates by extending the Tresca yield criterion and applied to circular plates.

Braestrup (115) strongly refuted the statement of Wood (116) and Jones and Wood (117) that yield line theory and limit analysis are inconsistent and demonstrated that both the 'normal moment' criterion of the modern yield line theory and the 'stepped' criterion of the classical theory correspond to a so called upper yield surface, which satisfies the requirements of limit analysis. It is also shown that the successive refinement of yield-line patterns does not converge to the yield load predicted by limit analysis, when the actual yield surface of the plate is different from the upper yield surface. The yield surface of an arbitrarily reinforced plate is derived.

Lance and Robinson (118) presented a theory of plastic behaviour of fibre reinforced composite materials which allows for several failure modes of the composite material such as the matrix failure, and the ductile failure of the fibres and the matrix. The plastic strain rates associated with each of the failure modes are specified.

Jain and Kennedy (119) considered equality of normal resisting ultimate moment with the normal applied moment at the yield line after examining all possible orientations of the yield line. The results were substantiated by data from experiments on reinforced concrete slabs.

Lenschow and Sozen (59) developed a general yield criterion for reinforced concrete slabs subjected to combination of flexural and twisting moments and compared with the experimental results. The analytical expression for the yield criterion derived was

$$wM_1 = M_2 = [M_x \sin^2(\alpha + \gamma) + M_y \cos^2(\alpha + \gamma)]/\cos^2\gamma \quad (6.3.4.1)$$

where M_i - the generalised stress, i = 1,2 and

α - the angle between the directions of M_1 and M_x and γ is determined by

$$-\tan^2\gamma - wC_1 \tan\gamma + w = 0 \quad \ldots \quad (6.3.4.2)$$

where

$$wC_1 = [(\mu - w)\tan^2\alpha + 1 - \mu w]/[(1 - \mu)\cot\alpha] \quad (6.3.4.3)$$

A graphical representation of their yield criterion is given in Figure 6.3. The yield criterion recognises that twisting moments may exist along the

line, which affect both the direction of the yield line and the moment capacity of the element. The yield criterion so developed was in good agreement with their test results. A general application of the yield criterion requires ductility of the considered section beyond the deformations at yielding. Lenschow and Sozen showed that for reinforced concrete the general ductility requirement limited the amount of reinforcement in plate elements far below the amount which is conventionally considered to result in dubtile behaviour as implied by various building codes. A simplified approximate expression was derived for the balanced amount of reinforcement

$$A_s \sigma_y = 0.125 \sigma_{ca} h \qquad \ldots (6.3.4.4)$$

where A_s - the area of steel reinforcement per unit width in one layer,

σ_y - the yield stress of reinforcement,

σ_{ca} - the average compressive concrete stress and

h - the height of the cross section.

6.3.5 The Yield Criterion for Ferrocement

The ferrocement plates under transverse set of loads have been observed to be as ductile as metal plates and the rotation of yield lines is quite appreciable at collapse, inspite of the fact the ferrocement plates are usually highly reinforced.

Austriaco, Lee and Pama (120) carried out trilinear analysis of ferrocement slabs and suggested a yield criterion shown in Figure 6.4. The

essentral features of the yield criterion are the square initial yield and limit surface in principal moment space. They assumed no significant interaction between the moments acting on any two orthogonal cross-sections of the composite material since the stresses in the skeletal steel and the wire mesh are independently transferred to the surrounding mortar by bond. Austriaco, Lee and Pama (120) substantiated the arguments by experiments on rectangular slabs subjected to cylindrical bending under central line load and circular slabs with concentric boss subjected to a punch load. These experiments, however, do not represent a general state of stress in a ferrocement.

The high ductility of the ferrocement slabs in bending and the homogeneity of the material suggests that the yield criterion similar to that of the Mises yield criterion may be more appropriate for determining the collapse loads. With a view to establishing a yield criterion relevant to ferrocement slabs under general state of stress of stress an experimental programme was carried out.

6.4 Test Procedure

The details of the test setups and brief descriptions of the test procedure are presented in Chapter III. Other pertinent information about the test procedures is given here.

6.4.1 Rectangular Slabs

The rectangular slabs clamped along the two shorter edges and free at the other two were tested under monotonically increasing central line load parallel to the clamped edges. The mid-span deflections at each increment of the load were recorded and development of cracks carefully observed. In all sixteen slabs were tested, two for each series to determine the collapse loads. The load-deflection curves for a few typical tested specimens are presented in Figure 6.5 and 6.6.

6.4.2 Circular Slab with a Concentric Boss

A circular slab with clear span of 1500, simply supported along its periphery, was subjected to a concentric punch load applied through a rigid core (boss) of 300 ϕ. Loads were applied in increments upto collapse. Deflection and strain measurements for each increment of load were taken at various points of interest. The cracks were noted carefully as the test progressed. The final deflections were recorded at collapse. To demonstrate the strength of ferrocement slab, the specimen was inverted and loads were applied again upto collapse. The Figures 6.7 and 6.8 show respectively the load-deflection curve of the rigid core and the deflection profiles of the circular slabs. The load-radial strains for circular slab at 170 from centre are shown in Figure 6.9 and the crack pattern at collapse is shown in Figure 6.10.

6.4.3 Uniaxial and Biaxial End Moment Series

Six square slabs, two for each series, were subjected to uniaxial end moments to determine the moment carrying capacity of the slabs. Fourteen slabs, five each for 6F and 8F series and four for 4F series, were subjected to biaxial end moments. The slabs tested under unidirectional moments were simply supported along two edges and free at other two and those tested under bidirectional moments were simply supported along all the four edges. The ratio of the moments in two orthogonal directions was varied. The slabs were tested for $M_2 = M_1$, $0.375\ M_1$, $0.5\ M_1$ and $0.675\ M_1$. The loads were applied in small increments and deflections were noted. The developments of cracks, their trend and directions were observed carefully when the test was in progress. The Figures 6.11 through 6.14 show the moment-deflection plots for a few tested specimens. A yield criterion obtained from the test results has been presented in Figure 6.15. The Figure 6.16 shows the typical crack pattern for 6F slab for $M_1 = M_2$.

6.5 Analysis: Determination of Collapse Loads

6.5.1 Rectangular Slabs

The dimensions and loads are given in Figure 6.17. For certain value of $P = P_c$, the bending moment at the built in ends and at the mid-span reaches the yield moment. It can be easily shown that

$$P_c = \frac{8M_0}{L} \qquad \ldots \quad (6.5.1.1)$$

where P_c - the collapse load, per unit width,

M_0 - the yield moment per unit width and

L - the clear span.

M_0 in equation (6.5.1.1) is given by equation (A.1.3.4) given in Appendix A.

6.5.2 Circular Slabs with Axisymmetric Loads and Supports

Consider any piecewise linear yield surface. The state of stress at the various points of the plate will be represented by stress points located on or inside the yield surface. The locus of these stress points is usually known as stress profile. Depending upon the geometry of the plate at collapse and the boundary conditions, a stress profile can easily be identified. For a linear stress profiles for circular plate subjected and loaded symmetrically about the axis, the radial and circumferential moment fields can be derived as follows.

Let the equation of a typical stress profile be

$$M_\theta = a + b M_r \qquad \ldots (6.5.2)$$

where M_θ - the circumferential moment,

M_r - the radial moment and

a,b - the constants.

The equilibrium equation of the plate under consideration is

$$(rM_r)'' - (M_\theta)' = - p(r)r \qquad \ldots (6.5.2.2)$$

where r - the radius at any point,

p(r) - the load as function of r and

prime - denotes differentiations with respect to r.

The equation (6.5.2.2) yields in view of equation (6.5.2.1)

$$M_r'' + \frac{(2 - b)}{r} M_r' = - p(r) \qquad \ldots (6.5.2.3)$$

For any load p, the equation (6.5.2.3) can be solved by the method of variation of parameters. For a uniformely distributed load $p(r) = p$, the radial moment M_r is given by

$$M_r = \frac{- pr^2}{2(3 - b)} + \frac{C_1 r^{b-1}}{b - 1} + C_2 \qquad \ldots (6.5.2.4)$$

Thus the equation (6.5.2.4) and (6.5.2.1) describe the moment field completely.

Example 1: Consider a circular slab of radius R, simply supported along the periphery and subjected to a uniformly distributed load p. At the centre of the plate, the axial symmetry requires that

$$M_r = M_\theta \qquad \ldots\ldots (6.5.2.5)$$

and M_r is a finite quantity. At the boundary,

$$r = R$$
$$M_r = 0 \qquad \ldots (6.5.2.6)$$

In view of equations (6.5.2.5) and (6.5.2.6), the governing stress profile

is CDE (Figure 6. 15) The limit load depends upon the radius ρR at which the stress regime changes from CD to DE. This radius is computed numerically using the moment and shear continuity conditions. The moment fields are,

for region $0 \leq r \leq \rho R$

$$M_{\theta 1} = a_1 + b_1 M_{r1} \qquad \ldots \quad (6.5.2.7)$$

$$M_{r1} = \frac{a_1}{2} + \frac{br^2}{2(b_1 - 3)} \qquad \ldots \quad (6.5.2.8)$$

for region $\rho R \leq r \leq R$

$$M_{\theta 2} = a_2 + b_2 M_{r2} \qquad \ldots \quad (6.5.2.9)$$

$$M_{r2} = \frac{a_2}{1 - b_2}\left[1 - \left(\frac{R}{r}\right)^{1-b_2}\right] + \frac{pr^2}{2(3 - b_2)}\left[\left(\frac{R}{r}\right)^{1-b_2} - \left(\frac{r}{R}\right)^2\right] \qquad \ldots \quad (6.5.2.10)$$

Let the coordinates of the points A,B,C,D and E on the proposed yield surface be, $(M_0,0)$, (d_2M_0,d_1M_0), $\left(\frac{d_1 + d_2}{2} M_0, \frac{d_1 + d_2}{2} M_0\right)$, (d_1M_0, d_2M_0) and $(0, M_0)$ respectively. Then

$$\begin{aligned} a_1 &= (d_1 + d_2) M_0 \\ b_1 &= -1 \\ a_2 &= M_0 \\ b_2 &= \frac{d_2 - 1}{d_1} \end{aligned} \qquad \ldots \quad (6.5.2.11)$$

By using the continuity and the boundary conditions, the non-dimensional is given by solving the equation

$$\rho^{3-b_2} - \rho^2 \frac{(3 - b_2)}{(1 - d_1 + b_2 + d_1 b_2^2)} + \frac{2(1 - b_2)}{(1 + b_2)} = 0 \quad .. (6.5.2.12)$$

The load capacity is given by

$$\frac{M_0}{pR^2} = \frac{(1 + b_2)\rho^{3-b_2} + 2(1 - b_2)}{4(3 - b_2)} \quad . . .(6.5.2.13)$$

In the proposed yield criterion

$$\begin{aligned} d_1 &= 0.7 \\ d_2 &= 1.1 \end{aligned} \quad . . .(6.5.2.14)$$

The equations (6.5.2.12) through (6.5.2.14) yield the region boundary

$$\rho = 0.51 \quad . . .(6.5.2.15)$$

and the load capacity

$$\frac{pR^2}{M_0} = 6.08 \quad . . .(6.5.2.16)$$

which lies in between the capacities based on the square yield criterion (6.00) and the Mises yield criterion (6.51) and hence justifies the statement made earlier.

Example 2: Consider a circular slab of radius R, simply supported along the boundary and subjected to a punch load applied through a concentric boss of

radius ΨR. Following the same arguments as for the previous example, it can be shown that the load capacity for this case is given by

$$\frac{M_0}{pR^2} = \frac{\Psi^2}{2}\left[1 - \frac{\Psi^2}{\rho(1 + b_2)}\right] \qquad \ldots (6.5.2.17)$$

in which ρ is obtained by solving the equation

$$\rho^2 - \frac{\Psi^2}{d_1 + d_2 - 1}(d_1 + d_2 - \frac{2}{1 - b_2})\rho^{1-b_2} - \frac{\Psi^2(1 + b_2)}{(d_1 + d_2 - 1)(1 - b_2)} = 0$$

Substituting the pertinent values of the equations (6.5.2.11) and (6.5.2.14) in euation (6.5.2.18) yields

$$\rho = 0.215 \qquad \ldots (6.5.2.18)$$

Hence

$$P_c = 8.175\, M_0 \qquad \ldots (6.5.2.19)$$

where P_c = the total collapse load applied through the boss.

Similarly the square, the rectangular and the circular slabs under axi - and non-axi symmetric loading can be analysed by using the piecewise linear programming technique.

6.6 Discussions of the Test Results

6.6.1 Rectangular Slabs

The cracks in rectangular slabs tested under monotonically increasing line load appeared at the mid-span, within 15 from the centre, at loads higher than the loads which cause mortar to crack. The cracks along clamped edges of the slab were observed slightly later. At the final collapse of the slab, three distinct yield lines, two along clamped edges and one at the mid-span were observed. The failure was characteristically the ductile failure of wires. The Table 6.1 shows the experimental collapse loads and the theoretical collapse loads calculated from equation (A.1.3.4). The specimens were observed to take loads beyond collapse due to the high ductility of ferrocement and the membrance action. The Figure 6.18 shows the yield lines in a tested specimen.

6.6.2 Circular Slab with a Concentric Boss

Under gradually increasing loads, the first cracks appeared along the periphery, i.e., the junction of the boss and the slab. A reasonably good agreement was observed between experimental cracking moment and the theoretical cracking moment. Under subsequent loading radial and circumferential cracks were observed as shown in Figure 6.10.

The slab carried a total load of 4500 kg and the total deflection of 48.22 was observed under the core. The collapse load in kg approximately was obtained from the load-strain curve shown in Figure 6.9 . This load

corresponds to the point where the curve changes its direction. Careful observation of the load strain-curve indicates that the slab started to pick-up the loads beyond collapse which is attributed to membrane action of the slab. The theoretical collapse load as calculated from equations (A.1.3.4) and (6.5.2.9) is 2650 kg which is in reasonably good agreement with experimental value.

The slab tested under a total load of 4100 kg was inverted and subjected to gradual loading under similar edge conditions. The slab was observed to be quite rigid during the first few increments of load. This was due to the fact that the slab was behaving as a conical shell and could resist considerable membrane forces. The slab was observed to be less rigid after it became flat. It is of interest to note that the slab resisted a maximum of 4000 kg (90% of the virgin load) and final deflection of 50.0 was observed. The test demonstrates the strength of ferrocement slab under single cycle of reverse loading.

The post yield load carrying capacity of the ferrocement slab can be estimated by considering the slab under its deformed state as a conical shell. The total load carrying capacity, following Massonnet and Save (122), is given by

$$P_l = P_c \left[1 + \frac{1}{3} \left(\frac{w}{h}\right)^2 \right] \qquad \ldots \quad (6.6.2.1)$$

P_l - the total load carried by the slab,

w - the total deflection and

h - the thickness of the composite section.

The load calculated from equation (6.6.2.1) is in reasonably good agreement with experimental value.

6.6.3 Uniaxial and Biaxial End Moment Series

The Figures 6.11 through 6.13 show the moment deflection curves for the slabs subjected to uniaxial end moment. The theoretical yield moments determined from equations A.1.3.4 compared well the experimental values as shown in respective figures. It was observed during gradual loading that any cracks, that appeared on the tension face, did not wide open under subsequent load increment. The further increase in strains was due to the formation of new cracks. The number of cracks at final failure were observed to be proportional to the specific surface of reinforcement. The Figure shows the crack pattern of 8UM1 specimen.

The Figures 6.11 through 6.13 show the moment-deflection curves for BM-series. The crack propagation, under gradual loading was observed to be from the corners to the centre of the slabs. The layout of the cracks at collapse was noticed to be a function of the ratio of two orthogonal applied moments. The Figure 6.16 shows the typical crack pattern for 6BM specimen. The slab finally failed with four yield lines starting from the corners and then becoming parallel to the edges of the slab.

The plot of M_1 vs M_2 indicates that the yield moments increase with increasing ratio of the applied moments upto 0.7 and then for $M_1 = M_2$, the yield moment is observed to be less than the unidirectional yield moment. The reason for the interaction of the applied moments two orthogonal

directions. Due to the presence of the woven mesh the behaviour at yield of a ferrocement slab element under general static of stress changes. The plastification of the mortar at yield causes local debonding of wire. The reduction in the ultimate moment capacity is due to the interference of the applied moments. The reason for increase in moment capacity in going from uniaxial moment to biaxial moment upto $M_2 = 0.7\ M_1$ is attributed to the biaxial compression of mortar on the compression side is analogous to the precompression of the specimen. Wood (121) reports that in experiments conducted by Hedley, on reinforced concrete simply supported slabs, a reduction in carrying capacity of the slab was observed. This is also in agreement with the Building Research Station (UK) tests. Hence the square yield criterion is common use is only an approximation of a more complicated yield criterion.

In view of the test results it is suggested the Mises yield criterion with depression in yield surface at 45° may be more appropriate to use in determination of the collapse loads of ferrocement slabs. However, an experimental test programme is necessary to establish the limit surface in II and IV quadrants.

Table 6.1 Load Capacities for S-Series

Specimen	Thickness	Ultimal Loads, kg	
		Theoretical	Experimental*
4S	25.0	1120	1080
6S	25.0	1380	1140
8S	25.0	1560	1400
6S	28.0	1480	1370
8S	30.0	1900	1780
4S**	25.0	767	720
6S**	28.0	1060	1000
8S**	30.0	1100	1020

* average of two specimens tested

** # 22 gauge wire

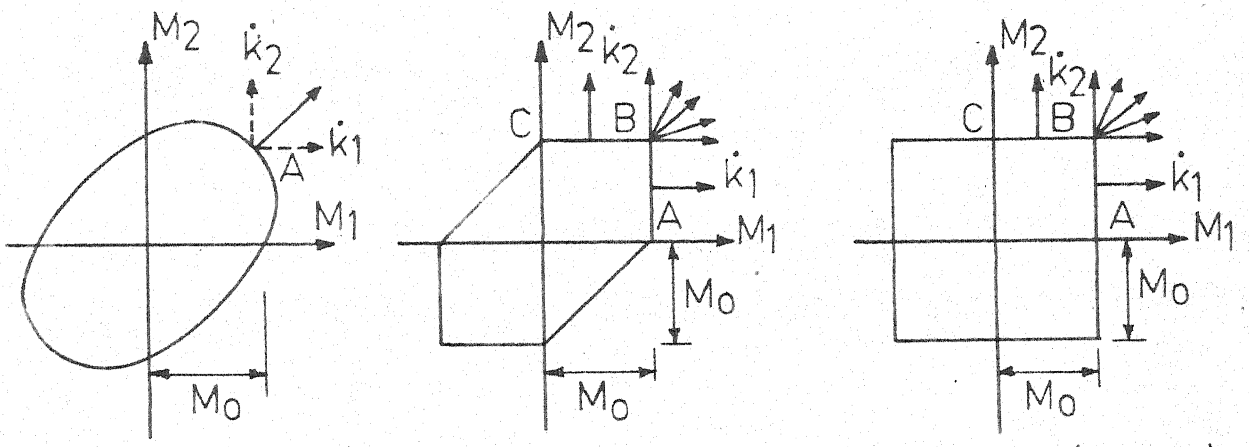

a)-The Mises yield criterion. (b)-The Tresca yield criterion. (c)-The 'Square' yield criterion(Johansen).

Figure 6.1-Yield Criteria.

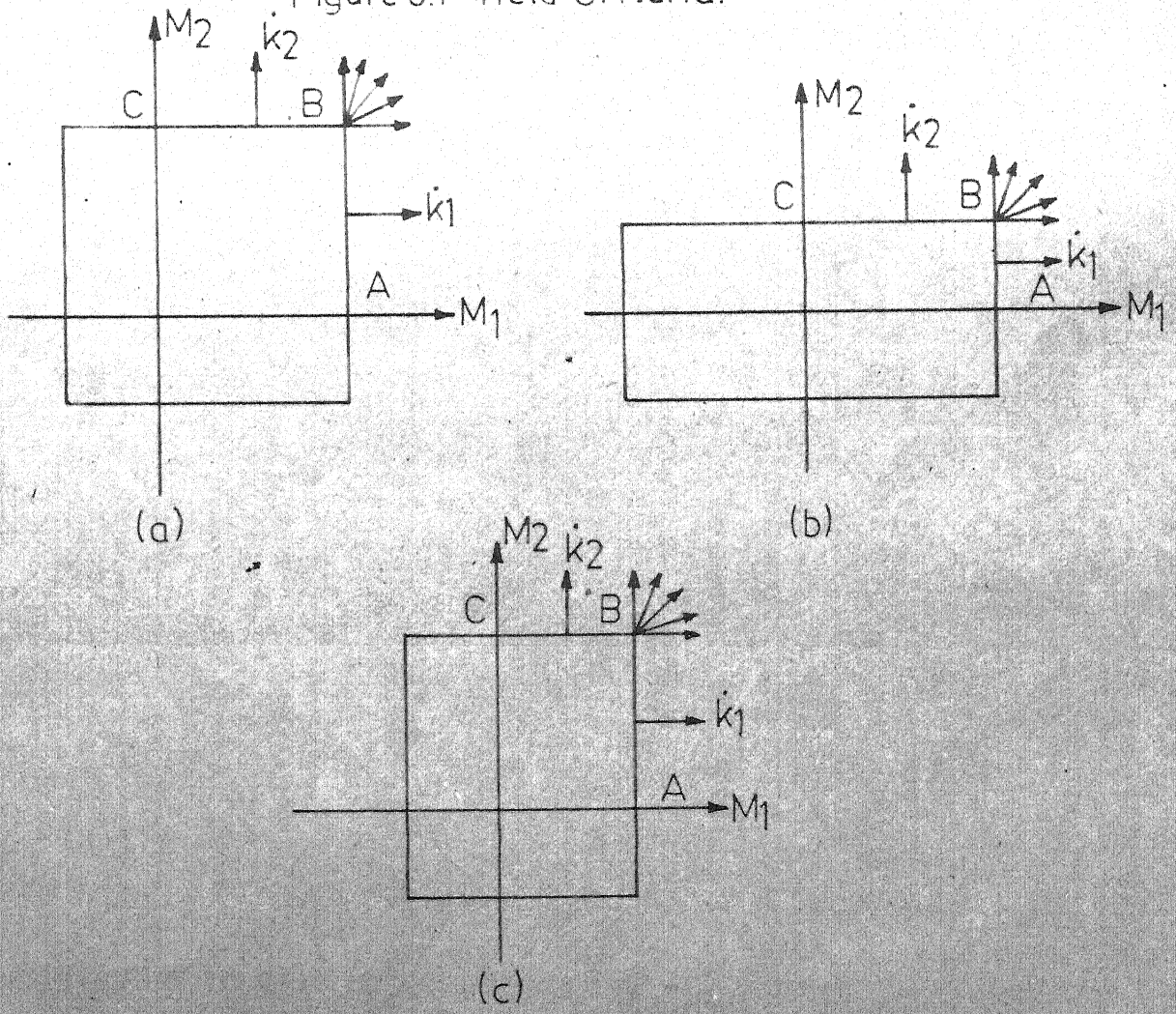

Figure 6.2-Yield Criteria (Johansen).

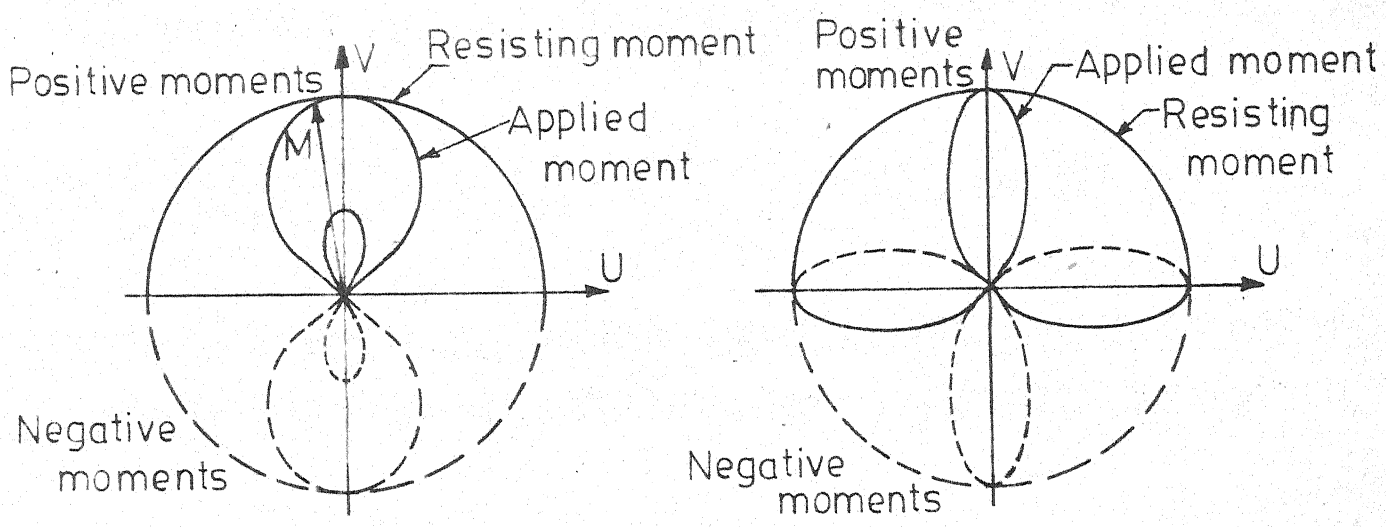

(i) Uniaxial moment. (ii) Pure torsion.

(a)-Isotropically reinforced element.

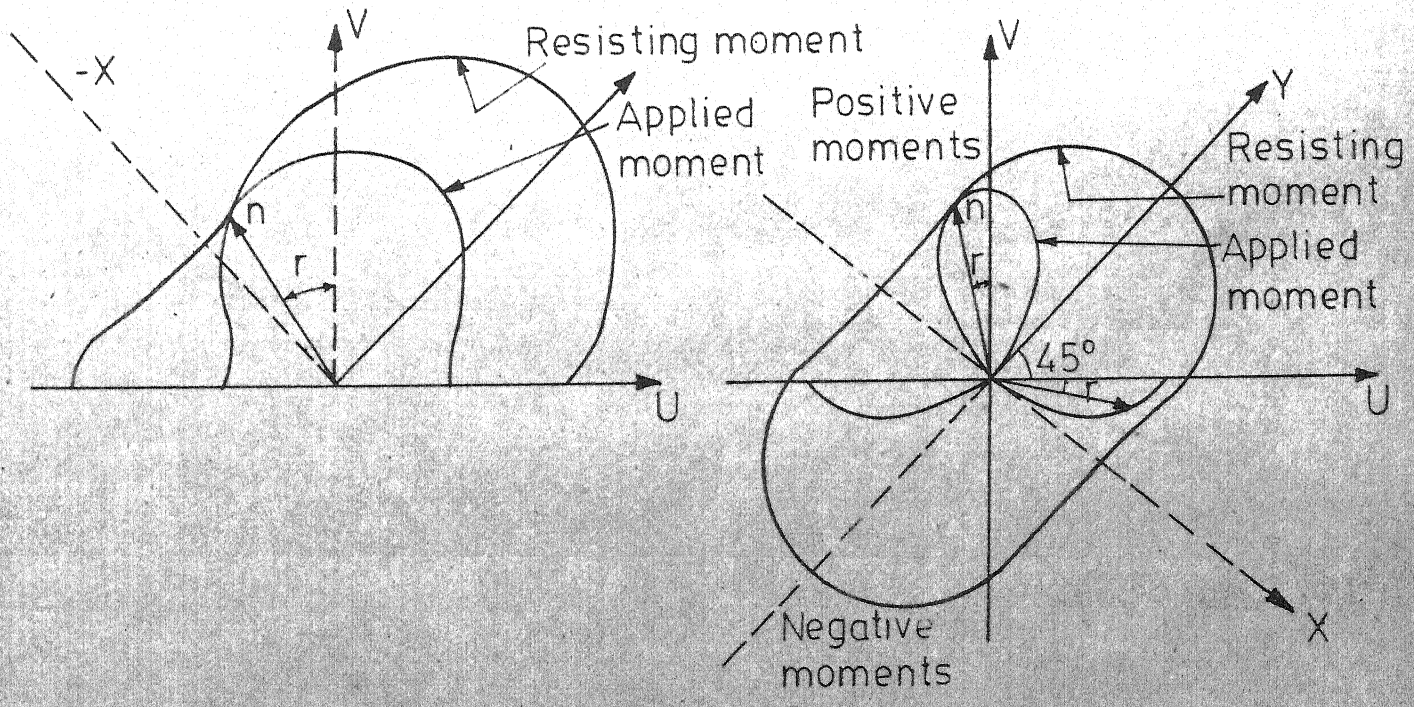

(i) Biaxial moment. (ii) Pure torsion.

(b)- Nonisotropically reinforced element.

Figure 6.3 -Yield Criteria (Lenschow and Sozen).

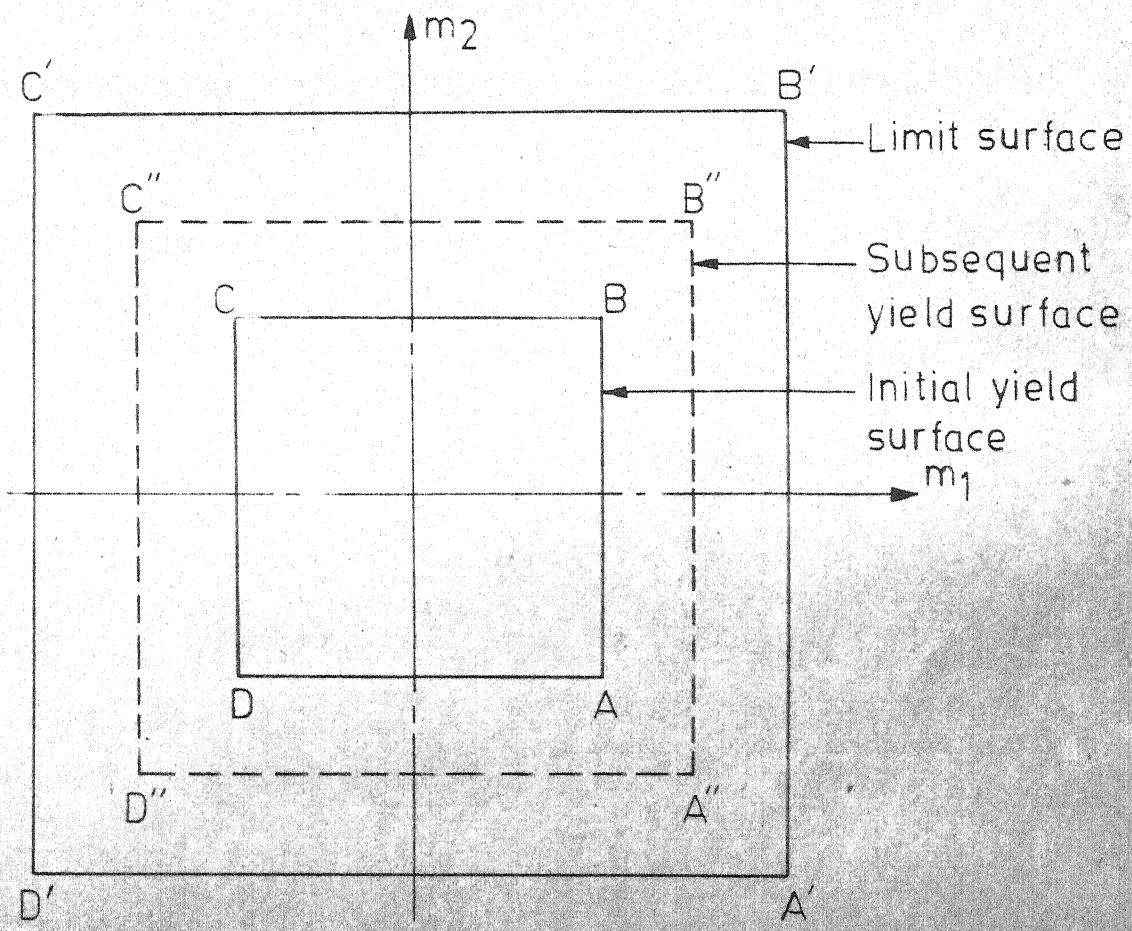

Figure 6.4 - Loading and Limit Surfaces for Ferrocement Slab (Austriaco, Lee & Pama).

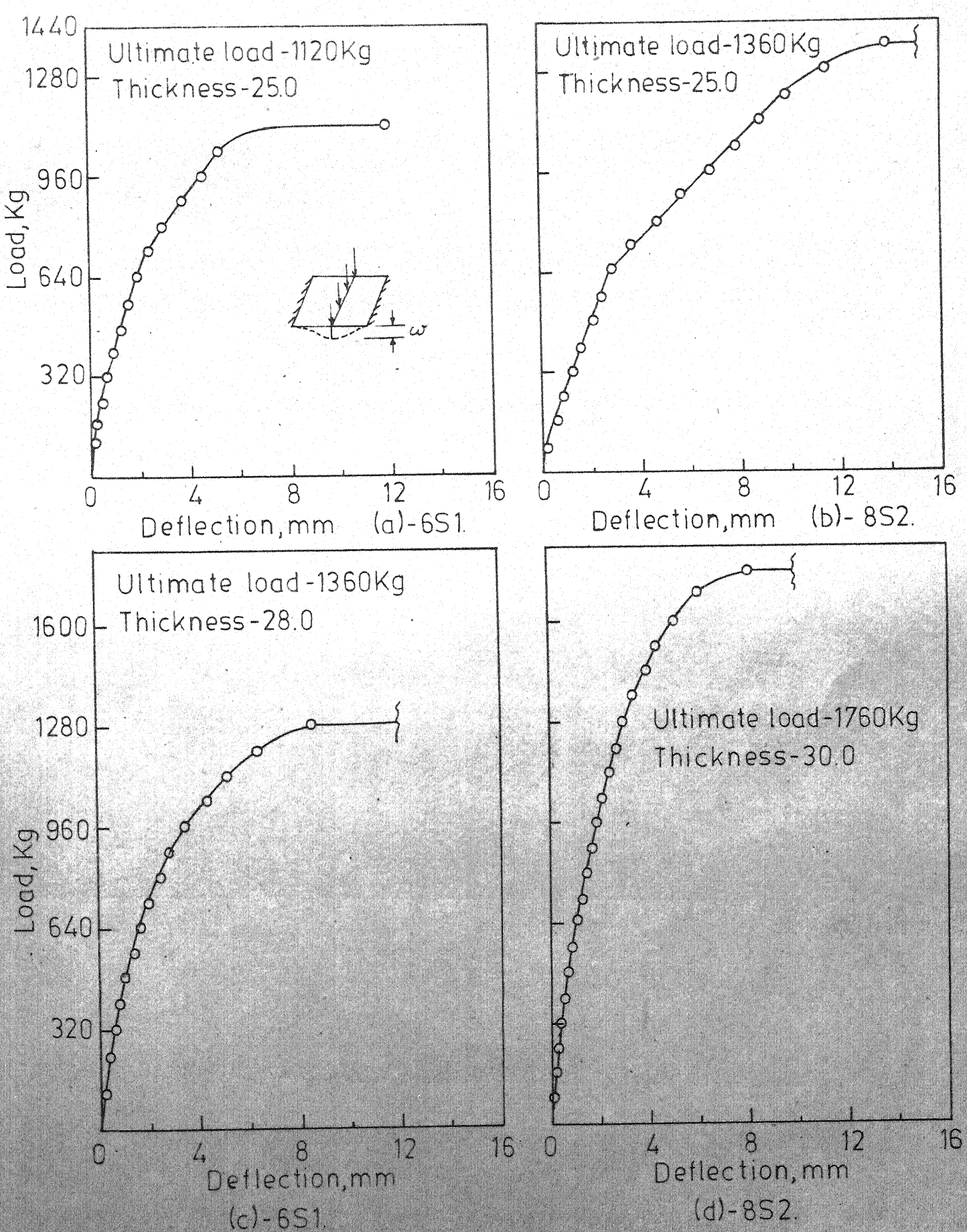

Figure 6.5- Load Deflection Curves for S-Series.

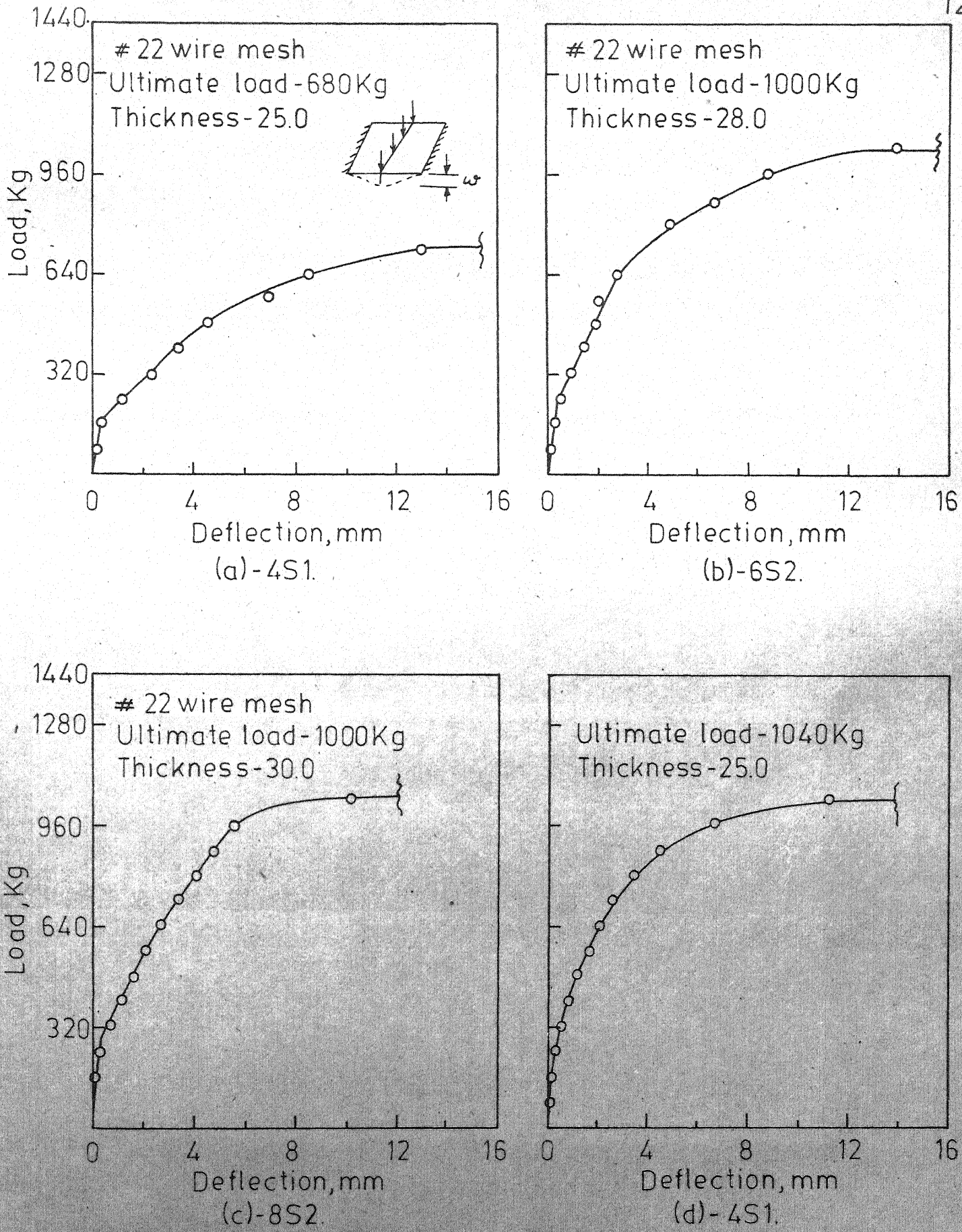

Figure 6.6 - Load - Deflection Curves for S-Series.

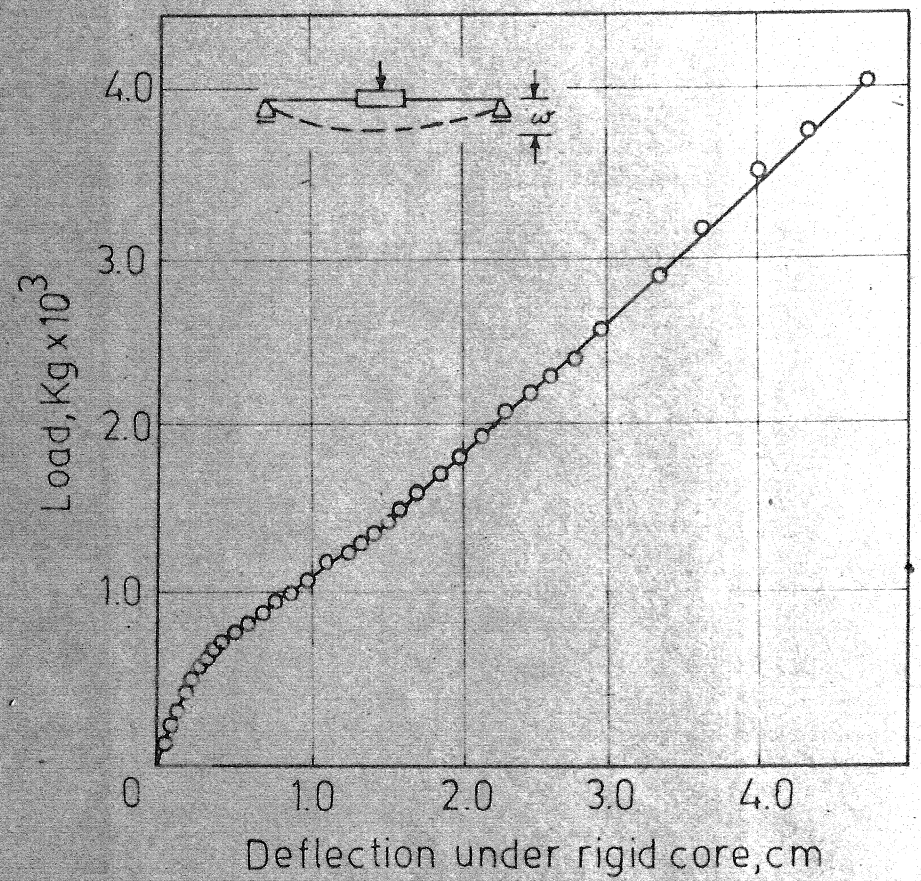

Figure 6.7 - Load-Deflection Curve for Circular Slab.

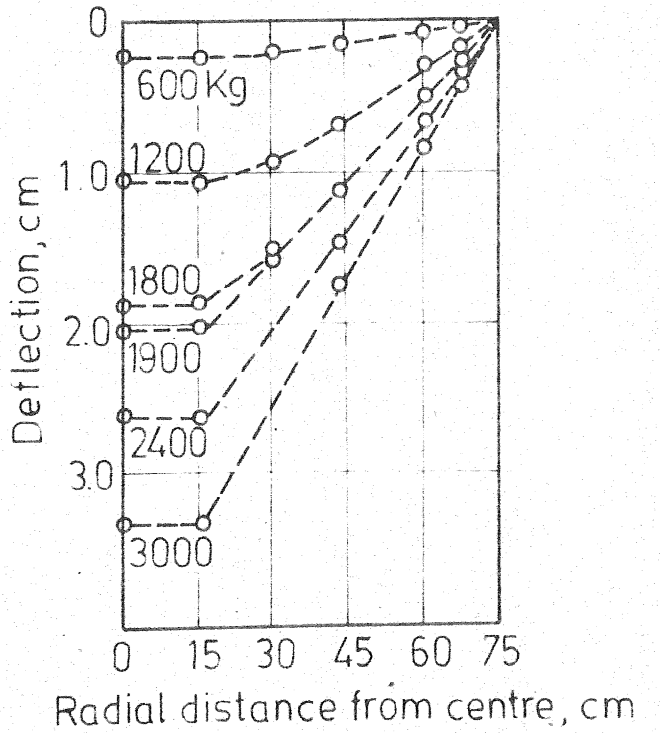

Figure 6.8 - Deflection Profile for Circular Slab.

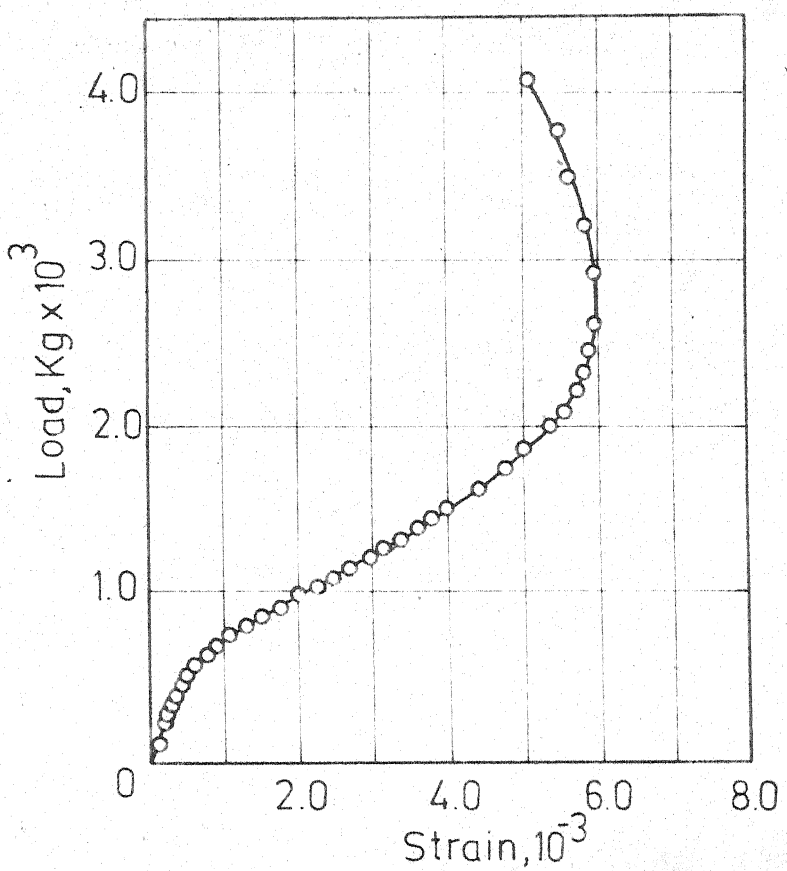

Figure 6.9-Load-Radial Strain Curve of Circular Slab. (170 from centre)

Figure6.10- Crack Pattern of Circular Slab.

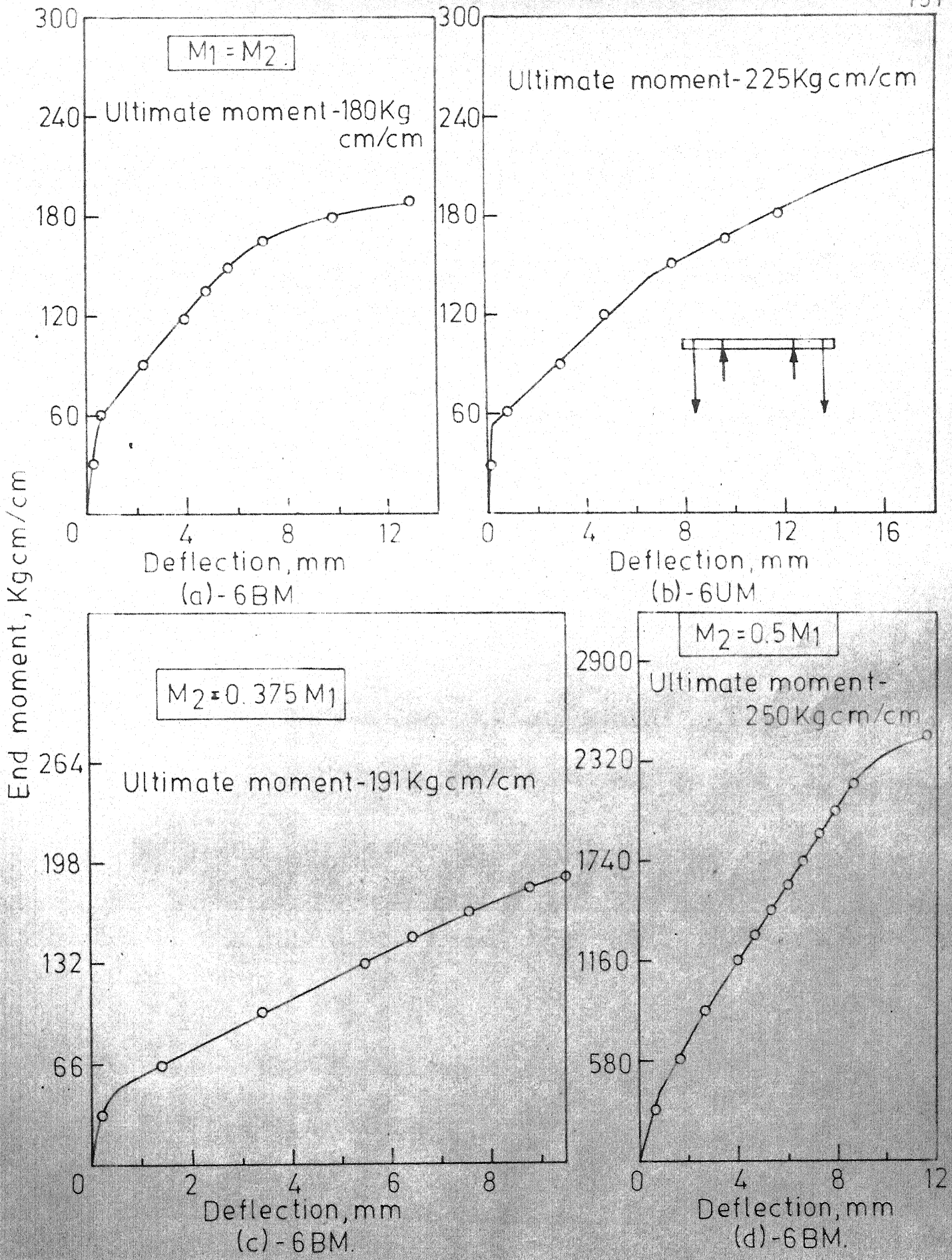

Figure 6.11- Moment - Deflection Curves for UM and BM Series.

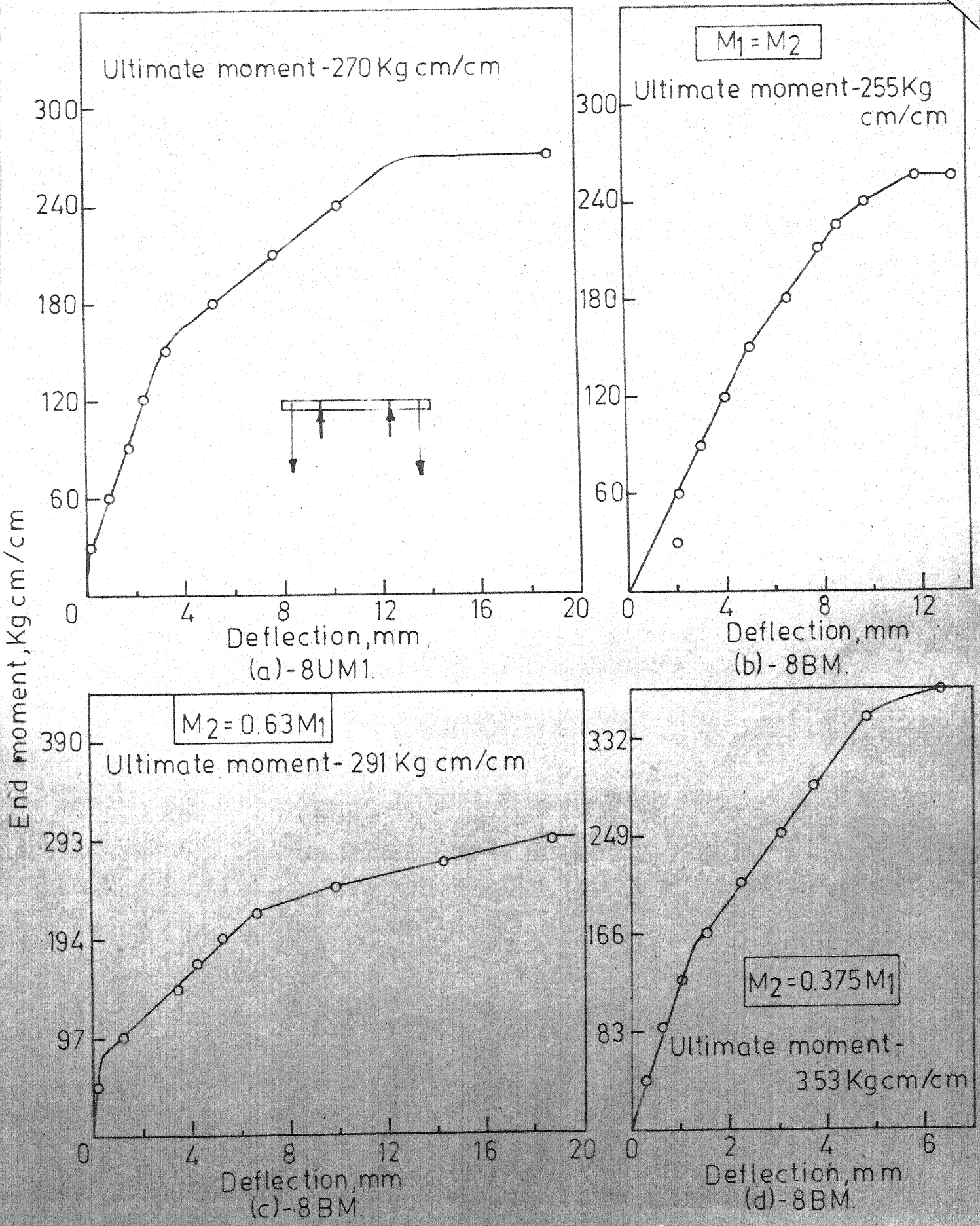

Figure 6.12 - Moment - Deflection Curves for UM and BM Series.

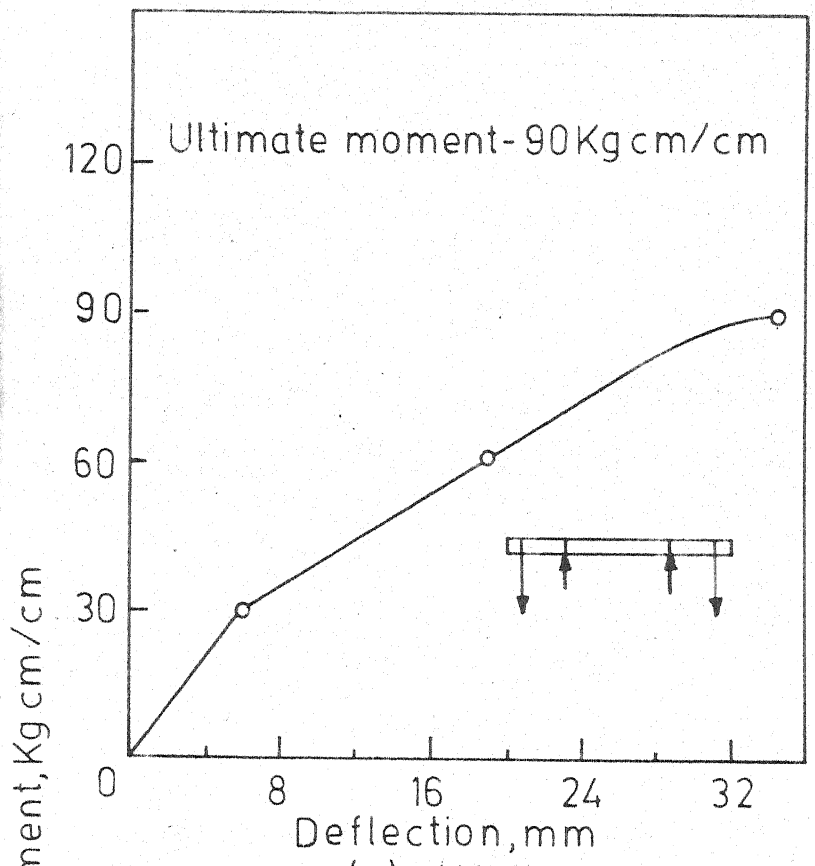

(a)-4UM1.

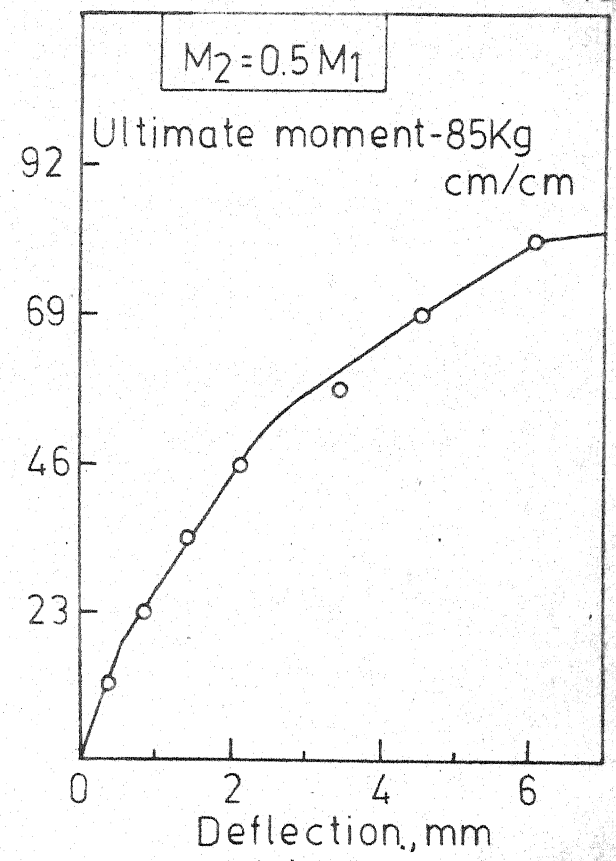

(b)-4BM.

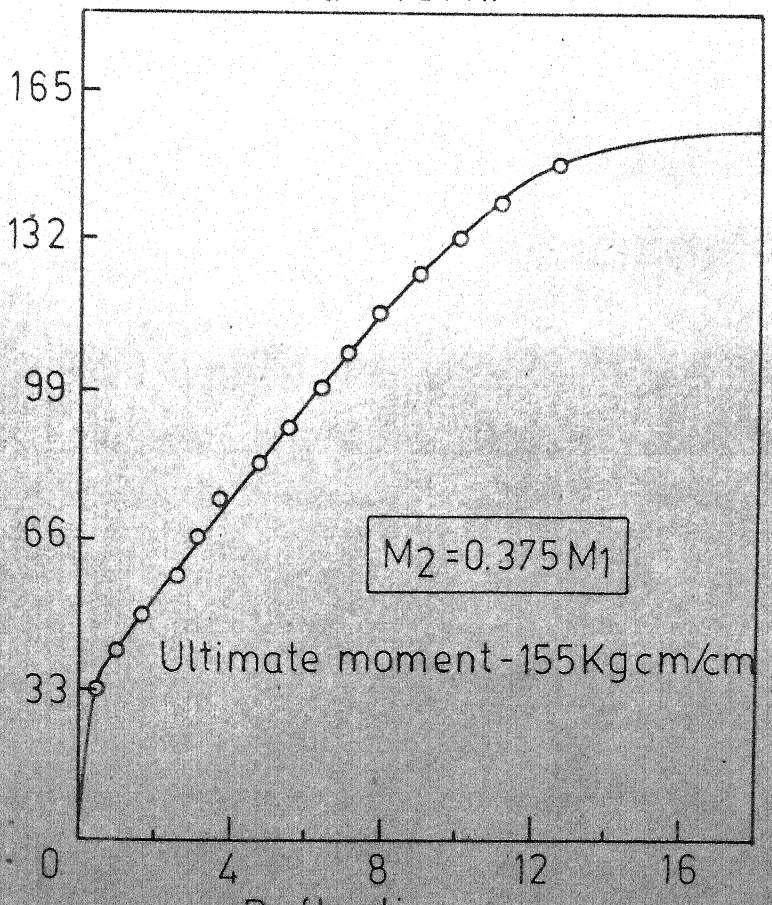

(c)-4BM.

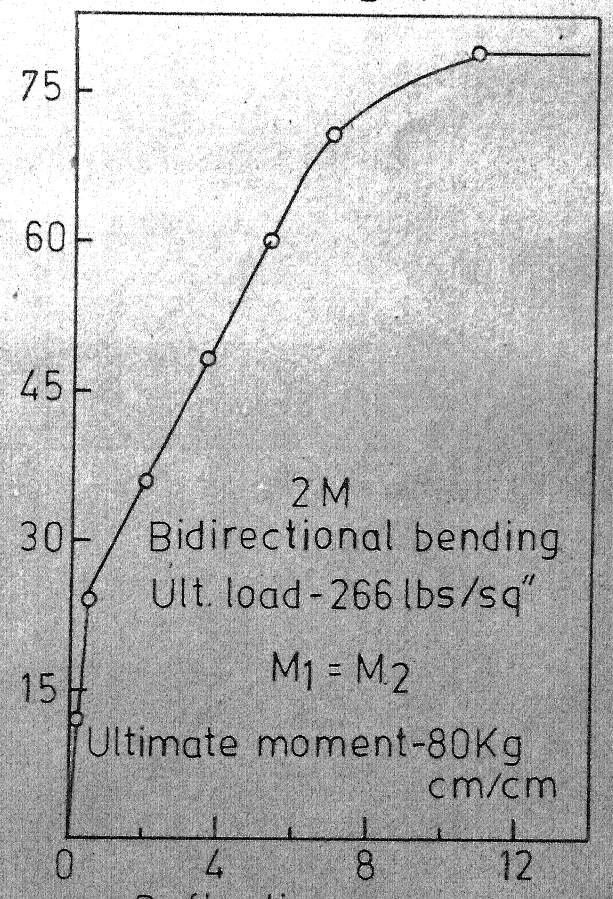

(d)-4BM.

Figure 6.13 - Moment - Deflection Curves for UM and BM Series.

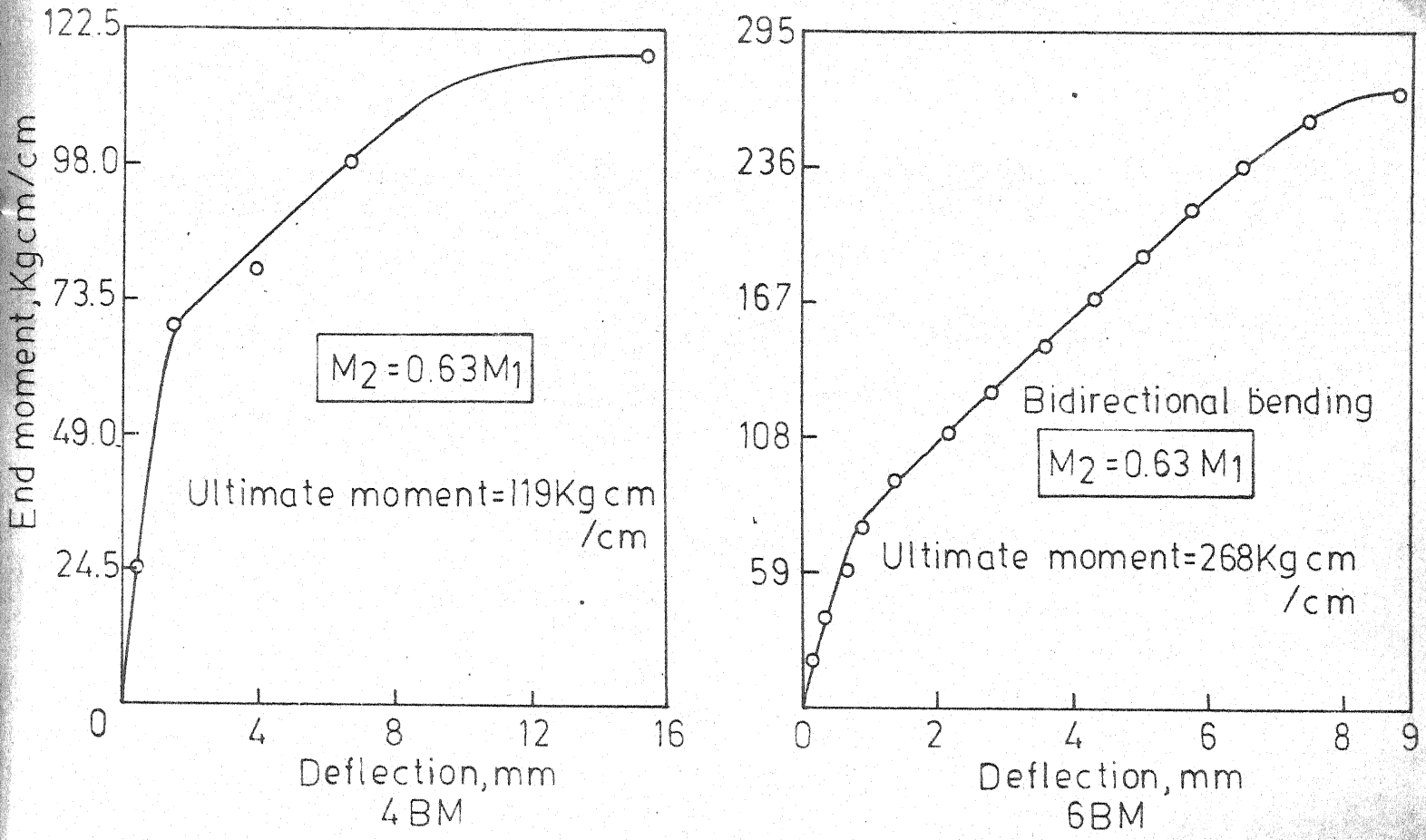

Figure 6.14- Moment - Deflection Curves for UM and BM Series.

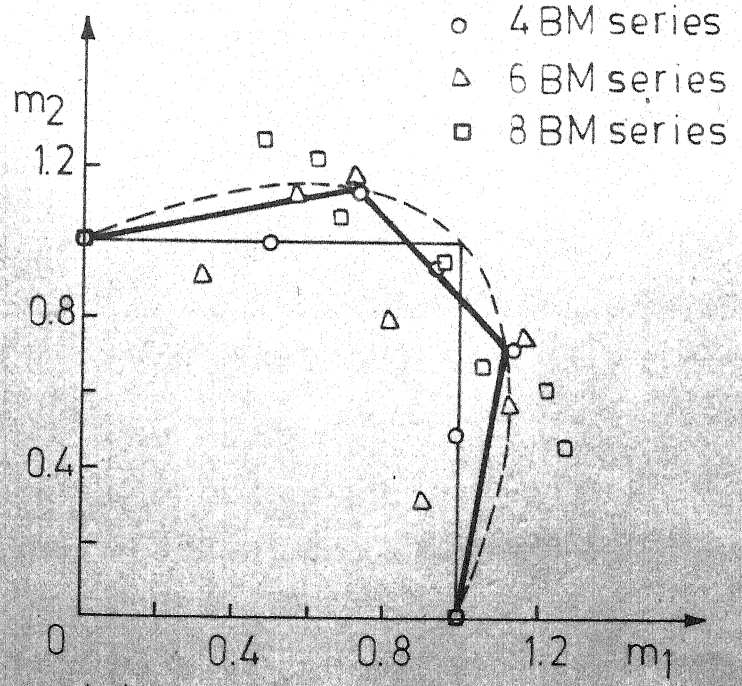

(a)-Proposed yield criterion.

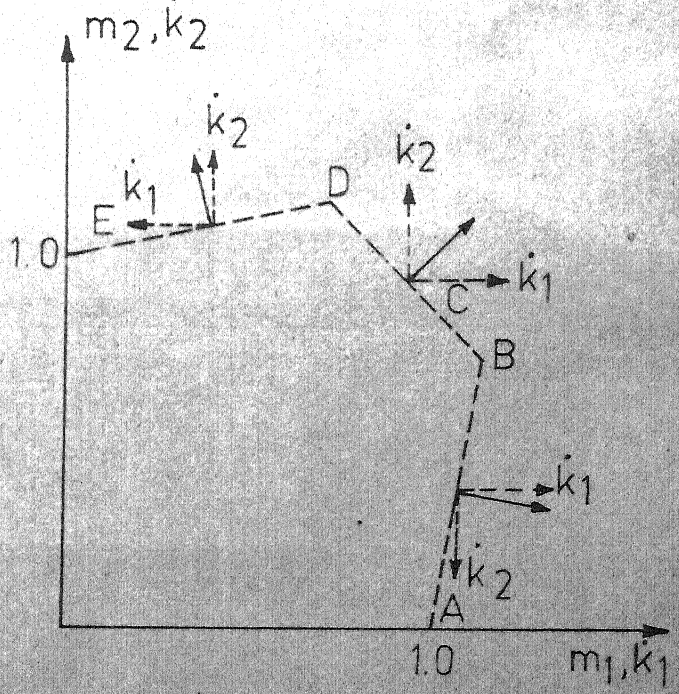

(b)-Gradient vectors.

Figure 6.15- Proposed Yield Criterion with Gradient Vectors.

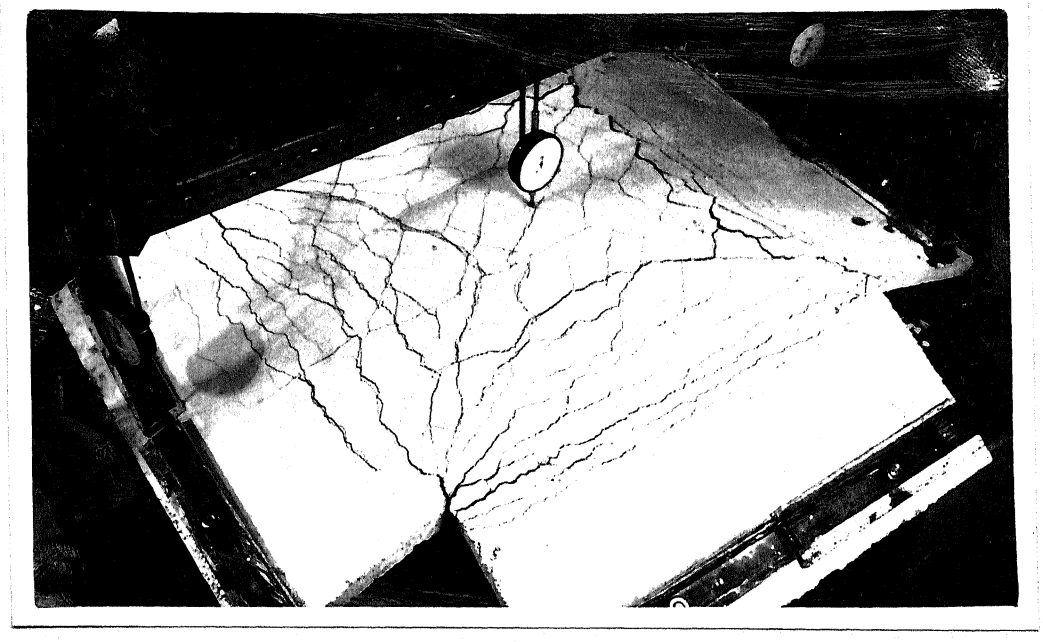

Figure 6.16 Crack Pattern for 6BM Specimen

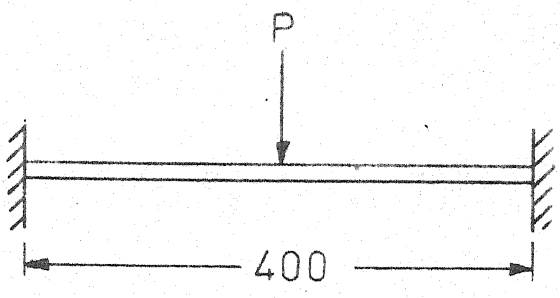

(a)- Before loading.

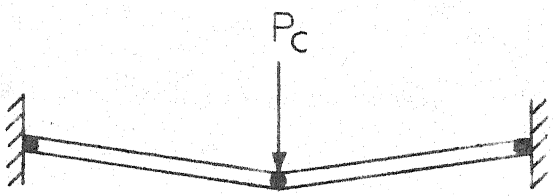

(b)- After collapse.

Figure 6.17 - Clamped Plate Under Central Line Loading.

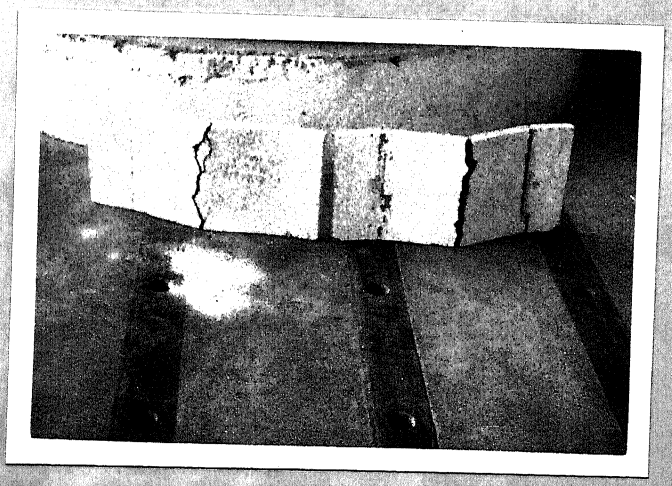

Figure 6.18- Yield Lines for Tested Rectangular Slab.

CHAPTER VII

EXPLOSIVE LOADING

7.1 General

Theoretical and experimental investigations into inelastic response of engineering materials under high intensity of short duration loads are necessary in order to permit reliable predictions of structural damage to pressure vessels, explosive containers, shiphulls etc. An extensive work in the area of damage to structures in underwater and air due to shock waves has been done by Kirkwood (123). The detailed description of the shock wave propagation, the energy released by the explosives, the mode of energy dissipation etc. has been given by him in a number of papers (123). However, all his studies are confined to materials other than ferrocement.

Ferrocement is a material with high resilience and can resist effectively shock and impulse loadings. To study the response of ferrocement material to explosive and detonation shock waves underwater and air, a test programme has been carried out, the details of which are given later. The test results have been discussed only qualitatively. An extended study of this nature would provide useful information, but due to lack of resources (viz. detonators and explosives), only a few tests could be carried out.

7.2 Detonation and Explosive Shock Waves

In the analysis of damage to structures by underwater explosion waves and by blast waves in air, a knowledge of pressure-time curve, peak pressure-time curves, peak pressure-distance curves of shock waves, produced by

explosives, is of primary importance.

The method of computing the magnitude of pressure and approximate durations of pressure-time pulse at any distance underwater from an explosion of a given spherical charge is given by Kirkwood (123). The computation starts with the initial pressure, the equation of state for burnt gases and other quantities which have been previously calculated theoretically. The pressure-time curve obeys the dimensional law, i.e., if the pressure, time and distance are measured in units proportional to the cube root of the mass of the charge, then the pressure curves for different masses of the same explosives will coincide if measured at equal distances (in the reduced units).

It has been found (123) that the peak pressure falls off as the inverse distance except near to the charge; where, within about twenty charge diameters, this law fails badly and the rate of fall is much more rapid. Furthermore, near to the charge, the duration of the pulse increases as the pulse moves away, although this spreading effect is scarcely noticeable beyond perhaps twenty five charge diameters. The absolute pressure calculated for 300 lb. of cast TNT at 50 ft. is 1.02 longtons/sq. in.

The damage to the structures in underwater explosion is attributed to the initial pressure pulse, although secondary pulses may also be important. The experimental investigation of initial pressure pulse is difficult due to non-availability of proper gauges and apparatus for recording gauge response. In the present investigation, the response was recorded through electrical resistance straingauges connected to Encordiorite viscicorder having eight channels.

7.3 Test Procedure

7.3.1 Underwater Blast

An underground excavation (2100 deep x 2400 dia) was made and the surfaces were properly levelled. At the bottom of the excavated pit, mass concreting (mix ratio 1:2:4 with water-cement ratio of 0.45 by weight) was done to get a base thickness of 600. The tank reinforcement cage prepared earlier, was lowered into excavated pit so that it hung centrally over the concrete base. The tank was then cast with rich cement mortar. The annular gap of 450 between the surrounding ground and the tank was then concreted. Curing was then done for 28 days. Other pertinent experimental details are given in Chapter III. The tank was fitted with strain gauges on the inner mortar surface as shown in Figure 3.2. Since the propagation of the initial pressure wave is spherical from the source of explosion, all the strain gauges were fixed at mid height and at the centre of the base of the tank. Cordtex explosives were used in this investigation. The cylindrical tank was filled with water upto the brim. The charge was lowered into the tank and subjected to explosion and the response of the tank recorded on automatic viscicorder. The explosive charges were varied from 1 metre to 3 metres in steps of 0.5 metres (1 metre = 10 gm of explosive approx). A few typical strain-time plots are shown in Figure 7.1.

7.3.2 Blast in Air

Six slab specimens were also subjected to explosive blast load tests in air. Ferrocement slabs (300 x 600) or (600 x 600) were kept on level ground

and a plastic charge of 5 to 15 gms was kept over the slab surface. Similar tests were conducted on the mild steel plates of 8-15 thickness for comparison. Figure 7.2 shows the damage caused by the explosive on ferrocement plates.

7.4 Discussion of Test Results

In the case of underwater explosion of the tank, it was observed that 15 gms of explosive charge did not produce any apparent damage to the ferrocement-tank and the surroundings. However, 20 gms of explosive resulted in cracks along the top periphery of the junction between the ferrocement tank and the surrounding concrete ring. It is felt that this blast must have resulted in a compression wave of rather high intensity, which, on travelling across the wall thickness, produced microcracks and also spalling off of concrete at the other end. No visible cracks were, however, observed in the ferrocement tank. 30 gms of the explosive charge did produce vertical cracks in the wall of the ferrocement tank at a few places, resulting in the complete emptying of the tank, water having obviously seeped through the cracks so formed. The Figure 7.1 shows this phenomenon in detail. It is apparent from the figure that the charge upto 20 gms resulted in quick damping of the system, whereas with the stronger charge, the vibrations continued upto almost half a second.

The blast tests in air carried out on rectangular ferrocement slabs of thicknesses 25, 28 and 30, resulted in through holes in the slabs, with the plastic charges of magnitudes 7.5, 10 and 15 gms, respectively. For

charge magnitudes less than these, only localized depressions with shattered mortar around it, were found. The damage caused to the slabs was found to be dependent on the shape of the plastic charge applied to the slabs. When the charge was put in the form of a thin flat shape, a localized depression was observed, the penetration being dependent on the amount of the charge. However, deeper penetration, resulting in through holes was observed, when the charge was applied in the shape of a cone on the slab. (Refer Figure 7.2).

The 15 gm charge in the conical form when applied on one side of a steel plate of thickness 15, resulted in spalling off of the material on the other side, whereas a charge of lesser magnitude, only produced a localized depression on one side and cracks on the opposite side.

From the above discussion, it is clear that the ferrocement material offers moderate to high resistance to blast loadings both in air and underwater. One particular advantage with this material is that the resulting damage (due to blast), being localized, can easily be repaired later on. It may be mentioned that no spalling off of the mortar was observed in case of ferrocement, unlike that in concrete and steel materials.

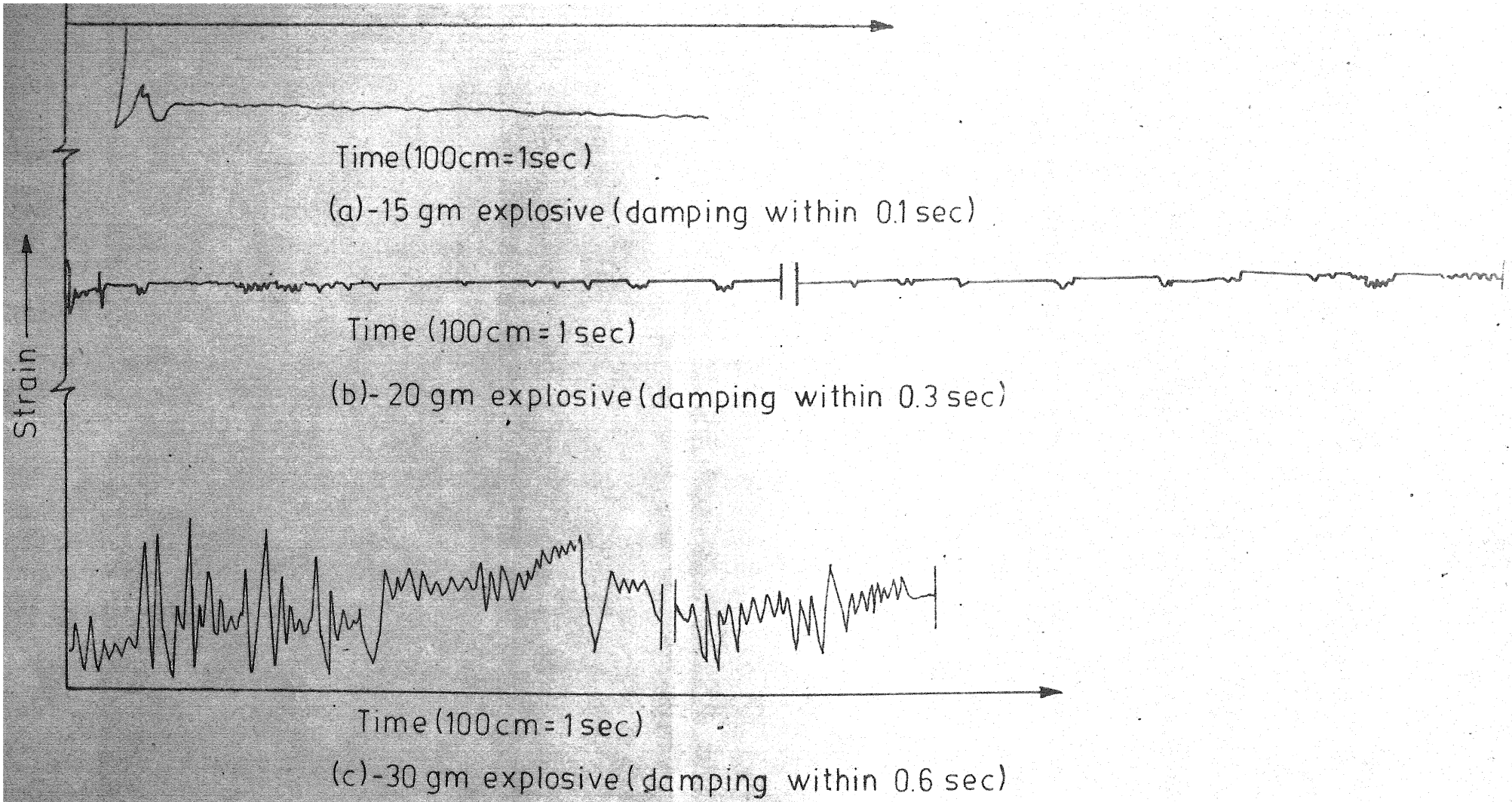

Figure 7.1 - Strain - Time Plots for Explosive Loading on an Ungerground Cylindrical Tank.

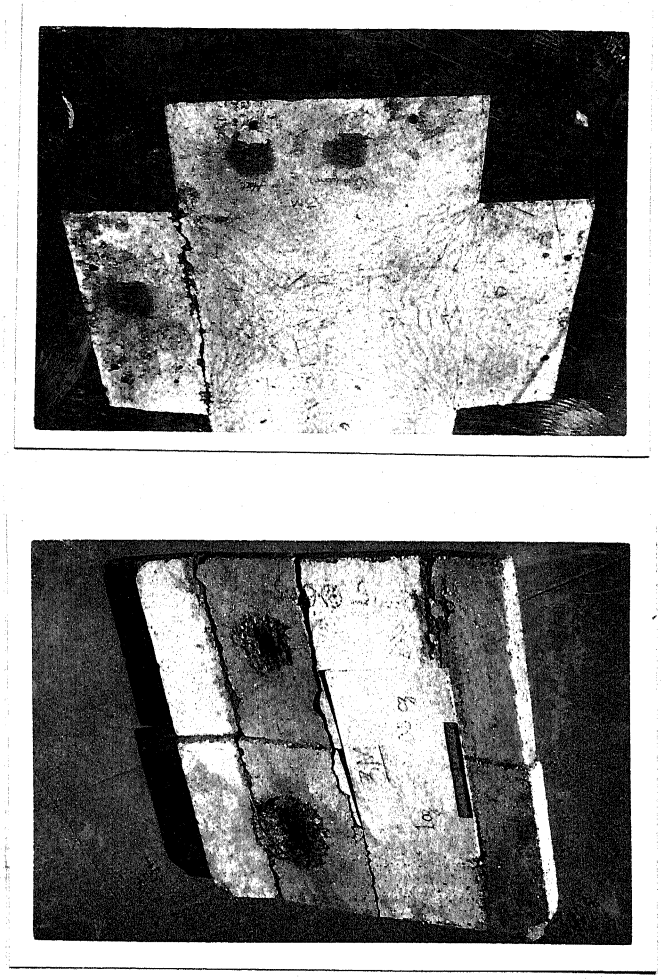

Figure 7.2 Damage to Rectangular Slabs due to Explosive Loading in Air.

CHAPTER VIII

CONCLUSIONS

8.1 General

An extensive experimental programme was conducted to understand the behaviour of ferrocement slabs under flexural sustained loads, flexural fatigue loads, biaxial bending and explosive blast loads. The variables in all the specimens were, the number of layers of wire mesh, the gauge size of the wire mesh and the thickness of the slabs. The conclusions drawn from these tests have been summarised below.

8.2 Creep

a. The creep specimens were observed to attain steady state in 40-45 days, when subjected to low tensile stresses (i.e., less than 35 kg/cm^2).

b. The creep rates for specimens (having a prior history of sustained loading for 30-45 days), were in general observed to be less than those observed for specimens without any earlier stress history. Also, more the age (curing period) of the specimen at the time of testing, the lower were the creep rates. The specimens subjected to sustained load, when tested to collapse under static loads, could carry 10-15% more load than their virgin parallels.

c. On the removal of the loads, instantaneous elastic recovery was of the order of forty percent for a test specimen subjected to a sustained load for a period of 45 days. The delayed recovery over a period of 10 days was another 10 percent. It was also observed that the cracks healed up with time on the removal of the load.

d. The creep observed in ferrocement slabs is usually less due to the even distribution of fine chicken wire mesh in both tension and compression zones. Logarithmic/hyperbolic relations appear to be

quite useful in prediction of creep. The load-creep relationship is linear prior to cracking and nonlinear in the post cracking range.

e. The effect due to the moderate changes in temperature and humidity on the creep is small, especially when matured samples are tested.

8.3 Fatigue

a. The presence of chicken wire mesh in ferrocement effectively arrests the crack propagation even under moderately high stress ranges of pulsating loads.

b. The specimens when subjected to repeated stresses of the order of 30 kg/cm^2 (the upper and the lower stress levels being 75-80 kg/cm^2 and 45-50 kg/cm^2 respectively) could withstand upto 2×10^6 cycles. A few pulsating peak loads of 15-20 percent of the upper stress level did not appreciably affect the endurance limit.

c. The incremental fatigue creep is linear in the low range of stress cycles and is almost recoverable over a rest period.

d. The flexural rigidities decrease and the stress strain relations become linear with increasing number of load cycles and then stabilize and also the energy stored due to hysteresis decreased with increasing load cycles. The nearness of failure of a specimen is indicated by the concavity in the load-deflection curve. The failure is usually sudden and is of brittle nature.

e. Those specimens that did not fail even at 2×10^6 cycles, when subjected to static loads, failed at 75-80 percent of the collapse load of their virgin parallels.

8.4 Yield Criterion

a. For slabs subjected to static loads, within the experimental limitations, the theoretical and experimental collapse loads and the yield patterns are in agreement. In particular, for slabs subjected to axi-symmetric loading and boundary conditions, the agreement was much better. Besides, considering the deformed slab of the truncated cone, the theoretical load capacity computed agrees well with the experimental value.

b. The proposed yield criterion is more closer to the Mises yield criterion due to the ductile nature of the ferrocement.

c. In the proposed yield criterion, the carrying capacity is increased in going from uniaxial to biaxial state upto a value of $M_2 = 0.7\ M_1$ and then decreased. The precompression of the mortar increases the load carrying capacity in the initial ranges, while the interference caused by the woven-mesh reduces the capacity at later stages $(M_1 = M_2)$.

8.5 Explosive Loading

The preliminary tests conducted indicate that ferrocement offers high resistance to blast loads. The damage caused to the structures is localised and hence can easily be repaired. This strong point of ferrocement makes it most suitable for the sea sailing structures like fishing vessels which are susceptible to collision in bad weather conditions. Unlike concrete, little or no spalling off of the mortar is observed under blast loading.

8.6 Recommendations for Further Research

a. Experiments should be carried out to find out a suitable workability agent available locally to improve the quality of the mortar mix.

b. The strength of ferrocement under low cycle fatigue must be determined. This is important for those structures which are occasionally subjected to high intensity dynamic loads.

c. To establish a complete generalized yield criterion and to obtain quantitative results for the structures subjected to blast loading, more experimental work is required.

d. Long term studies on the creep of ferrocement under general state of stress should be conducted.

e. The scatter in experimental data on fatigue and creep of composite materials like ferrocement is usually wide. Hence, an extensive experimental programme is necessary to get a compatible sample size for making use of the statistical methods of analysis in estimating the fatigue life of a structure.

f. The behaviour of twin ferrocement slabs with shear connectors under different loading conditions is of great interest and is presently under investigation.

Appendix A

Moment-Curvature Relationships for Ferrocement

A.1 Bending of Ferrocement Slabs

The load-deflection curve of a ferrocement slab element subjected to monotonically increasing bending moment is approximately trilinear as shown in Figure A.1(a).

A.1.1 Uncracked Range

In the uncracked range, the ferrocement can be treated as homogeneous composite material and the stress distributions, as shown in Figure A.1(b), are determined from the classical beam theory. The modulii of elasticity in tension and compression are assumed to be equal. The moment carrying capacity of the section is given by

$$M = \frac{\sigma_c h^2}{6} \qquad \ldots (A.1.1)$$

where M - the bending moment per unit width of section,

σ_c - the tensile or compressive stress in composite, and

h - the thickness of the composite section.

For a composite material reinforced with fibres oriented at an angle with the loading direction, the 'law of mixture' (9) yields

$$\sigma_c = \sigma_m V_m + F^2 \sigma_f V_f \qquad \ldots (A.1.2)$$

where σ_m - the tensile or compressive stress in mortar/matrix,

σ_f - the tensile or compressive stress in fibres, i.e. wire mesh,

V_m - the volume fraction of matrix,

V_f - the volume fraction of fibres and

F - the fibre efficiency factor and is given by the cosine of the angle that fibre makes with load direction.

It can be easily shown that

$$E_c = E_m V_m + F^2 E_f V_f \qquad \ldots (A.1.3)$$

where E_c - the modulus of elasticity of composite,

E_m - the modulus of elasticity of mortar and

E_f - the modulus of elasticity of fibres.

The cracking of the mortar corresponds to the limiting case of the uncracked range, for which equation A.1.1 is given by

$$M_{cr} = \frac{\sigma_{cr} h^2}{6} \qquad \ldots (A.1.4)$$

where M_{cr} - the cracking moment of the ferrocement section and

σ_{cr} - the modulus of rupture of the mortar determined from beam test.

A.1.2 Cracked Range

In the cracked range the modulus of elasticity of the uncracked zone is given by equation A.1.3. For the cracked zone the effective modulus of elasticity is obtained by dropping the term $E_m V_m$ in equation A.1.3, hence

$$E_t = F^2 E_f V_f \qquad \ldots (A.1.2.1)$$

where E_t - the modulus of elasticity of composite in tension in the cracked range.

The stress and strain distributions in the cracked range are shown in Figure A.1(c) where the neutral axis shifts upward relative to that of uncracked range. The more accurate stress distribution curve on the left may be replaced with very little loss of accuracy by the simpler on the right.

It can be shown that the position of the neutral axis is defined by

$$\frac{h_t}{h_c} = \sqrt{\frac{E_c}{E_t}} = \beta \qquad \ldots (A.1.2.2)$$

where h_t - the depth of tension zone and

h_c - the depth of compression zone.

The tensile and compressive stresses are respectively

$$\sigma_t^* = \alpha_1 \frac{6M}{h^2} \qquad \ldots (A.1.2.3)$$

$$\sigma_c^* = \alpha_2 \frac{6M}{h^2} \qquad \ldots (A.1.2.4)$$

where σ_t^* - the tensile stress in bending, and

σ_c^* - the compressive stress in bending.

In equations (A.1.2.3) and (A.1.2.4),

$$\alpha_1 = \frac{1+\beta}{2\beta} \qquad \ldots (A.1.2.5)$$

$$\alpha_2 = \frac{1+\beta}{2} \qquad \ldots (A.1.2.6)$$

It may be mentioned here that M in equations (A.1.2.3) and (A.1.2.4) corresponds to bending moment due to loads in excess of cracking load of mortar. The yielding of wire mesh and skeletal reinforcement denotes the end of the second range.

A.1.3 Yield Range

The stress and strain distributions in the yield range are shown in Figure A.1(d). Again the more accurate stress distribution curve shown on the left is replaced by simpler rectangular stress block on the right.

In the tension zone, the total tensile force per unit width of section is given by

$$T' = T_f + T_s = F^2 \sigma_{fy} V_f h_t' + A_s \sigma_{sy} \qquad \ldots (A.1.3.1)$$

where T' - the total tensile force,

T_f - the tensile force due to wire mesh/fibres,

T_s - the tensile force due to skeletal steel,

σ_{fy} - the yield strength of fibres,

σ_{sy} - the yield strength of skeletal steel,

A_s - the area of skeletal steel per unit width of the section and

h'_t - the depth of tensile zone.

The total compressive force C per unit width of the section is

$$C = 0.85 \ \sigma_{ca} \ h'_c \qquad \ldots (A.1.3.2)$$

where h'_c - the depth of the compression zone and

σ_{ca} - the average cube strength of the mortar.

In equation A.1.3.2, the cube compressive strength has been reduced by 15 percent due to the fact, that in compression the fibres have adverse effect on the strength of the composite due to local buckling of the wire mesh which causes premature failure.

The force equilibrium of the section yields

$$h'_c = \frac{A_s \ \sigma_{sy} + F^2 \ \sigma_{fy} \ V_f \ h}{0.85 \ \sigma_{ca} + F^2 \ \sigma_{fy} \ V_f} \qquad \ldots (A.1.3.3)$$

$$M_o = A_s \ \sigma_{sy} \left(h_s - \frac{h'_c}{2}\right) + F^2 \ \sigma_{fy} \ V_f \left(\frac{h}{2}\right) (h - h'_c) \qquad \ldots (A.1.3.4)$$

where M_o - the ultimate moment per unit width and

h_s - the depth of the skeletal steel from extreme force of slab.

It is suggested, based on experimental evidence, that F in equation (A.1.3.3) and (A.1.3.4) should be taken as 1 since at collapse the fibres of the wire mesh get oriented in the direction of the load due to kinking and hence are hundred percent effective.

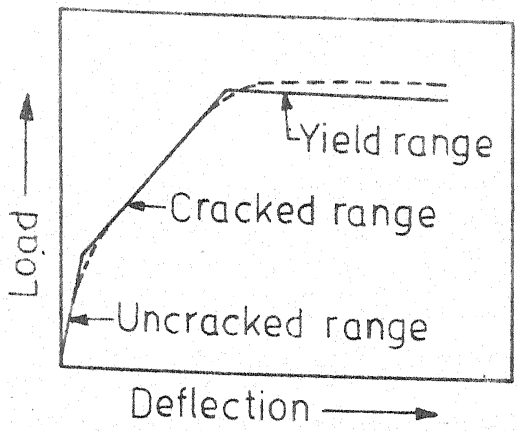

(a)-Load-deflection curve for ferrocement.

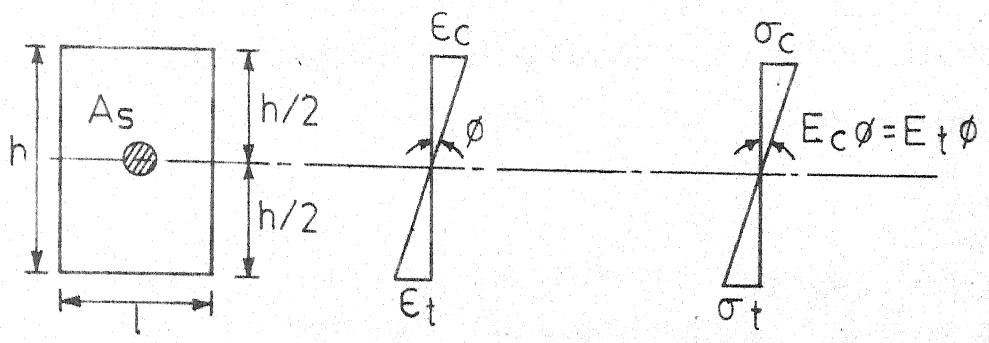

(b)-Uncracked range.

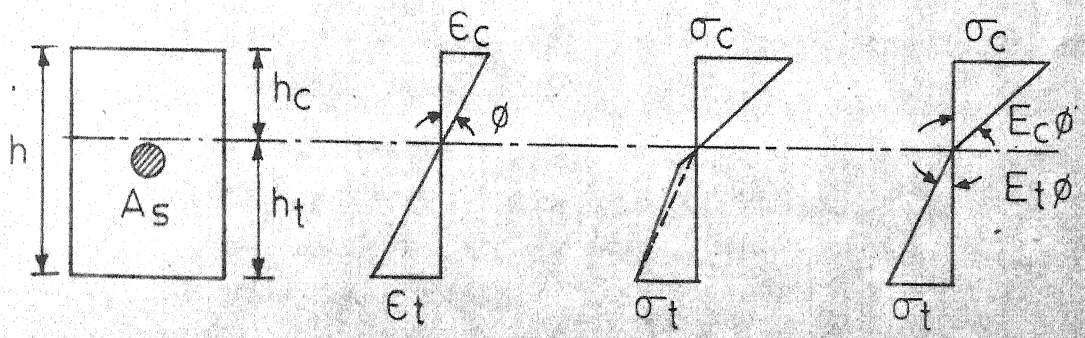

(c)-Cracked range.

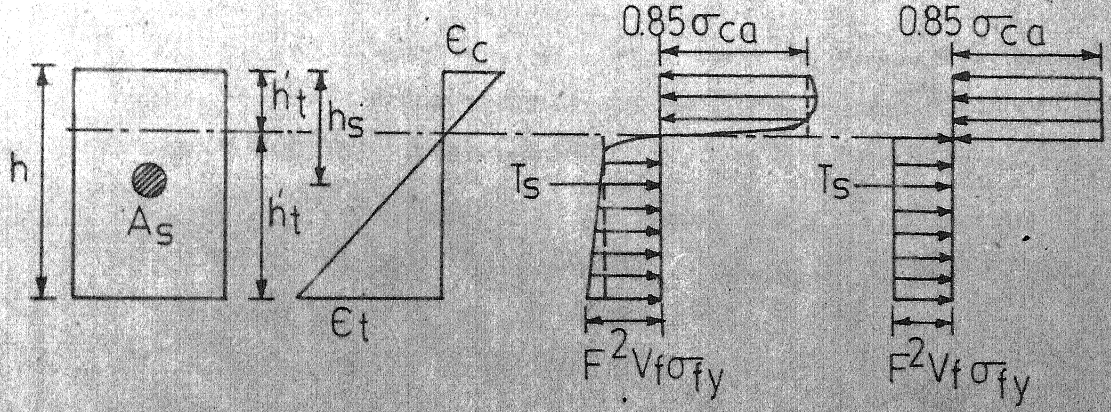

(d)-Yield range.

Figure A.1-Stress Strain Distribution.

REFERENCES

1. Nervi, P.L., 'Ferrocement, its Characteristics and Potentialities', L'Ingegnere, Jan. 1951 (English Translations by Cement and Concrete Association, London).

2. Smith, R.B.L. and Boon-Long, S., 'Ferrocement for Hermetic Storage of Rice', Research Report No. 12, AIT, Bangkok, 1970.

3. 'Ferrocement: Applications in Developing Countries', National Academy of Sciences, Washington, 1973.

4. Khaidukov, G.K., 'Development of Armocement Structures', Bulletin of IASS, Dec. 1968, No. 36, pp. 85-97.

5. Walkus, B.R., Maria Kamariska and Edward Szejkowski, 'Mechanical Method of Manufacture of Prefabricated Shells', IASS Symposium on Industrialized Spatial and Shell Structures, Kielec, Poland, June 1973, pp. 399-410.

6. Griffith, A.A., 'The Phenomenon of Rupture and Flow in Solids', Translations, Royal Philosophical Society, Glasgow, A221, 1920, pp. 163-198.

7. Romualdi, J.P. and Mandel, J.A., 'Tensile Strength of Concrete Affected by Uniformly Distributed and Closely Spaced Short Lengths of Wire Reinforcement', ACI Journal, Proc., Vol. 61, No. 6, June 1964, pp. 657-672.

8. Broutman, L.J. and Krock, R.H., 'Modern Composite Materials', Addison-Wesley Publishing Co., London, 1967, pp. 16-19.

9. Lee, S.L., Raisinghani, M. and Pama, R.P., 'Mechanical Properties of Ferrocement', FAO Seminar on the Design and Construction of Ferrocement Fishing Vessels, Wellington, New Zealand, Oct., 1972, pp.1-20.

10. Romualdi, J.P. and Batson, G.B., 'Mechanics of Crack Arrest in Concrete', Journal of Engineering Mechanics Devision, ASCE, Proc., Vol. 89, No. EM3, June 1963, pp. 147-168.

11. Aveston, J. and Kelly, A., 'Theory of Multiple Fracture of Fibrous Composites', Journal of Material Science, Vol. 8, No. 3, 1973, pp. 352-362.

12. Shah, S.P. and Rangan, B.V., 'Fiber Reinforced Concrete Properties', ACI Journal, Proc., Vol. 68, No. 2, Feb., 1971, pp. 126-134.

13. Naaman, A.E. and Shah, S.P., 'Tensile Tests in Ferrocement', ACI Journal, Proc., Vol. 68, No. 9, Sept., 1971, pp. 693-698.

14. Walkus, R., 'State of Cracking and Elongation of Ferrocement Under Axial Tensile Load', I and II. Buletinal Institulni Polytechnic Division. Iasi, Tonsul XIV, 1968 and Tonsul XVI, 1970.

15. Bezukladov, V.F., Amel Yanovich, K.K., Verbitakiy, V.D. and Bogo Yavlensky, L.P., 'Ship Hulls made of Reinforced Concrete', Noviships Translation No. 1148, Shipbuilding House, Leningrad, 1968.

16. Rao, K.A. and Gowder, K.C.C., 'A Study of Behaviour of Ferrocement in Direct Compression', Cement and Concrete, Oct. - Dec., 1969, pp. 231-237.

17. Kelly, A.M. and Monat, T.W., 'Ferrocement as a Fishing Vessel Construction Material', Proc. Conf. on Fishing Vessel Construction Materials, Montreal, Canada, Oct., 1968.

18. Claman, J.S., 'Bending of Ferrocement Plates', M.Sc. Thesis, Institute of Technology, Cambridge, Massachusetts, 1967.

19. Walkus, B.R., 'The Behaviour of Ferrocement in Bending', Journal of Structural Engg., Vol. 3, No. 3, Oct., 1975, pp. 113-125.

20. Nervi, P.L., 'Structures', Translation by Giuseppinna and Mario Salvadori, F.W. Dodge Corporation, New York, 1956.

21. Desayi, P. and Jacob, A.K., 'Strength and Behaviour of Ferrocement in Tension and Flexure', Proc. Symp. on Modern Trends in Civil Engineering, Vol. 1, University of Roorkee, Nov., 1972, pp. 274-79.

22. Muhlert, F.H., 'Analysis of Ferrocement in Bending', Eastern Canadian Section, Society of Naval Architects and Marine Engineers, Montreal, 1969.

23. Rajagopalan, K. and Parmeswaran, V.S., 'Cracking and Ultimate Strength Characteristics of Ferrocement in Direct Tension and Pure Bending', The Indian Concrete Journal, Vol. 48, No. 12, Dec., 1974, pp. 387-393.

24. Logan, D. and Shah, S.P., 'Moment Capacity and Cracking Behaviour of Ferrocement in Flexure', Journal of the American Concrete Institute, Vol. 20, No. 12, Dec., 1973, pp. 799-804.

25. Austriaco, N.C., 'Trilinear Behaviour of Ferrocement Slabs', Ph.D. Thesis, AIT, Bangkok, 1975.

26. Pama, R.P., Sutharatnachaiyaporn, C. and Lee, S.L., 'Rigidities and Strength of Ferrocement', Proc. First Australian Conf. on Engineering Materials, Sydney, Australia, 1974, pp. 287-308.

27. Sintzow, G.M., Libow, Y.A., Antipow, W.A. and Lapin Ye I, 'Konstrukja i Protchnost zhelie zobietonnyich Sudow' (Construction and Strength of Reinforced Concrete Ships) Izdat, Sudostroyienie, Leningrad, 1969, p. 384 (In Russian).

28. Shah, S.P. and Key, W.H. Jr., 'Impact Resistance of Ferrocement', Journal of Structural Engineering Division, ASCE, Vol. 98, No. ST1, Jan., 1972, pp. 111-123.

29. Chang, Wen F., Gibson, D.W., Gibbons, N.R., 'Flexural Behaviour of Ferrocement Panels', Civil Engineering in Oceans - II, pp. 1023-1044.

30. Lessard, Y., 'Propriete's et Applications do Ferro-Shotcrete', These de Maitrise, Department de Ge'nie Civil, Universite Laval, Canada 1971, X1 + 197, p. 19 (In French).

31. Lachance, L. and Fugeure, P., 'Ferro-Shotcrete for Thin Shell Structures', Bulletin IASS, No. 44, Dec., 1970, pp. 13-18.

32. Greenius, A.W., 'Behaviour of Ferrocement Under Repeated Stresses', Journal of Structural Engineering, Roorkee, Vol. 2, No. 4, Jan., 1975, pp. 129-136.

33. Surya Kumar, G.V., Narayanaswamy, V.P. and Sharma, P.C., 'Ferrocement-a Survey of Experimental Investigations', Journal of Structural Engineering, Vol. 1, No. 4, Jan., 1974, pp. 167-182.

34. Walkus, B.R. and Kowalski, T.G., 'Ferrocement - a Survey', Concrete, Cement and Concrete Association London, Feb., 1971, pp. 48-52.

35. Hill, R., 'The Mathematical Theory of Plasticity', Oxford University Press, 1967.

36. Westergaard, H.M., 'Theory of Elasticity and Plasticity', Harvard University Press, Cambridge, 1952.

37. Koiter, W.T., 'General Theorems for Elastic Plastic Solids', Progress in Solid Mechanics, edited by I.N. Sneddon and R. Hill, Amsterdam, 1960, North Holland, Vol. 1, pp. 165-221.

38. Kececioglu, D., 'Bibliography of Plasticity: Theory and Applications', ASME Publication, 1950.

39. Tresca, H., 'Memoire Sur l'ecoulment des Corps Solides Soumis a de fortes Pressions, Comptes Rendus Acad. Sci, Paris, Vol. 59, 1864, pp. 754-758.

40. Tresca, H., 'Memoire Sur L'e poinconnage et. la Theorie Mechanique de la Deformation des Metanx', Comptes Rendus Acad. Sci. Paris, Vol. 68, 1869, pp. 1197-1201.

41. Von Mises, R., 'Mechanik der Koerper in Plastisch Deformablen Zustand', Goettinger Nachrichten, Math. Phys. Klasse, 1913, pp. 582-592.

42. Von Mises, R., 'Mechanik der Plastischen Formaenderung Von Kristallen, Zeit and Math. Mech., Vol. 8, 1928, pp. 161-185.

43. Drucker, D.C., 'Some Implications of Work Hardening Ideal Plasticity', Quarterly of Applied Mathematics, Vol. 7, No. 4, 1950, pp. 411-418.

44. Drucker, D.C., 'A More Fundamental Approach to Plastic Stress-Strain Relationships', Proceedings, First U.S. National Congress of Applied Mechanics, Chicago, 1951, Ann Arbor, 1952, pp. 487-491.

45. Prager, W., 'An Introduction to Plasticity', Addison-Wesley Publishing Co., Reading, USA, pp. 57-68.

46. Melan, E., 'Zur Platizitat des Raumlichen Kontinuum', Ing-Archiv, Vol. 9, 1938, pp. 116-126.

47. Nielsen, M.P., 'Exact Solutions to the Plastic Plate Theory', Bygringsstatiske Meddelesen, Vol. 34, Copenhagen, 1963, p. 28.

48. Koiter, W.J., 'Stress-Strain Relations, Uniqueness and Variational Theorems for Elastic Plastic Materials with a Singular Yield Surface', Quarterly of Applied Mathematics, Vol. 11, 3, 1953, pp. 350-354.

49. Prager, W., 'A New Method of Analysing Stress and Strain in Work Hardening Plastic Solids', Journal of Applied Mechanics, Vol. 23, pp. 493-496.

50. Hodge, P.G. Jr., 'Piecewise Linear Plasticity', Proceedings Ninth International Congress of Applied Mechanics, Brussels, Vol. 8, 1957, pp. 65-72.

51. Hodge, P.G. Jr., 'A General Theory of Linear Piecewise Plasticity Based on Maximum Shear', Journal Mech. Phys. Solids, Vol. 5, 4, 1957, pp. 242-260.

52. Hodge, P.G. Jr., 'The Effect of Strain Hardening in Annular Slab', Journal of Applied Mechanics, Vol. 20, 1953, pp. 530-536.

53. Hodge, P.G. Jr., 'Boundary Value Problems in Plasticity', Plasticity, Proceedings, Second US Symposium of Naval Structural Mechanics, (edited by E.H. Lee and P.S. Symonds), New York, Pergamon Press, 1960, pp. 297-337.

54. Nielsen, M.P., 'Vridnings for sgmed Jernbeonpla der', Academy of Engineering, Copenhagen, 1965, p. 157.

55. Baus, R. and Tolaccia, S., 'Calcul à la Rupture des Dalles en Beton Arme et Etude Experimental du Crite're de Rupture en Flexion Pure', Annales de l'Institute Technique du Batiment et des Travaux Publics No. 189, Sept., 1963, pp. 871-894.

56. Kwiecinski, M.W., 'Some Tests on Yield Criterion for a Reinforced Concrete Slab', Magazine of Concrete Research, Vol. 17, No. 52, Sept., 1965, pp. 135-138.

57. Johansen, K.W., 'Yield Line Theory', Cement and Concrete Association, London, 1962, p. 181.

58. Wood, R.H., 'Plastic and Elastic Design of Slabs and Plates', The Ronald Press Co., New York, 1961, pp. 12-14.

59. Lenschow, R.J. and Sozen, M.A., 'A Yield Criterion for Reinforced Concrete Under Biaxial Moments and Forces', Civil Engineering Studies, Structural Research Series No. 311, University of Illinois, Urbana, Illinois, 1966.

60. McLaughlin, P.V., 'Properties of Work Hardening Materials with a Limit Surface', Journal of Applied Mechanics, Vol. 40, 1973, pp. 802-807.

61. Drucker, D.C., Prager, W. and Greenberg, H.J., 'Extended Limit Design Theorems for Continuous Media', Quarterly of Applied Mathematics, Vol. 9, 1952, pp. 381-389.

62. Thorn, B.J., Kao, J.S. and Lee, S.L., 'Non regular Progression in Strain Hardening Shells', Conference Preprint No. 269, ASCE, Structural Engineering Conference, Miami, Florida, 1966.

63. Ferguson, P.M., 'Reinforced Concrete Fundamentals', John Wiley & Sons, Inc., New York, p. 11.

64. Neville, A.M., 'Tests on the Influence of the Properties of Cement on the Creep of Mortar', R.I.L.E.M. Bull. No. 4, Oct., 1959, pp. 5-17.

65. Neville, A.M., 'Role of Cement in the Creep of Mortar', Journal of American Institute, March, 1959, pp. 963-984.

66. Ross, A.D., 'A Note on the Maturity and Creep of Concrete', R.I.L.E.M. Bull. No. 1, March, 1959, pp. 55-57.

67. Hope, B.B., Neville, A.M. and Guruswami, A., 'Influence of Admixtures on Creep of Concrete Containing Normal Weight Aggregate', R.I.L.E.M. Int. Symp. on Admixtures for Mortar and Concrete, September 1967, pp. 17-32.

68. Arnstein, A. and Reiner, M., 'Creep of Cement, Cement-Mortar and Concrete', Civil Engg. and Public Works Review, 40, No. 9, 1945, pp. 198-202.

69. L'Hermite, R.G., 'Volume Changes of Concrete', Proc. Fourth Int. Symposium on the Chemistry of Cement, Washington D.C., 1960, pp. 659-694.

70. Lorman, W.R., 'The Theory of Concrete Creep', ASTM Proc. 40, 1940, pp. 1082-1102.

71. Ishai, O., 'Influence of Sand Concentration on Deformations of Mortar Beams under Low Stresses, ACI Journal, Proc. 58, 1961, pp. 611-624.

72. de La Pena, C., 'Shrinkage and Creep of Specimens of Thin Sections', R.I.L.E.M. Bull. No. 3, July 1959, pp. 60-70.

73. Neville, A.M., 'Creep of Concrete: Plain, Reinforced and Prestressed', North Holland Publishing Company, Amsterdam, 1970.

74. Neville, A.M., 'Properties of Concrete', ELBS and Pitman Publishing, 1975.

75. Troxell, G.E., Davis, H.E. and Kelly, J.W., 'Composition and Properties of Concrete', McGraw Hill Book Company, Second Edition, 1968.

76. Ross, A.D., 'Concrete Creep Data', The Structural Engineer, 15, No. 8, 1937, pp. 314-326.

77. 'Investigation of Creep in Concrete', Review of Literature on Creep in Concrete, US Army Engineer Waterways Experiment Station, Corps of Engineers, Vicksburg, Miss., Misc. Paper No. 6-132, Report No. 1, June 1965, pp. 1-22.

78. Irwin, G.R., 'Fracture Dynamics, Fracturing of Metals', ASM, Novelty, Ohio, 1948, pp. 147-166.

79. Orwan, E., 'Fundamentals of Brittle Behaviour in Metal', Fatigue and Fracture of Metals, MIT, Symposium, June 1950, John Wiley and Sons.

80. Narayanawasy, R., 'Written Discussion in Session D', in the Structures of Concrete, Ed., Brookes, A., and Newman, K., C.C.A., 1968, pp. 212-214.

81. Sneddon, I.N., 'The Distribution of Stress in Neighbourhood of a Crack in a Elastic Solid', Proc. of Royal Society, Series A, Vol. 187, pp. 229-260.

82. Rao, C.V.S.K., 'Some Studies on Statistical Aspects of Size Effects on Strength and Fracture Behaviour of Materials and Fracture Resistance', Ph.D. Thesis, Department of Civil Engineering, Indian Institute of Technology, Kanpur, 1972.

83. Glucklich, J., 'Fracture of Plain Concrete', Journal of the Engineering Mechanics Division, ASCE, Dec., 1963, pp. 127-138.

84. Kaplan, M.F., 'Crack Propagation and the Fracture of Concrete', Journal of the American Concrete Institute, Nov., 1961, pp. 591-609.

85. Romualdi, J.P. and Batson, G.B., 'Behaviour of Reinforced Beams with Closely Spaced Reinforcement', Journal of American Concrete Institute, June, 1963, pp. 775-790.

86. 'Considerations for Design of Concrete Structures Subjected to Fatigue Loading', Recommendations of ACI Committee 215, Journal of American Concrete Institute, Vol. 71, No. 3, March, 1974, pp. 97-122.

87. Goodman, J., 'Mechanics Applied to Engineering', Vol. 1, 9th ed., Longmans Green, London, 1930.

88. Frost, N.E., Marsh, K.J. and Pook, L.P., 'Metal Fatigue', Clarendon Press, Oxford, 1974, p. 308.

89. Wood, R.H. and Armer, G.S.T., 'The Theory of the Strip Method for Design of Slabs', Proc. ICE, Vol. 41, 1968, pp. 285-312.

90. Clyde, D.H., 'Yield-Line Theory and Plasticity', Mag. Conc. Res., Vol. 24, 1972, pp. 37-42.

91. Kao, J.S., Mura, T. and Lee, S.L., 'Limit Analysis of Orthotropic Plates', Journal Mech. Phys. Sol., Vol. 11, 1963, pp. 429-436.

92. Hill, R., 'A Theory of the Yielding and Plastic Flow of Anisotropic Metals', Proc. Royal Society, London, Vol. 193, 1948, pp. 281-297.

93. Nielsen, M.P., 'Limit Analysis of Reinforced Concrete Slabs', Acta Polytechnica Scandinavica Civil Eng., Build. Const. Ser., No. Ci 26, 1964.

94. Kemp, K.O., 'The Yield Criterion for Orthotropically Reinforced Slab on Simple Supports', Int. Journal of Mechanical Science, Vol. 7, 1965, pp. 737-746.

95. Sawezuk, A., 'An Initiation of Membrane Action in Rigid Plastic Plates', Journal de Mecanique, Vol. 3, 1964, pp. 15-23.

96. Kwiecinski, M.W., 'Yield Criterion for Initially Isotropic Reinforced Slab', Mag. Conc. Res., Vol. 17, 1965, pp. 79-100.

97. Flügge, W. and Nakamura, T., 'Plastic Analysis of Shells of Revolution Under Axisymmetric Loads', Ingenieur-Archiv., Vol. 34, 1965, pp. 238-247.

98. Kwiecinski, M.W., 'Yield Condition for Orthotropically Reinforced Slab', Arch. Mech. Stos., Vol. 18, pp. 615-625.

99. Massonet, Ch., 'Complete Solutions Describing the Limit State of Reinforced Concrete Slabs', Mag. Conc. Res., Vol. 19, 1967, pp. 13-32.

100. Hopkins, H.G., 'On the Plastic Theory of Plates', Proc. Royal Society, Vol. 241, 1957, pp. 153-179.

101. Schumann, W., 'On Limit Analysis of Plates', Quart. Applied Math., Vol. 16, 1958, pp. 61-71.

102. Zawidzki, J. and Sawczuk, A., 'Plastic Analysis of Fibre Reinforced Plates Under Rotationally Symmetric Conditions', Int. Journal of Sol. and Struct., Vol. 3, 1967, pp. 413-425.

103. Prince, M.R. and Kemp, K.O., 'A New Approach to the Yield Criterion for Isotropically Reinforced Concrete Slabs', Mag. Con, Res., Vol. 20, 1968, pp. 13-20.

104. Beckette, D., 'An Introduction to Limit State Analysis of Reinforced Concrete Beams and Slabs', Build. Sci., Vol. 4, 1969, pp. 1-21.

105. Prager, W., 'Plastic Failure of Fibre Reinforced Materials', Trans. ASME, Journal Applied Mechanics, Vol. 36, 1969, pp. 542-544.

106. Biron, A., 'Limit Analysis of Cylinderical Shells with Longitudinal Rib Reinforcements, Int. J. Sol. Struct., Vol. 6, 1970, pp. 893-908.

107. McLaughlin, P.V. and Batterman, S.C., 'Limit Behaviour of Fibrous Materials', Int. J. Sol. Struct., Vol. 6, 1970, pp. 1357-1376.

108. McLaughlin, P.V. and Batterman, S.C., 'Limit Analysis of Plates Under a Concentrated Load', Journal of Engg. Mechanics Division, ASCE, Vol. 96, pp. 509-514.

109. Hopkins, H.G. and Prager, W., 'The Load Carrying Capacity of Circular Plates', J. Mech. Phys. Sol. Vol. 2, 1953, pp. 1-13.

110. Drucker, D.C. and Hopkins, H.G., 'Combined Concentrated and Distributed Load on Ideally Plastic Circular Plates', Proc. 2nd US Nat. Cong. App. Mech. (Ann Arbor, 1954), New York, 1955, pp. 517-520.

111. Hopkins, H.G. and Wang, A.J., 'Load Carrying Capacity for Circular Plates of Perfectly Plastic Material with Arbitrary Yield Condition', J. Mech. Phys. Sol., Vol. 3, 1954, pp. 117-129.

112. Haythornthwaite, R.M. and Shield, R.T., 'A Note on the Deformable Region in a Rigid-Plastic Structure', J.Mech.Phys.Solids, No.6, Vol.127,1958.

113. Zaid, M., 'On the Carrying Capacity of Plates of Arbitrary Shape and Variable Fixity Under a Concentrated Load', Trans. ASME, J. App. Mech. Div., Vol. 25, pp. 598-602.

114. Wasti, S.T., 'The Plastic Bending of Transversely Anisotropic Circular Plates', Int. J. Mech. Sci., Vol. 12, 1970, pp. 109-112.

115. Braestrup, M.W., 'Yield Line Theory and Limit Analysis of Plates and Slabs', Mag. Conc. Res., Vol. 22, 1970, pp. 99-106.

116. Wood, R.H., 'Some Controversial and Curious Developments in the Plastic Theory of Structures', Contribution to Engineering Plasticity, ed. J.H. Heyman and T.A. Leckie, Cambridge University Press, pp. 665-691.

117. Jones, L.L. and Wood, R.H., 'Yield-Line Analysis of Slabs', Thames and Hudson, Chatto and Widus, London, 1967.

118. Lance, R.H. and Robinson, D.N., 'A Maximum Shear Stress Theory of Plastic Failure of Fibre Reinforced Materials', J. Mech. Phy. Sol., Vol. 19, 1971, pp. 49-60.

119. Jain, S.C. and Kennedy, J.B., 'Yield Criterion for Reinforced Concrete Slabs', Journal of the Structural Division, ASCE, Vol. 100, SN.3, March, 1974, pp. 631-643.

120. Austriaco, N.C., Lee, S.L. and Rama, R.P., 'Inelastic Behaviour of Ferrocement Slabs and Bending', Magazine of Concrete Research, Vol. 27, No. 93, Dec. 1975, pp. 193-209.

121. Wood, R.H., 'Plastic Design of Slabs and Plates', Thames and Hudson, 1961, London, p. 13.

122. Massonnet, C.E. and Save, M.A., 'Plastic Analysis and Design of Plates, Shells and Disks', North Holland Publishing Company, London, 1972.

123. Kirkwood, J.G., 'Shock and Detonation Waves', Documents on Modern Physics, Gordon and Breach, New York, 1967.